ANALYSIS OF PAVEMENT STRUCTURES

Animesh Das

CRC Press
Taylor & Francis Group

ANALYSIS OF PAVEMENT STRUCTURES

This page intentionally left blank

ANALYSIS OF PAVEMENT STRUCTURES

Animesh Das
Professor, Department of Civil Engineering
Indian Institute of Technology Kanpur
Kanpur, India

CRC Press
Taylor & Francis Group
Boca Raton London New York

CRC Press is an imprint of the
Taylor & Francis Group, an **informa** business

CRC Press
Taylor & Francis Group
6000 Broken Sound Parkway NW, Suite 300
Boca Raton, FL 33487-2742

Version Date: 20140617

International Standard Book Number-13: 978-1-4665-5856-4 (eBook - PDF)

Visit the Taylor & Francis Web site at
http://www.taylorandfrancis.com

and the CRC Press Web site at
http://www.crcpress.com

Gifted to my beloved wife, Nibedita

This page intentionally left blank

Contents

This page intentionally left blank

List of Symbols

a	Radius of circular area or equivalent tire imprint
A	Area
a_{st}	Cross-sectional area of a single steel bar
A_{st}	Cross-sectional area of steel per unit length
B	Width of a concrete slab
BF	Body force
C_{crp}	Creep compliance
C^h	Heat capacity
D	Flexural rigidity of a plate
E	Young's modulus or elastic modulus
E'	Storage modulus
E''	Loss modulus
E^*	Complex modulus
E_d	Dynamic modulus
E_{rel}	Relaxation modulus
f	Coefficient of friction
g	Acceleration due to gravity
G	Shear modulus
h	Layer thickness
I_1	First stress invariant ($= \sigma_1 + \sigma_2 + \sigma_3$)
I_2	Second stress invariant
I_3	Third stress invariant
k	Modulus of subgrade reaction
k^{td}	Coefficient of thermal diffusivity
k_s	Spring constant
k_{ss}	Slider constant
l	Radius of relative stiffness

L	Length of a concrete slab
M	Moment
M_R	Resilient modulus
M_c	Unit cost of maintenance
M_u	Unit road user cost
n	Number of repetitions applied
$\boldsymbol{N}$	Number of traffic repetitions a material/pavement can sustain
P_a	Atmospheric pressure
q	Pressure
Q	Concentrated load
Q_h	Heat flow per unit area
r	Discount rate
R	Reliability
S	Structural health of a pavement
t	Time
T	Temperature
$\boldsymbol{T}$	Number of expected traffic repetitions
T_t	Temperature at the top surface
T_b	Temperature at the bottom surface
T_∞	Temperature at infinite depth
u	Displacement along X direction (Cartesian coordinate)
u_r	Displacement along R direction (cylindrical coordinate)
U	Universal gas constant
v	Displacement along Y direction (Cartesian coordinate)
V	Shear force
v_θ	Displacement along tangential direction (cylindrical coordinate)
V_o	Speed
x	Distance along X direction
y	Distance along Y direction
z	Distance along Z direction
z_s	Gap between two adjacent concrete slabs
α	Coefficient of thermal expansion
α_T	Time shift factor
β	An angle
γ	Engineering shear strain

δ	Phase angle
ΔH	Apparent activation energy
ϵ	Strain
ζ	Dummy variable for time
θ	An angle in cylindrical polar coordinate system
η_d	Viscosity of the dashpot
μ	Poisson's ratio
ρ	Density of the material
σ	Normal stress
σ^c	Confining pressure ($= \sigma_3$)
σ_d	Deviatoric stress
σ^S	Tensile strength
σ^{TA}	Axial stress component due to temperature
σ^{TB}	Bending stress component due to temperature
σ^{TN}	Nonlinear stress component due to temperature
ω	Displacement along Z direction (for both Cartesian and cylindrical coordinates)
ω_f	Angular frequency
τ^b	Bond strength

This page intentionally left blank

List of Figures

This page intentionally left blank

Preface

This is a simple book.

This book is about pavement analysis. A pavement is a multi-layered structure, made of a number of layers placed one over the other. These layers can be made of asphaltic material, cement concrete, bound or unbound stone aggregates, etc. These materials show complex mechanical response with the variation of stress, time, or temperature. Thus, understanding the performance of an in-service pavement structure subjected to vehicular loading and environmental variations is a difficult task.

However, this is a simple book. This book presents a step-by-step formulation for analyses of load and thermal stresses of idealized pavement structures. Some of these idealizations involve assumptions of the material being linear, elastic, homogeneous and isotropic; the load being static; the thermal profile being linear and so on.

Significant research has been done on analysis and design of pavements during the last half-century (some of the fundamental developments are, however, more than hundred years old) and a large number of research publications are already available. However, there is a need for the basic formulations to be systematically compiled and put together in one place. Hence this book. It is believed that such a compilation will provide an exposure to the basic approaches used in pavement analyses and subsequently help the readers formulate their own research or field problems—more difficult than those dealt with in this book.

The idea of this book originated when I initiated a post-graduate course on *Characterization of Pavement Materials and Analysis of Pavements* at IIT Kanpur. This course was introduced in 2007; that was the time we were revising the post-graduate course structure in our department. I must thank my colleague Dr. Partha Chakroborty for suggesting at that time that the Transportation Engineering program at IIT Kanpur should have a pavement engineering course with more analysis content. I also should thank him for his constant encouragement during the entire process of preparing this manuscript. One of our graduate students, Priyanka Khan, typed out portions of my lectures as class-notes. Those initial pages helped me to overcome the inertia of getting started to write this book. That is how it began.

This book has eight chapters. The first chapter introduces the sign convention followed in the book and mentions some of the basic solid mechanics formulations used in the subsequent chapters. The second chapter deals with the material characterization of various pavement materials. It introduces simple rheological models for asphaltic material. Beams and plates on elastic foundations are dealt with in the third chapter—these formulations form the basis of analysis of concrete pavement slabs due to load. The fourth chapter covers the thermal stress in concrete pavement, and it provides formulations for axial and bending stresses due to full and partial restraint conditions. The fifth chapter starts with the analysis of elastic half-space, and enlarges it to an analysis of multi-layered structure. A formulation for thermo-rheological analysis of asphalt pavement is presented in the sixth chapter. The seventh chapter discusses the pavement design principles where pavement analyses results are used. Finally, the last chapter discusses some miscellaneous topics which include analysis of a beam/plate resting on elastic half-space, analysis of dynamic loading conditions, analysis of composite pavement, reliability issues in pavement design, and the inverse problems in pavement engineering.

Since this book provides an overview of basic approaches for pavement analysis, rigorous derivations for complex situations have been deliberately skipped. However, references are provided in appropriate contexts for readers who want to explore further. I must place a disclaimer that those references are not necessarily the only and the best reading material, but they are just a representative few.

A number of my former and present students have contributed to the development of this book. They have asked me questions inside the classroom and outside. Discussions with some of them were quite useful, while others helped me to cross-check a few derivations. Dr. Pabitra Rajbongshi, Sudhir N. Varma, Vivek Agarwal, Pranamesh Chakraborty, Syed Abu Rehan, and Vishal Katariya are some of these students. I must also thank my former colleague, Dr. Ashwini Kumar, for the useful discussions with him on plate theories. I also thank all the people with whom I have interacted professionally from time to time for discussing various issues related to pavement engineering. I want to thank all the authors of numerous papers, books and other documents whose works have been referred to in this book.

I am most grateful to my parents for their care and thought involved in my education. I thank my father, Dr. Kali Charan Das, for teaching me formulations in physics using first principles. I thank my Ph.D. supervisor Dr. B. B. Pandey for training me as a researcher in pavement engineering. I also wish to thank my colleagues for the encouragement, and my Institute, IIT Kanpur, for providing an excellent academic ambiance.

I thank CRC Press and Taylor & Francis staff members, especially Dr. Gangandeep Singh and Joselyn Banks-Kyle for remaining in touch with me during the development of the manuscript and Karen Simon during the production process. I must thank my family members for bearing with me, and especially my daughter Anwesha for sacrificing her bedtime stories for months, while I was finalizing the manuscript.

Care has been taken as far as possible to check for editorial mistakes. If, however, you find any, or wish to provide your feedback on this book please drop me an e-mail at adas@iitk.ac.in.

This book now must go for printing.

Animesh Das

About the Author

Animesh Das, Ph.D., is presently working as a professor in the Department of Civil Engineering, Indian Institute of Technology Kanpur. He earned his Ph.D. degree from the Indian Institute of Technology Kharagpur. Dr. Das's areas of interest are pavement material characterization, analysis, pavement design, and pavement maintenance. He has authored many technical publications in various journals of repute and in conference proceedings. He has co-authored a textbook titled *Principles of Transportation Engineering* published by Prentice-Hall of India (currently, PHI Learning), and he co-developed a web-course titled *Advanced Transportation Engineering* under the National Programme on Technology Enhanced Learning (NPTEL), India. Dr. Das has received a number of awards in recognition of his contribution in the field, including an Indian National Academy of Engineers Young Engineer award (2004) and a Fulbright–Nehru Senior Research Fellowship (2012–13), etc. Details of his works can be found on his webpage: http://home.iitk.ac.in/∼adas.

This page intentionally left blank

Chapter 1

Introduction

1.1 Purpose of the book

Pavement is a multi-layered structure. It is made up of compacted soil, unbound granular material (stone aggregates), asphalt mix or cement concrete (or other bound material) put as horizontal layers one above the other. Figure 1.1 presents a typical cross section of an asphalt and a concrete pavement.

Generally, asphalt pavements do not have joints, whereas the concrete pavements (commonly known as jointed plain concrete pavement) have joints[1]. The concrete pavements are made of concrete slabs of finite dimensions with connections (generally of steels bars) to the adjacent slabs. Dowel bars are provided along the transverse joint and tie bars are provided along the longitudinal joint (refer to Figure 1.2). A block pavement or a segmental pavement is made up of inter-connected blocks (generally, cement concrete blocks), and its structural behavior is different from the usual asphalt or concrete pavements.

[1]Though exceptions are possible, for example, asphalt pavements in extremely cold climates may be provided with joints, continuously reinforced concrete pavements does not generally have joints etc.

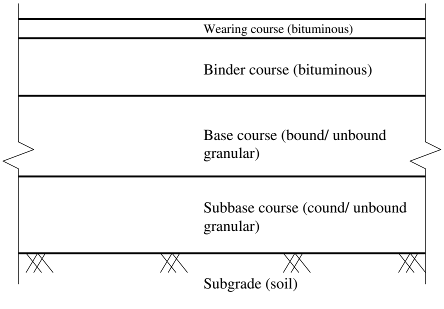

(a) An asphalt pavement section

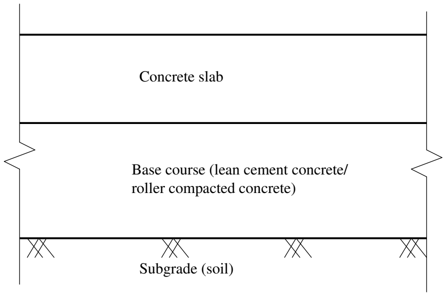

(b) A concrete pavement section

Figure 1.1: Typical cross-section of an asphalt and a concrete pavement.

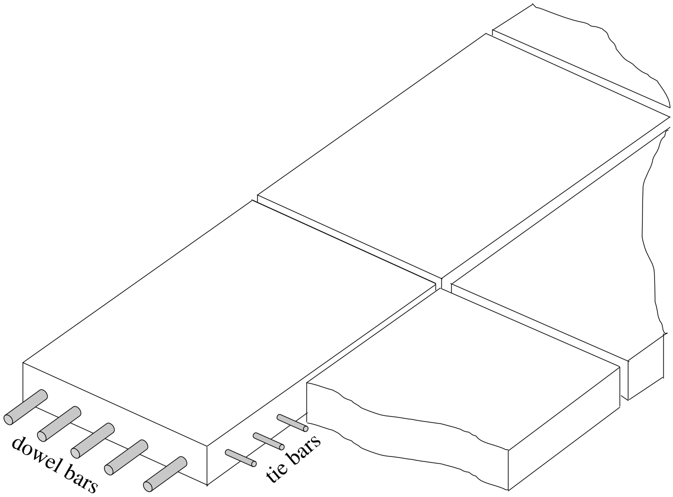

Figure 1.2: Dowel bar and tie bar arrangement in concrete pavement.

An in-service pavement is continuously subjected to traffic loading and temperature variations. The purpose of this book is to present a conceptual framework on the basic formulation of load and thermal stresses of typical (as shown in Figures 1.1 and 1.2) concrete and asphalt pavements.

Analysis of pavement structure enables one to predict or explain the pavement response to load from physical understanding of the governing principles, which can be corroborated later through experimental observations. This, in turn, builds confidence in structural design, evaluation, and maintenance planning of road infrastructure.

Generally speaking, a concrete pavement is idealized as a plate resting on an elastic foundation [124, 303, 304, 305]. It is assumed that the load is transferred through bending and the slab thickness does not undergo any change while it is subjected to a load. For an asphalt pavement, it is assumed that the load is transferred through contacts of particles, and the layer thicknesses do undergo changes due to application of load [34, 35, 142].

Pavement being a multi-layered structure, it is generally difficult to obtain a closed-form solution of its response due to load. For design purpose, pavement analysis may be done through some software(s) which may use certain numerical methods to perform the analysis. Ready-to-use analysis charts are also available in various codes/ guidelines. The algorithms used and the assumptions involved in the analysis process may not always be apparent to a pavement designer (as a user of these softwares/charts). Thus, there is a need to know the assumptions involved and the basic formulations needed for analyzing a pavement structure.

On the other hand, a large pool of research papers, books, reports, theses etc. is available dealing with pavement material characterization and structural analyses of pavements. The research publications typically deal with a rigorous theoretical development on a specific aspect and may choose to skip details of some of the of basic and well-known principles/techniques. Further, some of the basic formulations might have been developed many years ago (often with different notations and sign conventions than practiced today) and contributed by researchers from other areas of science and engineering. For instance, contributions to the theoretical formulation for pavement analysis have come from structural engineering (for example, the theory of plates), soil mechanics (for example, beams and plates on an elastic foundation), applied mechanics (for example, the stress-strain relationship, principles of rheology), mechanical engineering (for example, material modeling) and so on.

For a beginner (in pavement engineering) this may appear to be a hurdle—because, one may need to trace back to the original source, understand the assumptions/idealizations, and follow the subsequent theoretical development. Thus, there is a need for the approaches to pavement analyses to be collated in one place. This is the purpose of this book. The focus of the present book, therefore, can be identified as follows,

- This book is a compilation of the existing knowledge on analyses of pavement structure. Load and thermal stress analyses for both asphalt and concrete pavements are dealt with in this book. Attempts have been made to provide ready references to other publications/documents for further reading.
- Basic formulations for analysis of pavement structure have been presented in this book in a step-by-step manner—from a simple formulation to a more complex one. Attempts have been made to maintain a uniformity in symbol and sign conventions throughout the book.

1.2 Background and sign conventions

Some of the basic and widely used equations, which are also referred to and used in this book, are presented here almost without discussion. One can refer to books on the mechanics of solids

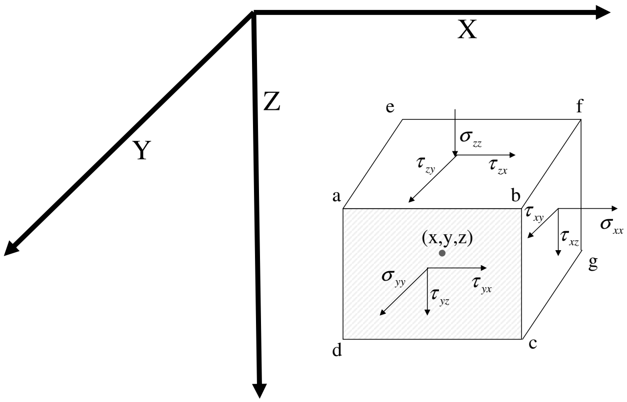

Figure 1.3: Sign convention in the Cartesian system followed in this book.

and the theory of elasticity [11, 99, 241, 277] for further study; applications of some of these formulations can also be found in books on soil mechanics [63, 104, 162, 222]. The sign convention followed in the present book is shown in Figure 1.3 for the Cartesian coordinate system and in Figure 1.4 for the cylindrical coordinate system. These figures also show the notations used to identify the stresses in different directions.

1.2.1 State of stress

The state of stress in a Cartesian coordinate system (refer to Figure 1.3) can be written as,

$$[\boldsymbol{\sigma}] = \begin{bmatrix} \sigma_{xx} & \tau_{xy} & \tau_{xz} \\ \tau_{yx} & \sigma_{yy} & \tau_{yz} \\ \tau_{zx} & \sigma_{zy} & \sigma_{zz} \end{bmatrix} \tag{1.1}$$

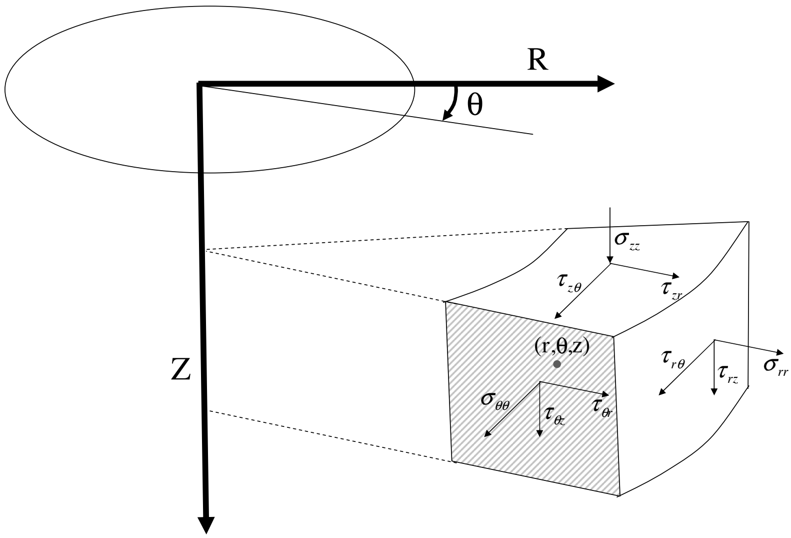

Figure 1.4: Sign convention in the cylindrical system followed in this book.

$\boldsymbol{\sigma}$ is also known as Cauchy's stress. For normal stresses on a body, a negative sign has been used in this book to indicate compression, and a positive sign to indicate tension.

Figure 1.5 shows a plane "afh," whose direction cosine values are l, m and n with respect to X, Y and Z axes respectively. If, p_{sx}, p_{sy} and p_{sz} represent the stresses (on plane "afh") parallel to X, Y and Z (refer Figure 1.5(a)), then,

$$\begin{Bmatrix} p_{sx} \\ p_{sy} \\ p_{sz} \end{Bmatrix} = \begin{bmatrix} \sigma_{xx} & \tau_{xy} & \tau_{xz} \\ \tau_{yx} & \sigma_{yy} & \tau_{yz} \\ \tau_{zx} & \sigma_{zy} & \sigma_{zz} \end{bmatrix} \begin{Bmatrix} l \\ m \\ n \end{Bmatrix} \tag{1.2}$$

The normal stress in the plane "afh" (refer to Figure 1.5b) can be obtained as,

$$\sigma_s = p_{sx}l + p_{sy}m + p_{sz}n \tag{1.3}$$

The shear stress on plane "afh" is obtained as,

$$\tau_s = \left(\left(p_{sx}^2 + p_{sy}^2 + p_{sz}^2\right) - \sigma_s^2\right)^{1/2} \tag{1.4}$$

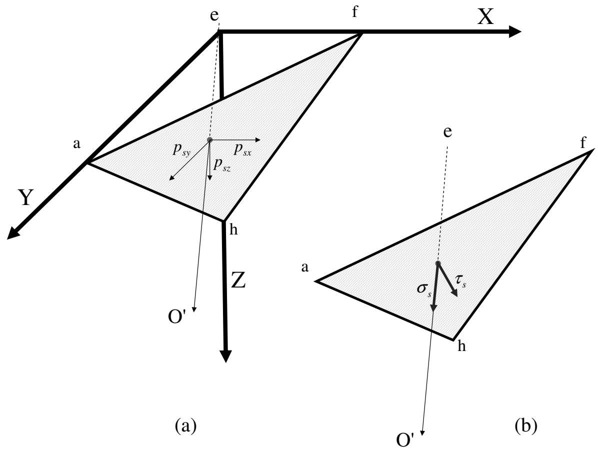

Figure 1.5: Stresses on plane "afh" plane with direction cosines as l, m and n.

For a special case, when the choice of the plane "afh" (that is choice of l, m and n) is such that the shear stress vanishes, and therefore, only the normal stress exists (that is, principal stress on that plane), it can be written as,

$$\left\{ \begin{array}{c} \sigma_s l \\ \sigma_s m \\ \sigma_s n \end{array} \right\} = \left[\begin{array}{ccc} \sigma_{xx} & \tau_{yx} & \tau_{zx} \\ \tau_{xy} & \sigma_{yy} & \tau_{zy} \\ \tau_{xz} & \sigma_{yz} & \sigma_{zz} \end{array} \right] \left\{ \begin{array}{c} l \\ m \\ n \end{array} \right\} \tag{1.5}$$

For a feasible solution to exist,

$$\left| \begin{array}{ccc} \sigma_{xx} - \sigma_s & \tau_{yx} & \tau_{zx} \\ \tau_{xy} & \sigma_{yy} - \sigma_s & \tau_{zy} \\ \tau_{xz} & \sigma_{yz} & \sigma_{zz} - \sigma_s \end{array} \right| = 0 \tag{1.6}$$

The Equation 1.6 gives rise to the characteristic equation as,

$$\sigma_s^3 - I_1 \sigma_s^2 + I_2 \sigma_s - I_3 = 0 \tag{1.7}$$

where, I_1, I_2 and I_3 are coefficients. Since the principal stress value for a given state of stress should not vary with the choice of the reference coordinate axes, the coefficients I_1, I_2 and I_3 must have constant values. These are known as stress invariants. Their expressions are provided as Equations 1.8–1.10.

$$I_1 = \sigma_{xx} + \sigma_{yy} + \sigma_{zz} \tag{1.8}$$

$$I_2 = \sigma_{xx}\sigma_{yy} + \sigma_{yy}\sigma_{zz} + \sigma_{zz}\sigma_{xx} - \tau_{xy}^2 - \tau_{yz}^2 - \tau_{zx}^2 \tag{1.9}$$

$$I_3 = \sigma_{xx}\sigma_{yy}\sigma_{zz} + 2\tau_{xy}\tau_{yz}\tau_{zx} - \sigma_{xx}\tau_{yz}^2 - \sigma_{yy}\tau_{xz}^2 - \sigma_{zz}\tau_{xy}^2 \tag{1.10}$$

In terms of principal stresses, these take the following form,

$$I_1 = \sigma_1 + \sigma_2 + \sigma_3 \tag{1.11}$$

$$I_2 = \sigma_1\sigma_2 + \sigma_2\sigma_3 + \sigma_3\sigma_1 \tag{1.12}$$

$$I_3 = \sigma_1\sigma_2\sigma_3 \tag{1.13}$$

There can be a special case when l, m, n values are all equal with references to the principal axes. That is, $l = m = n = \frac{1}{\sqrt{3}}$. The corresponding plane is known as an octahedral plane. The octahedral normal stress (σ_{oct}) can be obtained from Equation 1.3 as follows,

$$\sigma_{oct} = \frac{1}{3}\left(\sigma_1 + \sigma_2 + \sigma_3\right) \tag{1.14}$$

The octahedral shear stress (τ_{oct}) can be obtained from Equation 1.4 as follows,

$$\tau_{oct} = \frac{1}{3}\left((\sigma_1 - \sigma_2)^2 + (\sigma_1 - \sigma_3)^2 + (\sigma_3 - \sigma_1)^2\right)^{1/2} \tag{1.15}$$

The σ_{oct} and τ_{oct} in terms of the general state of stress can be expressed as,

$$\sigma_{oct} = \frac{1}{3}\left(\sigma_{nn} + \sigma_{yy} + \sigma_{zz}\right) \tag{1.16}$$

$$\begin{aligned} \tau_{oct}^2 &= \frac{1}{3}\Big((\sigma_{nn} - \sigma_{yy})^2 + (\sigma_{yy} - \sigma_{zz})^2 + (\sigma_{zz} - \sigma_{xx})^2 \\ &\quad + \sigma\tau_{ny}^2 + \sigma\tau_{yz}^2 + \sigma\tau_{zx}^2\Big)^{1/2} \end{aligned} \tag{1.17}$$

1.2.2 Strain-displacement and strain compatibility equations

If displacement fields in the direction of X, Y and Z are considered as u, v, and ω then,

$$\begin{aligned} \epsilon_{xx} &= \frac{\delta u}{\delta x} \\ \epsilon_{yy} &= \frac{\delta v}{\delta y} \\ \epsilon_{zz} &= \frac{\delta \omega}{\delta z} \\ \gamma_{xy} &= \frac{\delta u}{\delta y} + \frac{\delta v}{\delta x} \\ \gamma_{yz} &= \frac{\delta v}{\delta z} + \frac{\delta \omega}{\delta x} \\ \gamma_{zx} &= \frac{\delta \omega}{\delta x} + \frac{\delta u}{\delta z} \end{aligned} \tag{1.18}$$

where, ϵ_{xx}, ϵ_{yy} and ϵ_{zz} indicate normal strains (along X, Y and Z directions) and γ_{xy}, γ_{yz} and γ_{zx} indicate the engineering shear strains. By taking partial derivatives and suitably substituting, one can develop the following set of equations which do not contain the u, v and ω terms. These equations (Equation set 1.19) are known as strain compatibility equations.

$$
\begin{aligned}
\frac{\partial^2 \gamma_{xy}}{\partial x \partial y} &= \frac{\partial^2 \epsilon_{xx}}{\partial y^2} + \frac{\partial^2 \epsilon_{yy}}{\partial x^2} \\
\frac{\partial^2 \gamma_{yz}}{\partial y \partial z} &= \frac{\partial^2 \epsilon_{yy}}{\partial z^2} + \frac{\partial^2 \epsilon_{zz}}{\partial y^2} \\
\frac{\partial^2 \gamma_{zx}}{\partial z \partial x} &= \frac{\partial^2 \epsilon_{zz}}{\partial x^2} + \frac{\partial^2 \epsilon_{xx}}{\partial z^2} \\
2\frac{\partial^2 \epsilon_{xx}}{\partial y \partial z} &= -\frac{\partial^2 \gamma_{yz}}{\partial x^2} + \frac{\partial^2 \gamma_{zx}}{\partial x \partial y} + \frac{\partial^2 \gamma_{xy}}{\partial x \partial z} \\
2\frac{\partial^2 \epsilon_{yy}}{\partial z \partial x} &= -\frac{\partial^2 \gamma_{zx}}{\partial y^2} + \frac{\partial^2 \gamma_{xy}}{\partial y \partial z} + \frac{\partial^2 \gamma_{yz}}{\partial y \partial x} \\
2\frac{\partial^2 \epsilon_{zz}}{\partial x \partial y} &= -\frac{\partial^2 \gamma_{xy}}{\partial z^2} + \frac{\partial^2 \gamma_{yz}}{\partial z \partial x} + \frac{\partial^2 \gamma_{zx}}{\partial z \partial y}
\end{aligned} \tag{1.19}
$$

The strain-displacement relationships in the cylindrical coordinate are,

$$
\begin{aligned}
\epsilon_{rr} &= \frac{\partial u_r}{\partial r} \\
\epsilon_{\theta\theta} &= \frac{u_r}{r} + \frac{1}{r}\frac{\partial v_\theta}{\partial \theta} \\
\epsilon_{zz} &= \frac{\partial \omega}{\partial z} \\
\gamma_{r\theta} &= \frac{1}{r}\frac{\partial u_r}{\partial \theta} + \frac{\partial v_\theta}{\partial r} - \frac{v_\theta}{r} \\
\gamma_{rz} &= \frac{\partial u_r}{\partial z} + \frac{\partial \omega}{\partial r} \\
\gamma_{r\theta} &= \frac{\partial v_\theta}{\partial z} + \frac{1}{r}\frac{\partial \omega}{\partial \theta}
\end{aligned} \tag{1.20}
$$

where, u_r = displacement in r direction, v_θ = displacement along tangential direction, and ω = displacement along Z direction.

1.2.3 Constitutive relationship between stress and strain

The constitutive relationship for a linear anisotropic material can be written as,

$$\begin{Bmatrix} \sigma_{xx} \\ \sigma_{yy} \\ \sigma_{zz} \\ \tau_{xy} \\ \tau_{yz} \\ \tau_{zx} \end{Bmatrix} = \begin{bmatrix} C_{11} & C_{12} & C_{13} & C_{14} & C_{15} & C_{16} \\ C_{21} & C_{22} & C_{23} & C_{24} & C_{25} & C_{26} \\ C_{31} & C_{32} & C_{33} & C_{34} & C_{35} & C_{36} \\ C_{41} & C_{42} & C_{43} & C_{44} & C_{45} & C_{46} \\ C_{51} & C_{52} & C_{53} & C_{54} & C_{55} & C_{56} \\ C_{61} & C_{62} & C_{63} & C_{64} & C_{65} & C_{66} \end{bmatrix} \begin{Bmatrix} \epsilon_{xx} \\ \epsilon_{yy} \\ \epsilon_{zz} \\ \gamma_{xy} \\ \gamma_{yz} \\ \gamma_{zx} \end{Bmatrix} \tag{1.21}$$

where, C_{ij} are the material constants. For isotropic material (that is, when the properties are same along any direction) Equation 1.21 takes the following form:

$$\begin{Bmatrix} \sigma_{xx} \\ \sigma_{yy} \\ \sigma_{zz} \\ \tau_{xy} \\ \tau_{yz} \\ \tau_{zx} \end{Bmatrix} = \begin{bmatrix} C_{11} & C_{12} & C_{12} & 0 & 0 & 0 \\ C_{12} & C_{11} & C_{12} & 0 & 0 & 0 \\ C_{12} & C_{12} & C_{11} & 0 & 0 & 0 \\ 0 & 0 & 0 & \frac{1}{2}(C_{11}-C_{12}) & 0 & 0 \\ 0 & 0 & 0 & 0 & \frac{1}{2}(C_{11}-C_{12}) & 0 \\ 0 & 0 & 0 & 0 & 0 & \frac{1}{2}(C_{11}-C_{12}) \end{bmatrix} \begin{Bmatrix} \epsilon_{xx} \\ \epsilon_{yy} \\ \epsilon_{zz} \\ \gamma_{xy} \\ \gamma_{yz} \\ \gamma_{zx} \end{Bmatrix} \tag{1.22}$$

where, $C_{11} = \frac{E(1-\mu)}{(1+\mu)(1-2\mu)}$ and $C_{12} = \frac{E\mu}{(1+\mu)(1-2\mu)}$, E is the Young's modulus of the material. The inverted form of the Equation 1.22 can be presented (using the values of C_{11} and C_{12}) as following,

$$\begin{Bmatrix} \epsilon_{xx} \\ \epsilon_{yy} \\ \epsilon_{zz} \\ \gamma_{xy} \\ \gamma_{yz} \\ \gamma_{zx} \end{Bmatrix} = \frac{1}{E} \begin{bmatrix} 1 & -\mu & -\mu & 0 & 0 & 0 \\ -\mu & 1 & -\mu & 0 & 0 & 0 \\ -\mu & -\mu & 1 & 0 & 0 & 0 \\ 0 & 0 & 0 & 2(1+\mu) & 0 & 0 \\ 0 & 0 & 0 & 0 & 2(1+\mu) & 0 \\ 0 & 0 & 0 & 0 & 0 & 2(1+\mu) \end{bmatrix} \begin{Bmatrix} \sigma_{xx} \\ \sigma_{yy} \\ \sigma_{zz} \\ \tau_{xy} \\ \tau_{yz} \\ \tau_{zx} \end{Bmatrix} \tag{1.23}$$

Equation 1.23 can be written as,

$$
\begin{aligned}
\epsilon_{xx} &= \frac{1}{E}\left(\sigma_{xx} - \mu\left(\sigma_{yy} + \sigma_{zz}\right)\right) \\
\epsilon_{yy} &= \frac{1}{E}\left(\sigma_{yy} - \mu\left(\sigma_{zz} + \sigma_{xx}\right)\right) \\
\epsilon_{zz} &= \frac{1}{E}\left(\sigma_{zz} - \mu\left(\sigma_{xx} + \sigma_{yy}\right)\right)
\end{aligned} \tag{1.24}
$$

$$
\begin{aligned}
\gamma_{xy} &= \frac{1}{G}\tau_{xy} \\
\gamma_{yz} &= \frac{1}{G}\tau_{yz} \\
\gamma_{zx} &= \frac{1}{G}\tau_{zx}
\end{aligned} \tag{1.25}
$$

where, $G = \frac{E}{2(1+\mu)}$. In a cylindrical coordinate (for isotropic material), the equations are,

$$
\begin{aligned}
\sigma_{rr} &= \frac{E}{(1+\mu)(1-2\mu)}\left((1-\mu)\epsilon_{rr} + \mu\epsilon_{zz} + \mu\epsilon_{\theta\theta}\right) \\
\sigma_{zz} &= \frac{E}{(1+\mu)(1-2\mu)}\left(\mu\epsilon_{rr} + (1-\mu)\epsilon_{zz} + \mu\epsilon_{\theta\theta}\right) \\
\sigma_{\theta\theta} &= \frac{E}{(1+\mu)(1-2\mu)}\left(\mu\epsilon_{rr} + \mu\epsilon_{zz} + (1-\mu)\epsilon_{\theta\theta}\right)
\end{aligned} \tag{1.26}
$$

$$
\begin{aligned}
\tau_{rz} &= \frac{E}{2(1+\mu)}\gamma_{rz} \\
\tau_{r\theta} &= \frac{E}{2(1+\mu)}\gamma_{r\theta} \\
\tau_{z\theta} &= \frac{E}{2(1+\mu)}\gamma_{z\theta}
\end{aligned} \tag{1.27}
$$

For an axi-symmetric situation (that is, when the material property, geometry and loading are symmetric about the axis of revolution) the response of the material/ medium will be independent of θ, that is, $\frac{\partial}{\partial\theta} = 0$ and $v_\theta = 0$ (refer to Equation 1.20).

Plane stress condition (in Cartesian coordinate system)

For a plane stress condition, stress in one particular direction (say along Y direction) is zero. That is, $\sigma_{yy} = \sigma_{xy} = \sigma_{yz} = 0$. Such a situation arises, for example, for a disk with a negligible thickness. Putting these conditions in Equations 1.24 and 1.25, one can write,

$$\begin{aligned}
\epsilon_{xx} &= \frac{1}{E}\left(\sigma_{xx} - \mu\sigma_{zz}\right) \\
\epsilon_{yy} &= \frac{1}{E}\left(-\mu\sigma_{zz} - \mu\sigma_{xx}\right) \\
\epsilon_{zz} &= \frac{1}{E}\left(\sigma_{zz} - \mu\sigma_{xx}\right)
\end{aligned} \tag{1.28}$$

$$\begin{aligned}
\gamma_{xy} &= 0 \\
\gamma_{yz} &= 0 \\
\gamma_{zx} &= \frac{1}{G}\tau_{zx} = \frac{2\left(1+\mu\right)}{E}\tau_{zx}
\end{aligned} \tag{1.29}$$

Conversely, the stresses (in the plane stress case) can be expressed (considering, $G = \frac{E}{2(1+\mu)}$) in terms of strains as follows,

$$\begin{aligned}
\sigma_{xx} &= \frac{E}{1-\mu^2}\epsilon_{xx} + \frac{\mu E}{1-\mu^2}\epsilon_{zz} \\
\sigma_{zz} &= \frac{E}{1-\mu^2}\epsilon_{zz} + \frac{\mu E}{1-\mu^2}\epsilon_{xx} \\
\tau_{zx} &= \frac{E}{2(1+\mu)}\gamma_{zx}
\end{aligned} \tag{1.30}$$

Plane strain condition in (Cartesian coordinate system)

In a plane strain condition, strain in one particular direction (say along Y direction) is zero. That is, $\epsilon_{yy} = \gamma_{xy} = \gamma_{yz} = 0$. Such a situation arises for example, for an embankment, which has negligible strain along the longitudinal direction. Putting these conditions in Equations 1.24 and 1.25, one can write,

$$\begin{aligned}
\epsilon_{xx} &= \frac{1-\mu^2}{E}\sigma_{xx} - \frac{\mu(1+\mu)}{E}\sigma_{zz} \\
\epsilon_{zz} &= \frac{1-\mu^2}{E}\sigma_{zz} - \frac{\mu(1+\mu)}{E}\sigma_{xx} \\
\gamma_{zx} &= \frac{2(1+\mu)}{E}\tau_{zx}
\end{aligned} \tag{1.31}$$

Conversely, the stresses (in the plane strain case) can be expressed in terms of strains as follows,

$$\begin{aligned}
\sigma_{xx} &= \frac{E(1-\mu)}{(1+\mu)(1-2\mu)}\epsilon_{xx} + \frac{\mu E}{(1+\mu)(1-2\mu)}\epsilon_{zz} \\
\sigma_{zz} &= \frac{\mu E}{(1+\mu)(1-2\mu)}\epsilon_{xx} + \frac{(1-\mu E}{(1+\mu)(1-2\mu)}\epsilon_{zz} \\
\tau_{zx} &= \frac{E}{2(1+\mu)}\gamma_{zx}
\end{aligned} \tag{1.32}$$

1.2.4 Equilibrium equations

The equilibrium condition is derived by taking the force balance along each direction. The static equilibrium equation (in Cartesian coordinate system) can be written as,

$$\begin{aligned}
\frac{\partial \sigma_{xx}}{\partial x} + \frac{\partial \tau_{yx}}{\partial y} + \frac{\partial \tau_{zx}}{\partial z} + BF_x &= 0 \\
\frac{\partial \tau_{xy}}{\partial x} + \frac{\partial \sigma_{yy}}{\partial y} + \frac{\partial \tau_{zy}}{\partial z} + BF_y &= 0 \\
\frac{\partial \tau_{xz}}{\partial x} + \frac{\partial \tau_{yz}}{\partial y} + \frac{\partial \sigma_{zz}}{\partial z} + BF_z &= 0
\end{aligned} \tag{1.33}$$

where, BF_x, BF_y and BF_z are the body forces per unit volume (say, gravity, magnetic force etc., as applicable) along X, Y and Z directions respectively. For a dynamic equilibrium case, the right-hand side of the equations will have terms as $\rho\frac{\partial^2 u}{\partial t^2}$, $\rho\frac{\partial^2 v}{\partial t^2}$ and $\rho\frac{\partial^2 \omega}{\partial t^2}$, respectively, where ρ is the density of the material. The static equilibrium condition in a cylindrical coordinate system is obtained as,

$$\begin{aligned}
\frac{\partial \sigma_{rr}}{\partial r} + \frac{1}{r}\frac{\partial \tau_{r\theta}}{\partial \theta} + \frac{\partial \tau_{zr}}{\partial z} + \frac{\sigma_{rr} - \sigma_{\theta\theta}}{r} + BF_r = 0 \\
\frac{\partial \tau_{r\theta}}{\partial r} + \frac{1}{r}\frac{\partial \sigma_{\theta\theta}}{\partial \theta} + \frac{\partial \tau_{\theta z}}{\partial z} + \frac{2\tau_{r\theta}}{r} + BF_\theta = 0 \\
\frac{\partial \tau_{zr}}{\partial r} + \frac{1}{r}\frac{\partial \tau_{\theta z}}{\partial \theta} + \frac{\partial \sigma_{zz}}{\partial z} + \frac{\tau_{zr}}{r} + BF_z = 0
\end{aligned} \tag{1.34}$$

where, BF_r, BF_θ, and BF_z are the body forces per unit volume along r, θ, and Z directions respectively.

1.3 Closure

Some basic relationships in the mechanics of solids are recapitulated in this chapter as background material. These equations have been referred/used at various places in the subsequent chapters of this book. One can refer to any suitable book on the mechanics of solids and the theory of elasticity for further discussions on these.

This page intentionally left blank

Chapter 2

Material characterization

2.1 Introduction

As mentioned in Section 1.1, different materials are used to build a road. This chapter deals with the material characterization of some of the basic types of materials used in pavements. Material characterization for soil, unbound granular material, asphalt mix, cement concrete, and cemented material will be briefly discussed in this chapter.

2.2 Soil and unbound granular material

Compacted soil is used to build subgrade (refer Figure 2.1(a)). Unbound granular material is used to build the base/sub-base of a pavement structure (refer Figure 2.1(b)).

The resilient modulus (M_R) is generally the elastic modulus parameter used for the characterization of granular material (or soil). It is determined by applying a repetitive load to the sample in a

(a) Compacted soil used as sub-grade

(b) Unbound granular material can be used as a base/sub-base

Figure 2.1: Soil and unbound granular materials are used for building roads.

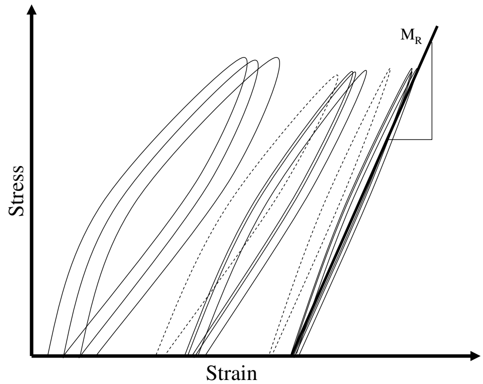

Figure 2.2: Repetitive load is applied to unbound granular material (or soil) in a triaxial setup to estimate M_R value.

triaxial cell [3]. The M_R is defined as,

$$M_R = \frac{\text{deviatoric stress}}{\text{recoverable strain}} \tag{2.1}$$

Experimental studies indicate granular material is a stress dependent material. A large number of M_R models (as functions of the state of stress) have been proposed by past researchers. One can refer to, for example, [163, 167, 278, 288] etc., for brief reviews on the various models of granular material and soil. One of such models is [75, 110],

$$M_R = c_1 \left(\sigma^c / P_a\right)^{c_2} \tag{2.2}$$

where, σ^c is the confining pressure ($= \sigma_3$) in a triaxial test, P_a is the atmospheric pressure, c_1 and c_2 are the material parameters. σ^c is divided by P_a to make the parameter dimensionless. Another model, popularly known as $k - \theta$ model ($\theta = I_1$), is represented as follows [1, 32, 110, 205]

$$M_R = k_1 \left(I_1\right)^{k_2} \tag{2.3}$$

where, k_1 and k_2 are the material parameters and I_1 is the first invariant of stress (refer to Equations 1.8 and 1.11). It was argued that the model represented by Equation 2.3 has certain limitations [163], and the following models were proposed [195, 293]

$$M_R = k_1 \left(I_1\right)^{k_2} \left(\sigma_d\right)^{k_3} \tag{2.4}$$

where, k_1, k_2 and k_2 are the material parameters, σ_d = deviatoric stress.

$$M_R = k_1 \left(I_1\right)^{k_2} \left(\tau_{oct}\right)^{k_3} \tag{2.5}$$

where, τ_{oct} is the octahedral shear stress (refer to Equation 1.15), and so on.

The resilient modulus of unbound granular material depends on a number of parameters, for example, aggregate gradation, level of compaction, moisture content, particle size, loading pattern, and stress level, etc. Further behavior of granular material in compression and in tension (because granular material can only sustain a small magnitude of tension) is different; therefore these need to be modeled separately [318]. It also behaves anisotropically [250]. One can, for example, refer to [163, 278] for a brief review on this topic.

Besides the above kind of models for M_R (where, M_R values are related to various stress parameters), a number of other (constitutive relationship based) models also have been proposed, in which volumetric and shear strains are considered [26, 29, 30, 160]. In these models, the material (that is, granular material or soil) is assumed to behave as an isotropic (refer Equation 1.22) and nonlinearly elastic material, (hence, there will be no loss in the strain energy) or the volumetric strain is path independent.

There are various other parameters which are used to characterize soil and granular materials, and some of these are related to M_R through empirical equations. Modulus of subgrade reaction [1, 217, 281] (k) is another parameter which is measured in situ, typically by a plate load test [102]. This is defined as the pressure needed to cause unit displacement of the plate. This conceptually represents the "spring constant" of the foundation on which the pavement is resting. The parameter k will be briefly discussed later in Section 3.2.1.

2.3 Asphalt mix

An asphalt mix is made up of an asphalt binder and aggregates mixed in specified proportion (refer to Figure 2.3). Volumetrically asphalt mix contains an asphalt binder, aggregates, and air-voids. Unlike cement concrete (where hydration of cement is involved during hardening), no chemical reaction takes place in asphalt mix, hence aggregates and asphalt binder retain their individual physical properties. The mixing can be done at an elevated temperature (for hot mix asphalt), a moderate temperature (for warm mix asphalt) or at ambient temperature (for cold mix asphalt).

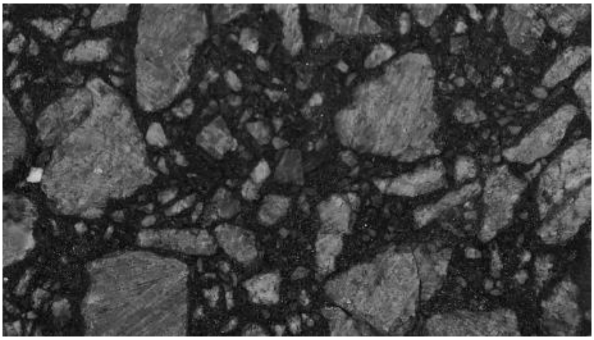

Figure 2.3: Cross-sectional image of an asphalt mix sample.

Various stiffness modulus parameters, measurement techniques, and modeling have been proposed to characterize asphalt mix [4, 70, 149, 172, 268, 291, 314]. Some of the simple rheological models and associated principles, which can be used to develop simple models for an asphalt mix, are discussed briefly in the following.

2.3.1 Rheological models for asphalt mix

Rheolgical models are widely used to describe the mechanical response of materials which varies with time. For a detailed understanding on rheological principles one can refer to, for example, [51, 84, 161] etc. A number of textbooks and synthesis documents are available on rheological modeling of materials.

Creep is a situation when stress (that is, load) is held constant, relaxation is a situation when the strain (that is, displacement) is held constant. For rheological materials like asphalt material, typically, under creep condition (that is, in a constant stress situation) the strain will keep on increasing (until it stabilizes to an almost constant level), and under relaxation condition (that is, at constant strain situation) the stress will keep on decreasing

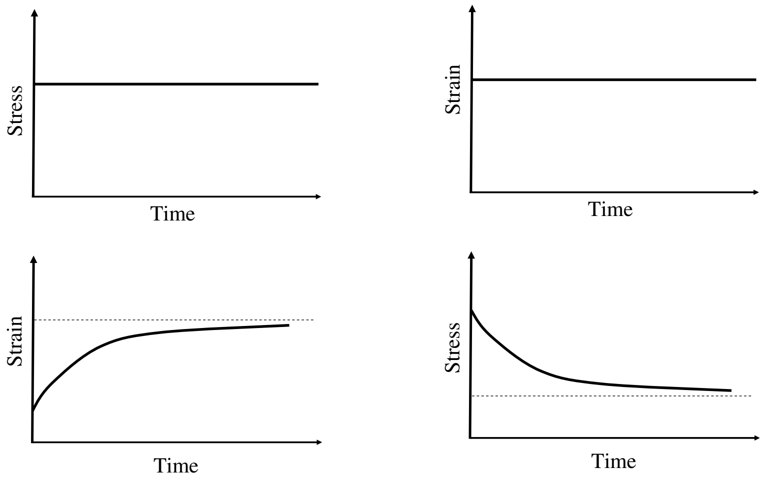

(a) Creep response (b) Relaxation response

Figure 2.4: Typical creep and relaxation response of asphalt mix.

(until it stabilizes to an almost constant level). A typical behavior, observed for asphalt mix, under creep and relaxation conditions is shown in Figures 2.4(a) and 2.4(b) respectively. Various curve fitting techniques (for example, power law, Prony series, etc.) have been suggested to fit the data, and the readers can, for example, refer to [149, 214] for further reading.

Creep modulus (E_{crp}) at any given time t can be defined as the stress divided by the strain at that time under creep condition, and the Creep compliance (C_{crp}) at any time t is defined as the strain divided by the stress at that time under creep condition. Similarly, the relaxation modulus (E_{rel}) at any given time t is defined as the stress divided by the strain at that time, under relaxation condition.

This behavior can be modeled using spring(s) and dashpot(s), as axial members (as a "mechanical analog"), connected in various

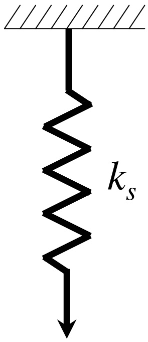

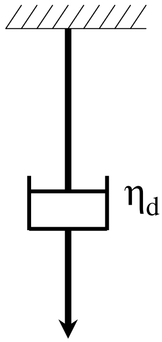

Figure 2.5: A spring and a dashpot.

combinations. The constitutive relationship of a (Hookean) spring (refer to Figure 2.5(a)) can be represented as,

$$\sigma = k_s \epsilon \tag{2.6}$$

where, σ = stress in the spring, k_s = spring constant, and ϵ = strain in the spring. The constitutive relationship of a dashpot (refer to Figure 2.5(b)) can be represented as,

$$\sigma = \eta_d \dot{\epsilon} \tag{2.7}$$

where, σ = stress in the dashpot, η_d = viscosity of the dashpot, and $\dot{\epsilon}$ = strain rate of the dashpot. Various combinations of spring and dashpot are used to develop various models. Since these models are made with elastic (that is, spring) and viscous (that is, dashpot) components, they are expected to capture the viscoelastic rheologic behavior of the material.

Two component models

A series combination of a spring and a dashpot is known as the Maxwell model, and a parallel combination of a spring and a dashpot is known as the Kelvin–Voigt model. These are discussed in the following.

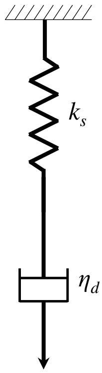

Figure 2.6: A Maxwell model.

Maxwell model

A Maxwell model is presented in Figure 2.6. Since, in this model, the spring and the dashpot are connected in series, the stresses are equal in each component and the total strain is equal to the sum of the strains in each of the components. Considering these two conditions, the constitutive equation can be written as,

$$\sigma + \dot{\sigma}\frac{\eta_s}{k_s} = \eta_d\dot{\epsilon} \tag{2.8}$$

where, σ = stress in the system and ϵ = strain in the system. For a creep case, the condition is σ= constant = σ_o (say), or $\dot{\sigma} = 0$. The Equation 2.8, therefore, takes the form

$$\sigma_o = \eta_s\dot{\epsilon} \tag{2.9}$$

Using the condition that at $t = 0$, $\epsilon = \frac{\sigma_o}{\eta_d}$, the solution of Equation 2.9 can be obtained as,

$$\epsilon(t) = \frac{\sigma_o}{\eta_d}t + \frac{\sigma_o}{k_s} \tag{2.10}$$

It can be seen that Equation 2.10 is an equation of a straight line and does not depict the typical creep trend (of asphalt mix) proposed in Figure 2.4(a). The creep compliance in this case can be obtained as,

$$\begin{aligned} C_{crp}(t) &= \epsilon(t)/\sigma_o \\ &= \frac{1}{\eta_d}t + \frac{1}{k_s} \end{aligned} \tag{2.11}$$

For the relaxation case, the condition is $\epsilon=$ constant $= \epsilon_o$ (say), or, $\dot{\epsilon} = 0$. Equation 2.8 takes the form

$$\sigma + \dot{\sigma}\frac{\eta_d}{k_s} = 0 \tag{2.12}$$

Using the condition that at $t = 0$, $\sigma = k_s \epsilon_o$, the solution of Equation 2.12 can be obtained as,

$$\sigma = k_s \epsilon_o e^{-\frac{k_s t}{\eta_d}} \tag{2.13}$$

The relaxation modulus, therefore, is obtained as,

$$\begin{aligned} E_{rel}(t) &= \sigma(t)/\epsilon_o \\ &= k_s e^{-\frac{k_s}{\eta_d}t} \end{aligned} \tag{2.14}$$

Kelvin–Voigt model

A Kelvin–Voigt model is presented in Figure 2.7. Since, in this model, the spring and the dashpot are connected in parallel, the strains are equal in each component and the total stress is equal to the sum of the stresses in each of the components. Taking these two conditions into account, the constitutive equation can be written as,

$$\sigma = k_s \epsilon + \eta_d \dot{\epsilon} \tag{2.15}$$

Equation 2.15 can be solved for creep condition (in a similar manner as above) and the response of the system can be obtained as following,

$$\epsilon = \frac{\sigma_o}{k_s}\left(1 - e^{-\frac{k_s}{\eta_d}t}\right) \tag{2.16}$$

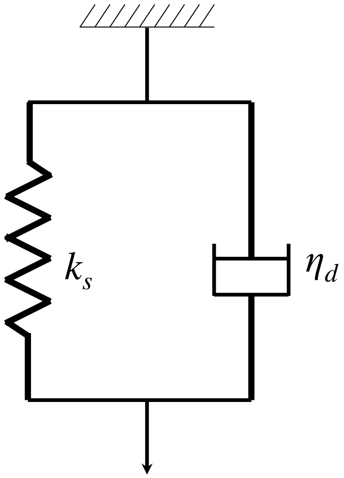

Figure 2.7: A Kelvin–Voigt model.

Similarly, Equation 2.15 can be solved for the relaxation condition and the response of the system can be obtained as following,

$$\sigma = k_s \epsilon_o \tag{2.17}$$

It can be seen that Equation 2.17 is an equation of a straight line (parallel to the time axis) and does not depict the typical relaxation trend (for asphalt mix) proposed in Figure 2.4(b).

Three component models

A three component model can be composed of a combination of either two springs and a dashpot or two dashpots and a spring. A three component model as shown in Figure 2.8 is taken up, here, for further analysis. In this model a spring (spring constant = k'') is connected in series to a parallel arrangement of another spring (spring constant = k') and a dashpot (viscosity = η_d). Identifying the components as 1, 2 and 3, as shown in Figure 2.8, one can

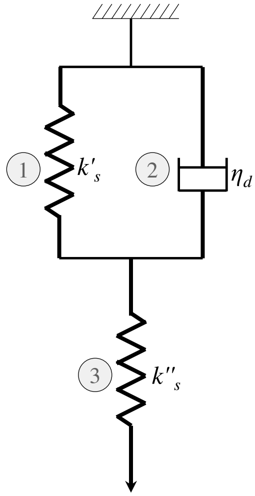

Figure 2.8: A three-component model.

write,

$$
\begin{aligned}
\sigma &= \sigma_3 = \sigma_1 + \sigma_2 \\
\epsilon_1 &= \epsilon_2 \\
\epsilon &= \epsilon_3 + \epsilon_2 \\
k'_s &= \frac{\sigma_1}{\epsilon_1} \\
\eta_d &= \frac{\sigma_2}{\dot{\epsilon}_2} \\
k''_s &= \frac{\sigma_3}{\epsilon_3}
\end{aligned}
\tag{2.18}
$$

Combining all the above equations, one can obtain the constitutive relationship as,

$$
\sigma + \frac{\eta_d}{k'_s + k''_s}\dot{\sigma} = \frac{k'_s k''_s}{k'_s + k''_s}\epsilon + \frac{k''_s \eta_d}{k'_s + k''_s}\dot{\epsilon} \tag{2.19}
$$

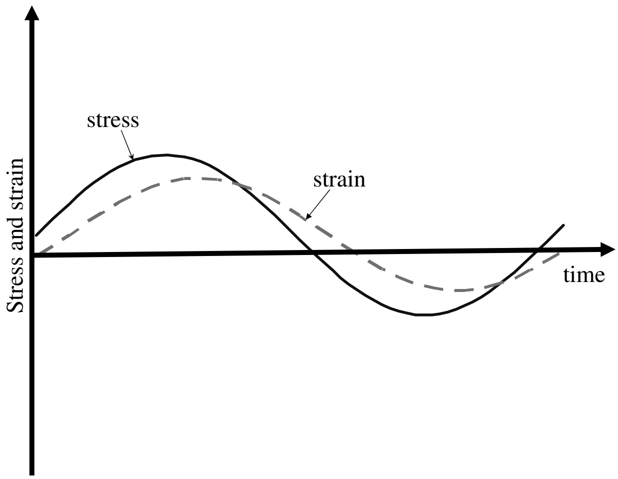

Figure 2.9: Sinusoidal loading on rheological material in stress controlled mode.

The solution for the creep case (that is, $\dot{\sigma} = 0$) is obtained as,

$$\epsilon = \sigma_o \left(\frac{k'_s + k''_s}{k'_s k''_s} \left(1 - e^{-\frac{k'_s}{\eta_d} t} \right) + \frac{1}{k''_s} e^{-\frac{k'_s}{\eta_d} t} \right) \tag{2.20}$$

The solution for the relaxation case (that is, $\dot{\epsilon} = 0$) is obtained as,

$$\sigma = \epsilon_o k''_s e^{-\frac{k'_s + k''_s}{\eta_d} t} + \frac{k'_s k''_s}{k'_s + k''_s} \epsilon_o \left(1 - e^{-\frac{k'_s + k''_s}{\eta_d} t} \right) \tag{2.21}$$

Under dynamic loading condition, a phase difference occurs between the stress and the strain for rheologic materials. Figure 2.9 shows a schematic diagram of a stress controlled dynamic loading. The stress can be expressed as,

$$\sigma = \sigma_o e^{i\omega_f t} \tag{2.22}$$

where ω_f is the angular velocity. The strain developed will have a phase angle lag of δ. That is,

$$\epsilon = \epsilon_o e^{i(\omega_f t - \delta)} \tag{2.23}$$

The energy dissipated per cycle per unit volume can be calculated as,

$$\int_0^{\frac{2\pi}{\omega_f}} \sigma d\epsilon = \int_0^{\frac{2\pi}{\omega_f}} \sigma \frac{d\epsilon}{dt} dt$$
$$= i\pi\sigma_o\epsilon_o \sin\delta \tag{2.24}$$

which is seen to be contributed from the out-of-phase portion. For elastic material $\delta = 0$ indicating that the loss of energy due to dissipation will be zero. The complex modulus (E^*) can be written as,

$$E^* = \frac{\sigma}{\epsilon} = \frac{\sigma_o e^{i\omega_f t}}{\epsilon_o e^{i(\omega_f t - \delta)}}$$
$$= \frac{\sigma_o}{\epsilon_o}\cos\delta + i\frac{\sigma_o}{\epsilon_o}\sin\delta$$
$$= E' + iE'' \tag{2.25}$$

where, E' is defined as the storage modulus, and E'' as the loss modulus. The dynamic modulus is defined as,

$$E_d = |E^*| = \sqrt{(E'^2 + E''^2)} \tag{2.26}$$

The phase angle, δ can be obtained as,

$$\delta = tan^{-1}\frac{E''}{E'} \tag{2.27}$$

The expression for E_d can be derived for any given model. For example, incorporating $\sigma = \sigma_o e^{i\omega_f t}$ (that is, Equation 2.22) and $\epsilon = \epsilon_o e^{i(\omega_f t - \delta)}$ (that is, Equation 2.23) in a three component model (represented by Equation 2.19), and considering that $\dot{\sigma} = i\omega_f \sigma$ and $\dot{\epsilon} = i\omega_f \epsilon$, and further assuming $k_s' = k_s'' = k_s$ (say), one obtains,

$$E^* = \frac{k_s^2 + i\omega_f \eta_d k_s}{2k_s + i\omega_f \eta_d} \tag{2.28}$$

and this can be expressed in $E' + iE''$ form, as

$$E^* = \frac{2k_s + k_s\omega_f^2\eta_d^2}{4k_s^2 + \omega_f^2\eta_d^2} + i\frac{\omega_f\eta_d k_s^2}{4k_s^2 + \omega_f^2\eta_d^2} \tag{2.29}$$

Thus, the E_d (refer to Equation 2.26) is obtained as,

$$E_d = |E^*| \tag{2.30}$$

$$= \frac{\left[(2k_s + k_s\omega_f^2\eta^2)^2 + (\omega_f\eta_d k_s^2)^2\right]^{\frac{1}{2}}}{4k_s^2 + \omega_f^2\eta^2} \tag{2.31}$$

and the phase angle (refer to Equation 2.27) is obtained as,

$$\delta = \tan^{-1}\left(\frac{\omega_f\eta_d k_s}{2 + \omega_f^2\eta_d^2}\right) \tag{2.32}$$

The E_d value of the asphalt mix is dependent on a number of parameters, for example, aggregate gradation, asphalt binder viscosity, temperature, volumetric parameters, level of compaction, and so on. A number of predictive models have been developed to estimate the E_d value of the asphalt mix from the known parameters. Interested readers can refer to, for example, [19, 41, 149] etc. for more details.

Generalized models

In generalized models a large/infinite number of components are used. An example of a generalized Maxwell model is shown in Figure 2.10. Here, a number of Maxwell elements are connected in parallel. For this model, for the relaxation case, one can write,

$$\begin{aligned} \epsilon_1 &= \epsilon_2 = \cdots = \epsilon_i = \cdots = \epsilon_o \\ \sigma &= \sigma_1 + \sigma_2 + \cdots + \sigma_i + \cdots \end{aligned} \tag{2.33}$$

Thus, the relaxation response can be written as,

$$\sigma(t) = \sum_{\forall i} \sigma_i = \epsilon_o \sum_{\forall i} k_s^i e^{\frac{-k_s^i}{\eta_d^i}t} \tag{2.34}$$

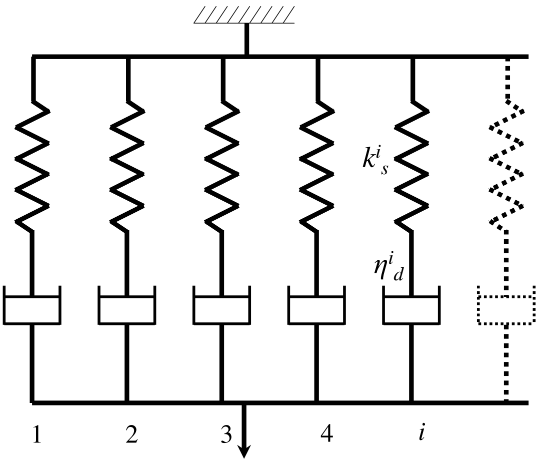

Figure 2.10: A generalized Maxwell model.

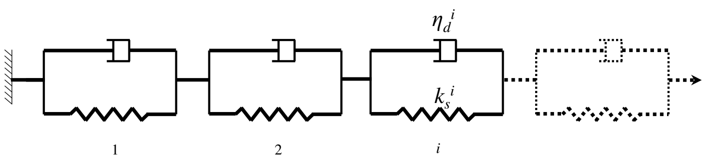

Figure 2.11: A generalized Kelvin model.

One can add various other components to the model, for example, if another spring is added in parallel, it is known as a Wiechert or Maxwell–Weichert model.

An example of a generalized Kelvin model is shown in Figure 2.11[1]. For this model, for a creep case, one can write,

$$\begin{aligned} \sigma_1 &= \sigma_2 = \cdots = \sigma_i = \cdots = \sigma_o \\ \epsilon &= \epsilon_1 + \epsilon_2 + \cdots + \epsilon_i + \cdots \end{aligned} \tag{2.35}$$

[1] Variants are possible and one can add various other components

Thus, the creep response can be written as,

$$\epsilon(t) = \sum_{\forall i} \epsilon_i = \sigma_o \sum_{\forall i} \frac{1}{k_s^i} \left(1 - e^{-\frac{k_s^i}{\eta_d^i} t} \right) \tag{2.36}$$

Other than the above examples of two-component, three-component and generalized models discussed, various other combinations of components are possible, and accordingly various models have been proposed (for example, the Burger model, the Huet model, the Huet–Sayegh model and so on). Researchers use various models to capture the time-dependent behavior of asphaltic material. One can refer to [55, 149] for example, for further study.

Linear viscoelasticity

A rheologic material can be called linearly viscoelastic, if the following two conditions are satisfied.

- Homogeneity: For a stress controlled experiment, double the strain is observed at a particular time, if double the original stress has been applied. Similarly, for a strain controlled experiment, double the stress is observed at a particular time, if double the original strain has been applied.
- Superposition: The response at a given time to a number of individual excitations applied at different times is the sum of the responses that would have occurred by each excitation acting alone at those respective timings.

The application of conditions of linear viscoelasticity gives rise to Boltzman's linear superposition principle. This is explained in the following.

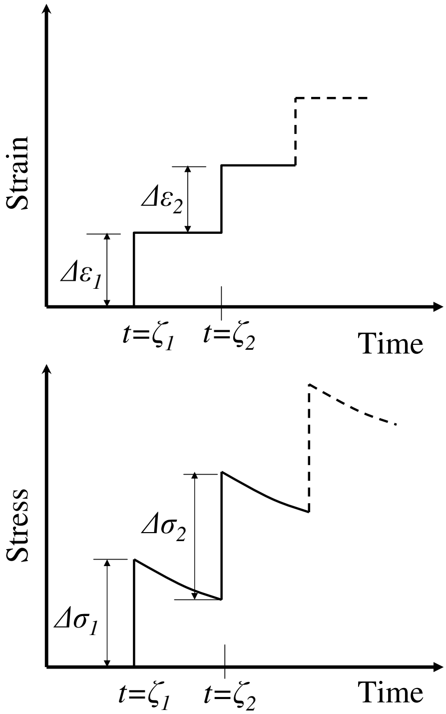

Figure 2.12: A strain-controlled thought experiment.

Figure 2.12 shows a strain controlled thought experiment on any rheologic material, like asphalt mix. In this experiment, an incremental strain of $\Delta\epsilon_1$ is applied at time $t = \zeta_1$, then, another incremental of strain $\Delta\epsilon_2$ is applied at time $t = \zeta_2$ and so on.

If these cause increments of stress by $\Delta\sigma_1$, at time $t = \zeta_1$ and then, $\Delta\sigma_2$ at $t = \zeta_2$ and so on, then, by using the above mentioned conditions of linear viscoelasticity, one can add for all these time steps to obtain,

$$\begin{aligned} \Delta\sigma_1 &= E_{rel}\left(t - \zeta_1\right)\Delta\epsilon_1 \\ \Delta\sigma_2 &= E_{rel}\left(t - \zeta_2\right)\Delta\epsilon_2 \end{aligned}$$

and so on.

Assuming that the initial stress level of the material was zero (that is, $\sigma|_{t=-\infty} = 0$) in this experiment, one can write,

$$\sigma(t) = \sigma|_{t=-\infty} + \sum_{\forall i} E_{rel}(t - \zeta_i)\Delta\epsilon_i \tag{2.37}$$

Thus, if a varying strain is applied to a rheologic material, it can be discretized into small time steps, and the above formulation (Equation 2.37) can be used to obtain the stress at a time t. In a similar manner, for a stress controlled experiment, one can derive,

$$\epsilon(t) = \epsilon|_{t=-\infty} + \sum_{\forall i} C_{crp}(t - \zeta_i)\Delta\sigma_i \tag{2.38}$$

For a continuous domain, these equations can be equivalently written as,

$$\sigma(t) = \int_{-\infty}^{t} E_{rel}(t - \zeta)\frac{d\epsilon(\zeta)}{d\zeta}d\zeta \quad \text{(for a strain controlled case)} \tag{2.39}$$

$$\epsilon(t) = \int_{-\infty}^{t} C_{crp}(t - \zeta)\frac{d\sigma(\zeta)}{d\zeta}d\zeta \quad \text{(for a stress controlled case)} \tag{2.40}$$

This is known as Boltzman's superposition principle for linear viscoelastic material. By taking the Laplace transform to Equations 2.39 and 2.40 one obtains [84],

$$\overline{\sigma}(s) = s\overline{E_{rel}}(s)\overline{\epsilon}(s) \tag{2.41}$$

$$\overline{\epsilon}(s) = s\overline{C_{crp}}(s)\overline{\sigma}(s) \tag{2.42}$$

where, $\overline{\sigma}(s)$, $\overline{\epsilon}(s)$, $\overline{E_{rel}}(s)$, $\overline{C_{crp}}(s)$ are the stress, strain, relaxation modulus and creep modulus in the Laplacian domain. From Equations 2.41 and 2.42 one can write,

$$\overline{C_{crp}}(s)\ \overline{E_{rel}}(s) = \frac{1}{s^2} \tag{2.43}$$

It is interesting to note that in general $E_{rel} \neq \frac{1}{C_{crp}}$ (except for some special situations), but, C_{crp} and E_{rel}, for linearly viscoelastic material maintains the above (given by, Equation 2.43) relationship in the Laplacian domain.

Equation 2.43 provides a link between the moduli value obtained from creep and relaxation tests for linear viscoelastic material. For a gluon expression for the creep response, it may be possible to find out the expression for the relaxation response, without using the component structure of the model. Some illustrative problems are presented below. One may refer to, for example, [84, 161, 203] for further studies on the concepts of linear viscoelasticity and various inter-relationships that may exist among the parameters.

Example problem

A stress of magnitude σ_o is applied at $t = \zeta_1$ on a rheologic material (which was initially stress-free) given as Equation 2.15, then withdrawn at $t = \zeta_2$ (refer to Figure 2.13). Predict the strain response.

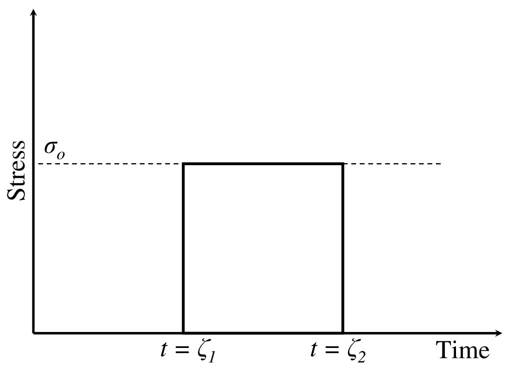

Figure 2.13: A stress of magnitude σ_o applied at $t = \zeta_1$ on a rheologic material, then withdrawn at $t = \zeta_2$.

Solution

Equation 2.15 represents a Kelvin–Voigt model, whose creep response is given by Equation 2.16. From Equation 2.16 one can write,

$$C_{crp} = \frac{1}{k_s}\left(1 - e^{-\frac{k_s t}{\eta_d}}\right) \tag{2.44}$$

Using Equation 2.38, one can write,

$$\epsilon(t) = \frac{\sigma_o}{k_s}\left(1 - e^{-\frac{k_s(t-\zeta_1)}{\eta_d}}\right) \quad \text{for } \zeta_2 < t < \zeta_1 \tag{2.45}$$

$$\epsilon(t) = \frac{\sigma_o}{k_s}\left(e^{-\frac{k_s(t-\zeta_2)}{\eta_d}} - e^{-\frac{k_s(t-\zeta_1)}{\eta_d}}\right) \quad \text{for } t > \zeta_2 \tag{2.46}$$

The above strain response is shown schematically in Figure 2.14. Since the Kelvin–Voigt model has a spring and a dashpot connected in parallel (and no springs in series), the strain response does not show any (i) instantaneous deformation on the application of stress and (ii) instantaneous recovery on the withdrawal of stress (refer to Figure 2.14).

Example problem

A stress of magnitude σ_o is applied over a rheologic material (which was initially stress-free) over a period of ζ_1 as shown in Figure 2.15. If $C_{crp} = \left(\frac{t}{\eta_d} + \frac{1}{k_s}\right)$ for the material, estimate the strain at time t, for $t > \zeta_1$.

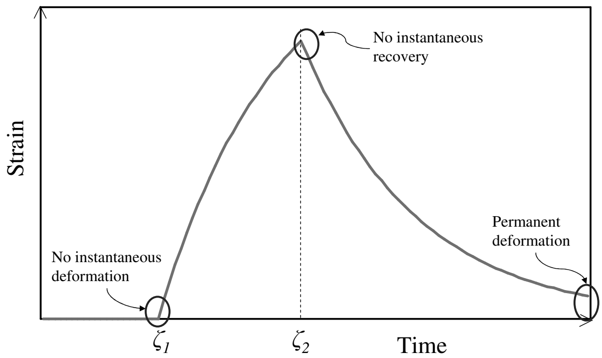

Figure 2.14: Strain response of Kelvin–Voigt model with a stress of magnitude σ_o applied at $t = \zeta_1$ and then withdrawn at $t = \zeta_2$.

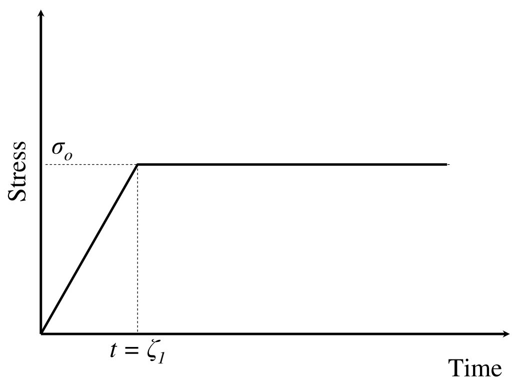

Figure 2.15: A stress of magnitude σ_o is applied linearly by $t = \zeta_1$ to a rheologic material.

Solution

The strain at time t (where, $t > \zeta_1$) is given as,

$$\epsilon_t\big|_{t>\zeta_1} = \int_0^{\zeta_1} \left(\frac{t-\zeta}{\eta_d} + \frac{1}{k_s}\right) \frac{\sigma_o}{\zeta_1} d\zeta + \int_{\zeta_1}^{t} \left(\frac{t-\zeta}{\eta_d} + \frac{1}{k_s}\right) 0 \, d\zeta$$
$$= \sigma_o \left(\frac{(t-\zeta_1/2)}{\eta_d} + \frac{1}{k_d}\right) \tag{2.47}$$

Example problem

Creep compliance of a rheological model is given as

$$C_{crp}(t) = \frac{t}{\eta_d} + \frac{1}{k_s}$$

Find an expression for the relaxation modulus ($E_{rel}(t)$).

Solution

After taking the Laplace transformation one obtains,

$$\overline{C_{crp}}(s) = \frac{1}{\eta_d s^2} + \frac{1}{k_s s}$$

Using Equation 2.43 one obtains,

$$\overline{E_{rel}}(s) = \frac{1}{s^2 C_{crp}(s)}$$
$$= \frac{k_s}{\frac{k_s}{\eta} + s}$$

By taking an inverse Laplace transform one obtains,

$$E_{rel}(t) = k_s e^{\frac{-k_s}{\eta} t}$$

Example problem

A load of $\sigma(t) = \sigma_o e^{i\omega_f t}$ is applied on a three component model (shown in Figure 2.8). The creep response of the model is given as Equation 2.20. Calculate the E^* using Boltzman's superposition principle. Assume $k'_s = k''_s = k_s$.

Solution

Considering Equation 2.20 and assuming $k'_s = k''_s = k_s$

$$\begin{aligned} C_{crp} &= \left(\frac{2}{k_s} \left(1 - e^{-\frac{k_s}{\eta_d} t} \right) + \frac{1}{k_s} e^{-\frac{k_s}{\eta_d} t} \right) \\ &= \frac{1}{k_s} \left(2 - e^{-\frac{k_s}{\eta_d} t} \right) \end{aligned} \tag{2.48}$$

From Equation 2.40, one can write,

$$\begin{aligned} \epsilon(t) &= \int_{-\infty}^{t} \frac{1}{k_s} \left(2 - e^{-\frac{k_s}{\eta_d}(t-\zeta)} \right) (i\omega_f \zeta) \sigma_o e^{i\omega_f \zeta} d\zeta \\ &= \frac{\sigma_o e^{i\omega_f t}}{k_s} \left(2 - \frac{1}{\frac{k_s}{\eta_d} + i\omega_f} \right) \\ &= \frac{\sigma(t)}{k_s} \frac{(2k_s + i\omega_f \eta_d)}{(k_s + i\omega_f \eta_d)} \end{aligned} \tag{2.49}$$

Or,

$$\frac{\sigma(t)}{\epsilon(t)} = \frac{k_s^2 + i\omega_f \eta_d k_s}{2k_s + i\omega_f \eta_d} = E^* \tag{2.50}$$

It may be noted that the above expression for E^* (that is, Equation 2.50) obtained using Boltzman's superposition principle is the same as Equation 2.28.

Time–temperature superposition

The response of an asphaltic material shows dependency on time as well as on temperature. For example, the variation of creep

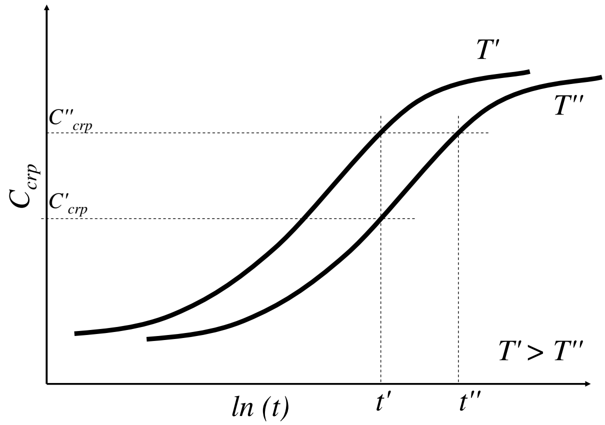

Figure 2.16: Schematic diagram illustrating the principle of time–temperature superposition.

compliance at different times and at two temperatures (say, T' and T'', where, $T' > T''$) has been plotted schematically in Figure 2.16. From Figure 2.16, it can be seen that at a given temperature, say at T'', the C_{crp} at time t' is lower than that of time t'', (i.e., $C'_{crp} < C''_{crp}$)—this is because, as time increases the strain keeps on increasing. Further, it can be seen that at a given time, say at t', the C_{crp} at temperature T'' is lower than that of temperature T' (i.e., $C'_{crp} < C''_{crp}$)—this is because, if the temperature is higher, the strain will be more at the same given time.

This behavior speaks for an equivalency that may exist between time and temperature, for example, the C_{crp} measured at time t'' at temperature T'' is equal to the C_{crp} measured at time t' at temperature T' (and its value is C''_{crp}, as shown in Figure 2.16). That means, one may perform a test at a specific temperature and time to obtain a rheological parameter for some other temperature and time. This forms the basis of time-temperature superposition.

Thus, a relationship between the two time scales can be proposed as,

$$t' = \frac{t''}{\alpha_T} \tag{2.51}$$

$$ln(t') = ln(t'') - ln(\alpha_T) \tag{2.52}$$

where, t' can be called the reduced time of t'' for shifting the test temperature from T'' to T', and α_T is called the time-temperature shift factor. Obviously, α_T is a function of these two temperatures, so one of them can be treated as a standard temperature. Material for which α_T value is not a dependent of time, can be called as a thermorheologically simple material.

Certain formulations are proposed for calculation of α_T for thermo-rheologically simple material. The following two formulae are typically used for asphalt mixes. The Williams–Landel-Ferry (WLF) equation is given as [308],

$$log_e(\alpha_T) = \frac{-C_1\left(T - T_{\text{ref}}\right)}{C_2 + \left(T - T_{\text{ref}}\right)} \tag{2.53}$$

where, $log_e(\alpha_T)$ is the natural logarithm of α_T, T_{ref} is the reference temperature, T is a temperature where α_T is being determined, and C_1 and C_2 are constants.

The Arrhenius Equation [85, 315] is given as,

$$log_e(\alpha_T) = \frac{\Delta H}{log_e(10)U}\left(\frac{1}{T} - \frac{1}{T_{\text{ref}}}\right) \tag{2.54}$$

where ΔH is the apparent activation energy, and U is the universal gas constant.

If rheological tests are conducted at various temperatures[2], it is possible (and, more easily for a thermo-rheologically simple materials) to develop the complete spectrum of rheologoical behavior of

[2]depending on the test convenience and available experimental facilities.

the material at any specified reference temperature (T_{ref}). This is known as the master curve. Further, for dynamic testing it is possible to establish equivalency with the frequency of loading (w_f) to time (for tests with static loading conditions) or temperature. One can, for example, refer to [149, 203, 219, 245, 291] on the (i) development of a master curve, (ii) interconversion between time, temperature, frequency, and (iii) techniques to obtain the curve fit parameters.

Discussions

Simple rheological models have been presented and some of these are used as descriptors of rheological behavior of asphalt mix [316, 321]. However, asphalt mix, as well as asphalt binder, show a more complex behavior in terms of their dependency on time, temperature, and stress state. Further, asphalt mix is an anisotropic [292] and heterogeneous [10] material. Researchers have been trying to develop various models to capture the response and damage mechanism of this complex material [17, 71, 76, 150, 157, 192, 242]. Interested readers may refer to [149, 156] for a review and further study on rheological modeling of asphalt mix (and asphalt binder).

2.3.2 Fatigue characterization

Bound materials (like asphalt mix) undergo fatigue damage due to repetitive application of load. In the laboratory, the loading may be applied in a stress or strain controlled manner on samples of various geometries. The repetitive loading may be flexural, axial, or torsional in nature; however, flexural fatigue loading is generally used for pavement engineering applications. Loading can be simple (where stress or strain amplitude level is maintained constant) or compound (where stress or strain amplitude level is varied during the course of testing) in nature.

Figure 2.17 shows typical fatigue characteristics of bound materials due to simple flexural fatigue loading. The fatigue life is

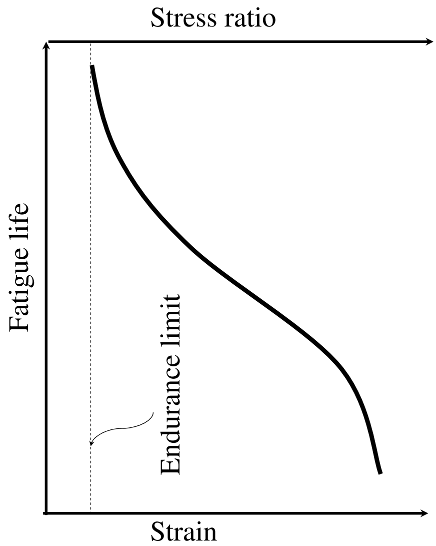

Figure 2.17: Schematic diagram showing a possible fatigue behavior of bound materials in simple flexural fatigue testing.

generally expressed as the number of repetitions at which the elastic modulus reaches a predefined fraction of the original elastic modulus value [2, 176]. The stress ratio is defined as the ratio between the applied stress amplitude (for constant stress amplitude testing) and the flexural strength (known as the modulus of rupture) of the bound material. From Figure 2.17 it can be seen that if the strain (or stress ratio) level is high, the fatigue life is expected to be low and vice versa. Typically, strain is used as a parameter for fatigue characterization of asphalt material, and the stress ratio is used for cement concrete or cemented material. It has been observed that at a very low level of strain (or stress ratio), the sample does not fail due to such repetitive loading[3] and this is known as the endurance limit. This property later formed the basis of perpetual pavement design [209, 300].

[3]That is, the fatigue life virtually becomes infinity.

For compound fatigue loading, the following empirical relationship generally satisfies,

$$\sum_{\forall i} \frac{n_i}{N_i} \approx 1 \tag{2.55}$$

where, n_i = the number of repetitions applied at a given strain (or stress ratio) level, and N_i is the fatigue life of the material at that strain (or stress ratio) level. Equation 2.55 was originally developed based on experiments conducted on aluminum [200], and subsequently adopted in pavement engineering for characterizing the fatigue behavior of asphalt mix, cement concrete, and cemented material [67, 98, 124, 206, 217, 269, 281]. By using Equation 2.55 one assumes that fractional damages caused due to repetitions at various levels of strains (or stresses) are linearly accumulative [82].

A significantly large number of research studies is available on fatigue characterization of asphaltic material, covering the issues related to the mode/process of testing [2, 67, 191, 236, 269], factors affecting the fatigue behavior [70, 176, 236], variability in test results [67, 236, 269], fracture and damage modeling of asphalt mix [57, 95, 150, 235], stiffness reduction [2, 176], asphalt healing [118, 151], endurance limit [309] and so on. One can refer to articles, like [15, 156, 177] for an overview on the fatigue behavior of asphalt mix.

2.4 Cement concrete and cemented material

Cement concrete is made up of aggregates, cement, admixtures (if required) and water. Hydration of cement and the subsequent hardening contribute to the strength of the material. Cement concrete, in a hardened state, is characterized by its elastic modulus, compressive strength, tensile strength, bending strength (that is, modulus of rupture) etc. Empirical equations are suggested for the interrelationships between these physical properties [5, 207, 208].

An elastic modulus of cement concrete can be measured as a tangent modulus, a secant modulus or, dynamic modulus [207]. Fatigue performance of cement concrete is an important consideration in the concrete pavement design [1, 132, 206, 211, 217, 281, 285]. One can, for example, refer to textbooks such as [207, 208] etc. for a detailed study of the properties and characterization of cement concrete.

Cemented materials (generally locally available/marginal materials are utilized as the bound form) are bound material, hence these can be characterized in a manner similar to other bound material. Interested readers can refer to, for example [86, 106, 169, 217], for further study on the characterization of cemented material and its application in pavement construction.

2.5 Closure

This chapter has discussed the concept of "elastic modulus" (stiffness) of various materials used for road construction. The elastic moduli of materials are used as an essential input during pavement analyses discussed in subsequent chapters (Chapters 3 to 6). The issues related to time dependency (for asphaltic material) and stress dependency (for unbound granular material) of elastic modulus have been highlighted. Pavement layers undergo damage (for example, damage due to fatigue for bound materials, permanent deformation, etc.). Generally, such damages propagate with the load repetitions. The number of repetitions a pavement can sustain until failure is an important consideration in pavement design. This will be discussed further in Chapter 7. Considerable literature is available on the choice of Poisson's ratio value of pavement materials [1, 32, 141, 201, 207]; there are instances where the Poisson's ratio value is measured as more than 0.5 [178, 294]. It is generally considered that variation of Poisson's ratio values does not significantly affect the pavement analysis results [201].

This page intentionally left blank

Chapter 3

Load stress in concrete pavement

3.1 Introduction

Concrete pavements are often idealized as beams or plates on an elastic foundation. Numerous hypothetical springs placed at the bottom of the beam/plate represent the elastic foundation for such models. In this chapter, first the analysis of a beam resting on an elastic foundation is presented, followed by analysis of a thin plate resting on elastic foundation. Further, it is discussed how the plate theory can be utilized for analysis of an isolated concrete pavement slab (of finite dimension) resting on a base/sub-base.

3.2 Analysis of beam resting on elastic foundation

A beam is a one-dimensional member. A schematic diagram of a beam (of unit width) resting on numerous springs with spring constant k (known as Winkler's model, discussed later in

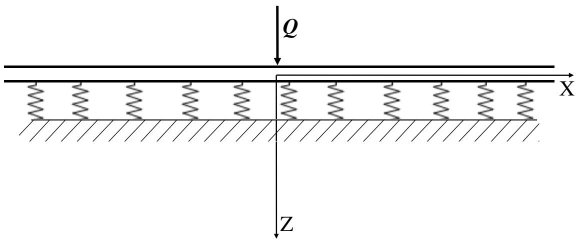

Figure 3.1: A beam resting on numerous springs is acted on by a concentrated load Q.

Section 3.2.1) subjected to a pointed loading Q at $x = 0$ is presented as Figure 3.1. The free-body diagram of a portion of the beam (other than the load application point) is shown in Figure 3.2. The moment (M) and shear force (V) are shown in the free-body diagram. The upward force of the spring on the element of length dx is $\omega k dx$, where ω is the displacement of the beam in the Z direction. From Figure 3.2, using the force equilibrium one can write,

$$V - (V + dV) + k\omega dx = 0 \tag{3.1}$$

Taking the moment equilibrium one obtains,

$$V = \frac{dM}{dx} \tag{3.2}$$

Putting Equation 3.2 in Equation 3.1 and considering that $EI\frac{d^2\omega}{dx^2} = -M$, (that is, for the Euler−Bernoulli beam) one obtains,

$$EI\frac{d^4\omega}{dx^4} - k\omega = 0 \tag{3.3}$$

where, EI is the flexural rigidity of the beam. This is a widely used basic expression for a beam resting on an elastic foundation

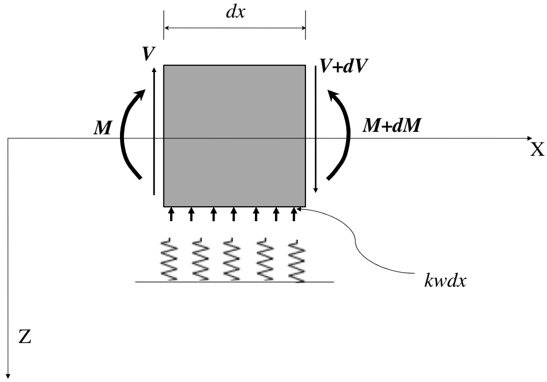

Figure 3.2: Free-body diagram of dx elemental length of the beam presented in Figure 3.1.

applied to foundation engineering [109, 136, 144, 247]. The general solution of Equation 3.3 is given as,

$$\omega = e^{\lambda x}\left(c_1 \cos \lambda x + c_2 \sin \lambda x\right) + e^{-\lambda x}\left(c_3 \cos \lambda x + c_4 \sin \lambda x\right) \quad (3.4)$$

where, $\lambda = \left(\frac{k}{4EI}\right)^{\frac{1}{4}}$, and c_1, c_2, c_3 and c_4 are constants. These constants can be determined from the boundary conditions pertaining to the specific geometry of the problem. Considering one side of the beam (for instance, the right side) with respect to the load application point of the infinite beam (as shown in Figure 3.1), one can write the following boundary conditions and subsequently derive the following results [109].

- $\lim_{x\to\infty} \omega = 0$. This condition leads to $c_1 = c_2 = 0$. Thus, the equation reduces to $\omega = e^{-\lambda x}\left(c_3 \cos \lambda x + c_4 \sin \lambda x\right)$
- Due to symmetry, $\frac{d\omega}{dx}\ |_{x\to 0} = 0$. This leads to $c_3 = c_4 = c$ (say)
- Total upward force generated by the springs must be equal

to the downward force Q applied, that is, $2\int_0^\infty k\omega\,dx = Q$. This leads to $c = \frac{Q\lambda}{2k}$

Hence, the expression for deflection of an infinite beam resting on an elastic foundation is obtained as,

$$\omega = \frac{Q\lambda}{2k}e^{-\lambda x}\left(\cos\lambda x + \sin\lambda x\right) \tag{3.5}$$

It may be noted that the developed equation (Equation 3.5) is valid only for the right side (i.e., $x \geq 0$) of the infinite beam. In a similar manner, an expression can be developed for the left side of the beam. Then, the first boundary condition changes as, $\lim_{x\to-\infty} = 0$; the other two conditions remain the same. From these boundary conditions, the constants are obtained as $c_3 = c_4 = 0$, and $c_1 = -c_2 = \frac{Q\lambda}{2k}$. The equation (for the left side of the infinite beam from $x = 0$) takes the form of,

$$\omega = \frac{Q\lambda}{2k}e^{\lambda x}\left(\cos\lambda x - \sin\lambda x\right) \tag{3.6}$$

Equations 3.5 or 3.6 can be utilized (by successive differentiation) to obtain the rotation, bending moment, and shear profile [109]. The maximum deflection is under the load and is obtained as,

$$\omega\text{max} = \frac{Q\lambda}{2k} \tag{3.7}$$

In case there is a uniformly distributed loading (instead of point loading) of q per unit length, the deflection can be obtained by integration.

For the loading diagram shown as in Figure 3.3, the deflection at AA' ($\omega_{AA'}$) can be obtained by using superposition of deflection calculated from Equations 3.5 and 3.6, and can be expressed as follows:

$$\begin{aligned}\omega_{AA'} = &\int_0^n \frac{q\lambda}{2k}e^{-\lambda x}\left(\cos\lambda x + \sin\lambda x\right)dx\\ &+\int_0^m \frac{q\lambda}{2k}e^{\lambda x}\left(\cos\lambda x - \sin\lambda x\right)dx\end{aligned} \tag{3.8}$$

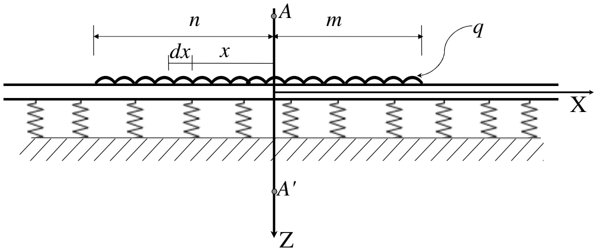

Figure 3.3: Analysis of an infinite beam with distributed loading.

If the section AA' is outside the loaded area (of length $n + m$), Equation 3.5 or 3.6 needs be used with appropriate integration limits. Further, the beam can be assumed as semi-infinite (that is, the beam has a definite ending at one side, and the other side is infinite), or finite (that, is the beam has a finite length). In such cases, an appropriate boundary condition can be used. Alternatively, one can solve it as a superposition of two infinite beams. One can refer to [109, 247], for example, for the details of the various approaches.

Such one dimensional analysis is useful, for example, for analysis of the problem of the dowel bar. Figure 3.4 illustrates how a single dowel bar can be idealized as a finite beam resting on an elastic foundation. However, additional considerations are involved in the dowel bar analysis problem (refer to Figure 3.4), for example, (i) there is a discontinuity of support in the middle portion, (ii) one side of the dowel bar is embedded in concrete but the other side is free to move horizontally, (iii) the wheel load does not directly act on the dowel bar, etc. Interested readers can refer to past works by Friberg [87, 88] and Bradbury [27] and a relatively recent study by Porter [223] on dowel bar analysis and the assumptions involved.

In line with the development of Equation 3.3, an equilibrium condition of a beam (refer to Equation 3.1) with an arbitrary loading

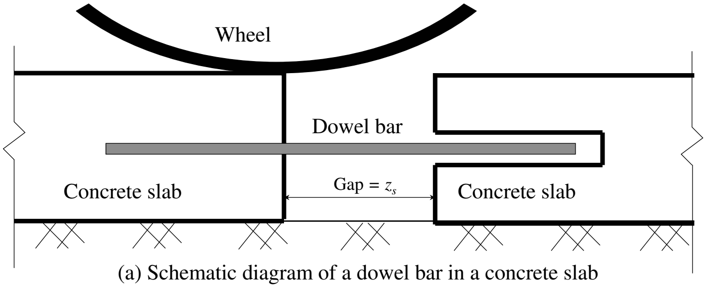

(a) Schematic diagram of a dowel bar in a concrete slab

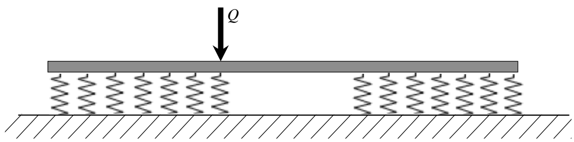

(b) Idealized representation of dowel bar

Figure 3.4: Idealization of a dowel bar for analysis.

(of q per unit length, which may include self-weight) and arbitrary foundation support (of p per unit length) condition (refer to Figure 3.5) can be written as:

$$\frac{dV}{dx} = p - q \tag{3.9}$$

Or,

$$EI\frac{d^4\omega}{dx^4} = q - p = q^* \tag{3.10}$$

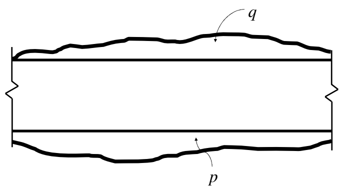

Figure 3.5: A beam with an arbitrary loading.

where, q^* is the net loading per unit length in the downward direction. Depending on the foundation support, the expression for p may become different. It may be noted that if $p = 0$, it becomes equivalent to the beam bending equation, without any spring support. Winkler, Pasternak, and Kerr are the examples of different types of supports, and are briefly discussed in the following.

3.2.1 Beam resting on a Winkler foundation

Unconnected (linear) springs are known as Winkler's springs [124, 142, 144, 182]. Formulation for a beam resting on a Winkler spring for a pointed loading was already discussed in the beginning of this section (Section 3.2). That is, for a Winkler spring, $p = k\omega$. Thus, a beam resting on a Winkler spring subjected to loading q (following Equation 3.3) can be represented as,

$$EI\frac{d^4\omega}{dx^4} = q - k\omega \tag{3.11}$$

The Winkler spring constant (k) used here in the formulation indicates the pressure needed on the spring system to cause unit displacement.[1] Its unit is therefore MPa/mm. As discussed in Section 2.2, the modulus of subgrade reaction (k) is also the pressure needed to cause unit deformation to the medium (that is, subgrade or sub-base or base layer). Thus, the spring constant used in the present formulation is conceptually equivalent to the modulus of subgrade reaction of the supporting layer.

One can refer to the paper written by Terzaghi [270] for a detailed discussion on the evaluation of the k value. Non-uniqueness of the modulus of the subgrade reaction in terms of the prediction of the (i) deflected shape (especially at the edges and corners of the slab) or (ii) stresses, is an issue raised by past researchers.

[1] The Winkler model is also known as the dense liquid model, and k represents the pressure needed to cause unit vertical displacement to a hypothetical floating body against buoyancy.

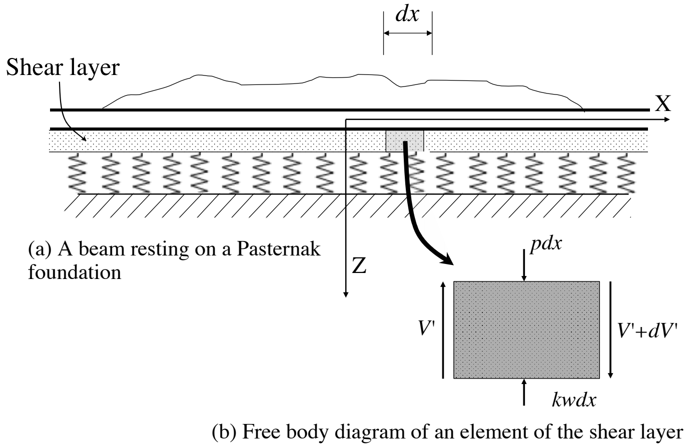

Figure 3.6: A beam resting on a Pasternak foundation and a free-body-diagram of the shear layer.

One can, for example, refer to [62, 117, 233] for discussions on the issues involved. This has prompted researchers in the past to develop multi-parameter models to capture the response of structures resting on soil. Some of these are discussed in the following.

Beam resting on a Pasternak foundation

In a Pasternak foundation, it is assumed that there is a hypothetical shear layer placed at the top of the spring system (refer to Figure 3.6(a)). Thus, considering the equilibrium of an element of length dx of shear layer (refer to Figure 3.6(b)), one can write,

$$pdx - V' + (V' + dV') - k\omega dx = 0$$

$$p = k\omega - \frac{dV'}{dx} \tag{3.12}$$

If the shear force developed within the shear layer is assumed to be proportional to the slope, then it can be written,

$$V' = G_s \frac{d\omega}{dx} \tag{3.13}$$

where G_s is the shear modulus of the foundation. Putting Equation 3.13 in Equation 3.12, one obtains,

$$p = k\omega - G_s \frac{d^2\omega}{dx^2} \tag{3.14}$$

Putting, Equation 3.14 in Equation 3.10 (i.e., the general equation for a beam resting on an elastic foundation) the equation for a one-dimensional beam resting on a Pasternak foundation becomes,

$$EI \frac{d^4\omega}{dx^4} - G_s \frac{d^2\omega}{dx^2} + k\omega = q \tag{3.15}$$

One can refer to, for example, [37] for the solutions for various problem geometries on a Pasternak foundation.

3.2.2 Beam resting on a Kerr foundation

The Kerr foundation model [144, 145] consists of two layers of Winkler springs (with spring constants k_1 and k_2, say) with a shear layer in between (refer to Figure 3.7(a)). The free-body diagram of an element of length dx of the shear layer in the Kerr foundation is shown in Figure 3.7(b). The pressures transmitted on the top and the bottom of the shear layer are shown as p_1 and p_2, and the displacements that the top and the bottom set of springs undergo are ω_1 and ω_2 respectively.

Considering the equilibrium of the shear layer,

$$\begin{aligned} p_1 - p_2 &= -\frac{dV'}{dx} \\ &= -G_s \frac{d\omega_2}{dx} \quad \text{(Similar to Equation 3.13)} \end{aligned} \tag{3.16}$$

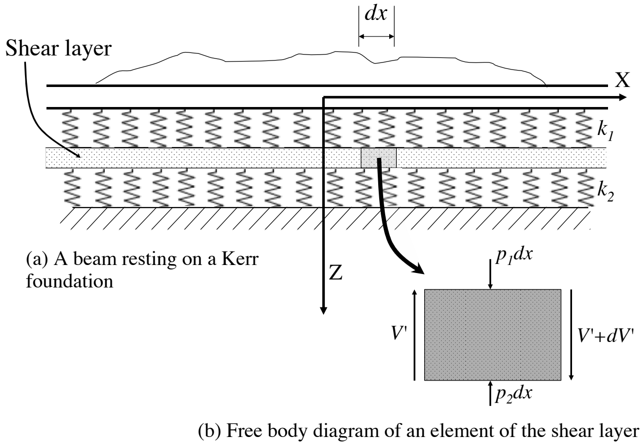

Figure 3.7: A beam resting on a Kerr foundation and a free-body diagram of the shear layer.

Further,

$$\omega = \omega_1 + \omega_2 \tag{3.17}$$

where, ω is the deflection of the beam. The spring conditions can be written as,

$$\begin{aligned} p_1 &= k_1\omega_1 \\ p_2 &= k_2\omega_2 \end{aligned}$$

Putting Equations 3.17 and 3.18 in Equation 3.16, one can write

$$\begin{aligned} p_1 &= k_2\omega_2 - G\frac{d^2\omega_2}{dx^2} \\ &= k_2\left(\omega - \frac{p_1}{k_1}\right) - G\frac{d^2}{dx^2}\left(\omega - \frac{p_1}{k_1}\right) \end{aligned} \tag{3.18}$$

Putting Equation 3.18 in Equation 3.10 (i.e., the general equation for a beam resting on an elastic foundation and considering that

$p = p_1$ in the present case) it can be written as,

$$\frac{G_s EI}{k_1}\frac{d^6\omega}{dx^6} - \left(1 + \frac{k_2}{k_1}\right) EI\frac{d^4\omega}{dx^4} + G_s\frac{d^2\omega}{dx^2} - k_2\omega = \frac{G}{k_1}\frac{d^2q}{dx^2} - \left(1 + \frac{k_2}{k_1}\right) q \tag{3.19}$$

3.2.3 Various other models

There is a large number of models of beams on elastic foundations (for example, the Filonenko–Borodich model, the Vlasov model, the Rhines model, the Reissner model, the Heténi model, etc., some of which are continuum models) and varieties of solution techniques proposed and studied by various researchers [73, 137, 237, 299]. Interested readers may refer to, for example, papers/reports such as [124, 142, 144, 153] for a review of various types of foundation models, or refer to the book by Selvadurai [247] for a detailed discussion.

If a beam resting on a Winkler spring is subjected to tensile axial force N, it can be shown (from the free-body diagram, in a similar manner the other equations are developed) [109],

$$EI\frac{d^4\omega}{dx^4} - N\frac{d^2\omega}{dx^2} + k\omega = q \tag{3.20}$$

It can be seen that the form of Equation 3.20 is similar to Equation 3.15 (hence the solution approach will be similar), even though these have been derived for two different types of problems.

Starting from the above approach, models can be further developed to represent a geotextile/geogrid placed within the shear layer [179, 181]. Other than the spring models (generally classified as "lumped parameter models"), continuum models are also used to represent subgrade support. This will be discussed in Chapter 5.

3.3 Analysis of a thin plate resting on an elastic foundation

Concrete slabs are generally idealized as thin plates resting on elastic foundations. In the following, the theory of thin plates resting on elastic foundations (a Winkler, Pasternak or Kerr foundation) has been presented. The principles and formulations of plate theories are widely used in practice and research. One can refer to, for example, [99, 134, 247, 276, 295] for detailed discussions. Here, the discussion on the theory of plate has been kept brief, and interested readers may refer to the above books, for instance, for further study.

The assumptions a for thin plate with a small deflection are as follows [99, 134, 153, 247, 276],

- The thickness of the plate (h) is small compared to its other dimensions.
- The deflection ω is small compared to the thickness of the plate.
- The middle plane does not get stretched due to the application of load.
- Plane sections perpendicular to the middle plane remain plane before and after bending.
- The plate can deform in only two ways; it can expand or contract axially, or it can bend with its cross section remaining a plane. Therefore, normal stresses along the transverse direction can be ignored i.e., $\sigma_{zz} = 0$.

3.3.1 Plate resting on a Winkler foundation

The thickness of the plate is h and its middle plane assumed to coincide with the X$-$Y plane, therefore z varies from $-\frac{h}{2}$ to $\frac{h}{2}$. The

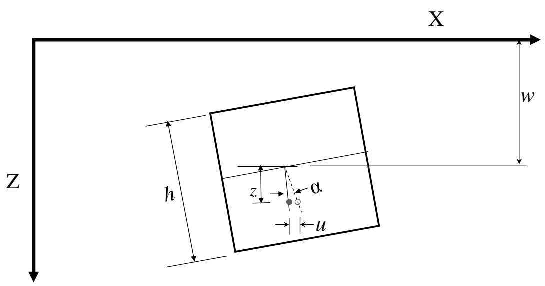

Figure 3.8: Deflected position of an element of a thin plate.

deflection of the plate is assumed as u and v in the directions of X and Y respectively. Figure 3.8 shows an element of the deflected plate and deflection is shown along the X direction only. From Figure 3.8, one can write,

$$\begin{aligned} u &= -z \sin \alpha \\ &\approx -z \tan \alpha \\ &\approx -z \frac{\delta \omega}{\delta x} \end{aligned} \tag{3.21}$$

Similarly, there will be deflection along the Y direction, hence

$$v \approx -z \frac{\delta \omega}{\delta y}$$

Using Equations 3.21 and 3.22 in Equation 1.18, one can write,

$$\begin{aligned} \epsilon_{xx} &= -z \frac{\delta^2 \omega}{\delta x^2} \\ \epsilon_{yy} &= -z \frac{\delta^2 \omega}{\delta y^2} \\ \gamma_{xy} &= -z \frac{\delta^2 \omega}{\delta x \delta y} \end{aligned} \tag{3.22}$$

Substituting the expressions in Equation 3.22 in Equation 1.30 (that is, for plane stress conditions), one obtains,

$$\begin{aligned}
\sigma_{xx} &= -\frac{Ez}{1-\mu^2}\left(\frac{\delta^2\omega}{\delta x^2}+\mu\frac{\delta^2\omega}{\delta y^2}\right) \\
\sigma_{yy} &= \frac{E}{1-\mu^2}\left(\epsilon_{yy}+\mu\epsilon_{xx}\right) = -\frac{Ez}{1-\mu^2}\left(\frac{\delta^2\omega}{\delta y^2}+\mu\frac{\delta^2\omega}{\delta x^2}\right) \\
\tau_{xy} &= \frac{E\gamma_{xy}}{2(1+\mu)} = -\frac{Ez}{2(1+\mu}\frac{\delta^2\omega}{\delta x\delta y)}
\end{aligned} \quad (3.23)$$

Using Equation 3.23, the moments are obtained as,

$$\begin{aligned}
M_{xx} &= \int_{-\frac{h}{2}}^{\frac{h}{2}} \sigma_{xx} z dz \\
&= -\frac{Eh^3}{12(1-\mu^2)}\left(\frac{\delta^2\omega}{\delta x^2}+\mu\frac{\delta^2\omega}{\delta y^2}\right) = -D\left[\frac{\delta^2\omega}{\delta x^2}+\mu\frac{\delta^2\omega}{\delta y^2}\right]
\end{aligned} \quad (3.24)$$

where, $D = \frac{Eh^3}{12(1-\mu^2)}$ is the flexural rigidity of a plate.

$$\begin{aligned}
M_{yy} &= \int_{-\frac{h}{2}}^{\frac{h}{2}} \sigma_{yy} z dz \\
&= -\frac{Eh^3}{12(1-\mu^2)}\left(\frac{\delta^2\omega}{\delta y^2}+\mu\frac{\delta^2\omega}{\delta x^2}\right) = -D\left[\frac{\delta^2\omega}{\delta y^2}+\mu\frac{\delta^2\omega}{\delta x^2}\right]
\end{aligned} \quad (3.25)$$

$$\begin{aligned}
M_{xy} &= \int_{-\frac{h}{2}}^{\frac{h}{2}} \sigma_{xy} z dz \\
&= \frac{Eh^3}{12(1+\mu)}\frac{\delta^2\omega}{\delta x\delta y} = D(1-\mu)\frac{\delta^2\omega}{\delta x\delta y}
\end{aligned} \quad (3.26)$$

Equations 3.24 to 3.26 are the widely used moment equations in thin plate theories. It may be recalled that in the present case the thin plate is assumed to be resting on an elastic foundation. Let the net vertical downward pressure be assumed as q^* per unit area (that is $q^* = q - p$, where q is the applied load per unit area), which may include the self-weight of the slab, and p is the foundation per unit area support, provided by the springs (for example, Winkler, Pasternak, Kerr, etc.) per unit area.

Figure 3.9 shows the various forces and moments acting on a small element ($dx \times dy$) of the plate. The assumed positive directions are also shown on the diagram. For the purpose of clarity, the diagram has been divided in three parts (a), (b), and (c). It may be noted that the moments and shear forces are acting per unit length, whereas q^* is acting per unit area. By taking vertical force equilibrium (refer Figure 3.9(a)), one obtains,

$$\frac{\delta V_{xx}}{\delta x}dxdy + \frac{\delta V_{yy}}{\delta y}dxdy + q^* dxdy = 0$$

$$\text{Or,} \quad \frac{\delta V_{xx}}{\delta x} + \frac{\delta V_{yy}}{\delta y} = -q^* \tag{3.27}$$

By taking moment along DC one obtains,

$$-\frac{\delta M_{yy}}{\delta y}dxdy + \frac{\delta M_{xy}}{\delta x}dxdy + V_{yy}dxdy - q^* dxdy\frac{dy}{2} - \frac{\delta V_{xx}}{dx}dxdy\frac{dy}{2} = 0 \tag{3.28}$$

Neglecting smaller order terms and rearranging,

$$\frac{\delta M_{xy}}{\delta x} - \frac{\delta M_{yy}}{\delta y} + V_{yy} = 0 \tag{3.29}$$

Similarly, by taking moment along BC one obtains,

$$\frac{\delta M_{xx}}{\delta x}dxdy + \frac{\delta M_{yx}}{\delta y}dxdy - V_{xx}dxdy - q^* dxdy\frac{dx}{2} - \frac{\delta V_{yy}}{dx}dxdy\frac{dx}{2} = 0 \tag{3.30}$$

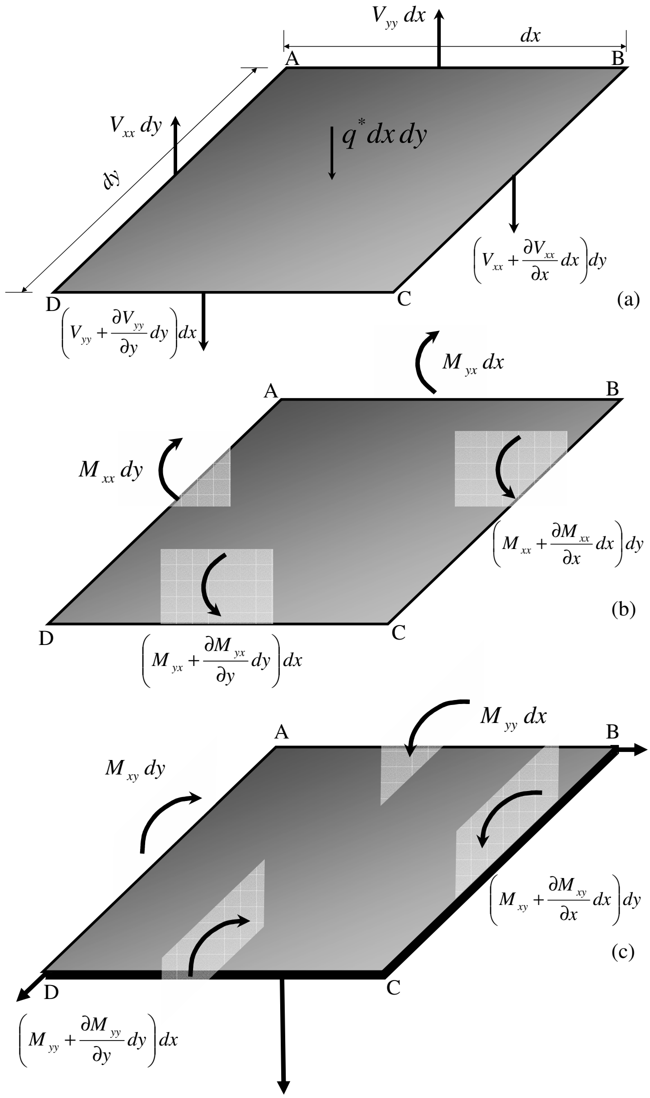

Figure 3.9: Free-body diagram of an element of a thin plate.

Similarly, neglecting smaller order terms and rearranging,

$$\frac{\delta M_{xx}}{\delta x} + \frac{\delta M_{yx}}{\delta y} - V_{xx} = 0 \tag{3.31}$$

Putting Equations 3.29 and 3.31 in Equation 3.27, one obtains [99, 134, 247, 276],

$$\frac{\delta^2 M_{yy}}{\delta y^2} - \frac{\delta^2 M_{xy}}{\delta x \delta y} + \frac{\delta^2 M_{xx}}{\delta x^2} + \frac{\delta^2 M_{yx}}{\delta x \delta y} + q^* = 0$$

$$\text{Or,} \quad \frac{\delta^2 M_{xx}}{\delta x^2} - 2\frac{\delta^2 M_{xy}}{\delta x \delta y} + \frac{\delta^2 M_{yy}}{\delta y^2} + q^* = 0 \tag{3.32}$$

since, $M_{xy} = -M_{yx}$

Now, putting expressions for M_{xx}, M_{yy} and M_{xy} from Equations 3.24, 3.25 and 3.26 respectively, one obtains [99, 134, 247, 276]

$$-D\frac{\delta^2}{\delta x^2}\left[\frac{\delta^2\omega}{\delta x^2} + \mu\frac{\delta^2\omega}{\delta y^2}\right] - 2D(1-\mu)\frac{\delta^4\omega}{\delta x^2 \delta y^2}$$
$$-D\frac{\delta^2}{\delta y^2}\left[\frac{\delta^2\omega}{\delta y^2} + \mu\frac{\delta^2\omega}{\delta x^2}\right] + q^* = 0$$

$$\text{Or,} \quad -D\left[\frac{\delta^4\omega}{\delta x^4} + 2\frac{\delta^4\omega}{\delta x^2\delta y^2} + \frac{\delta^4\omega}{\delta y^4}\right] + q^* = 0$$

$$\text{Or,} \quad D\nabla^4\omega = q^* \tag{3.33}$$

where, $\nabla^2 = \frac{\delta^2}{\delta x^2} + \frac{\delta^2}{\delta y^2}$

The Equation 3.33 is a well-known equation for a plate resting on spring foundation [99, 134, 247, 276, 295]. For the Winkler's foundation case, the equation can be rearranged as,

$$D\nabla^4\omega + k\omega = 0 \tag{3.34}$$

The equation can also be written as,

$$l^4\nabla^4\omega + \omega = 0 \tag{3.35}$$

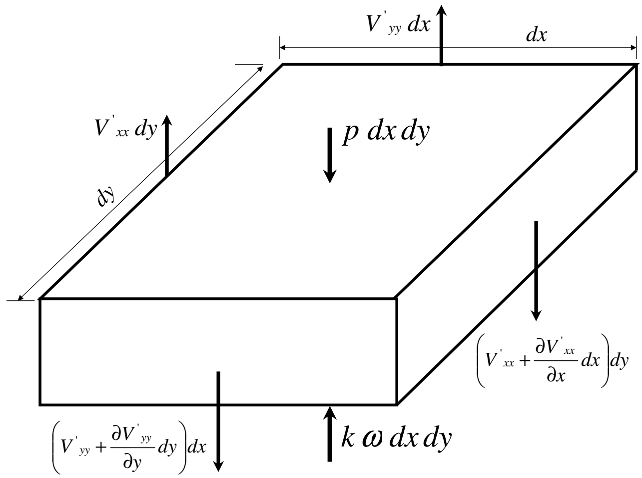

Figure 3.10: Free-body diagram of the shear layer of a two-dimensional Pasternak foundation.

where, $l = \frac{Eh^3}{12(1-\mu^2)k}$. l is known as the radius of relative stiffness [126, 304].

Further, the cases of plates resting on Pasternak and Kerr foundations are discussed briefly in the following sections. Proceeding in the similar manner in a cylindrical coordinate system one can also show that the Equation 3.33 holds, where, $\nabla^2 = \frac{\partial^2}{\partial r^2} + \frac{1}{r}\frac{\partial}{\partial r} + \frac{1}{r^2}\frac{\partial^2}{\partial \theta^2}$. One can, for example, refer to [134, 276] for the derivation.

3.3.2 Plate resting on a Pasternak foundation

The free-body diagram of the shear layer for a two-dimensional Pasternak foundation is shown in Figure 3.10. Considering the force equilibrium of the shear layer, one can write,

$$pdxdy + \frac{\partial V'_{xx}}{\partial x}dxdy + \frac{\partial V'_{yy}}{\partial y}dxdy - k\omega dxdy = 0 \qquad (3.36)$$

Assuming that a shear force developed in the shear layer is proportional to the slope (in a similar manner as done in Section 3.2.1), one can write,

$$V'_{xx} = G\frac{\partial \omega}{\partial x}, \quad \text{and} \quad V'_{yy} = G\frac{\partial \omega}{\partial y} \tag{3.37}$$

Thus, one can write,

$$p = k\omega - G\nabla^2\omega \tag{3.38}$$

Therefore, considering Equation 3.33, the governing equation for a plate resting on a Pasternak foundation becomes:

$$D\nabla^4\omega = q^* = q - p = \quad q - (k\omega - G\nabla^2\omega)$$

$$\text{Or,}\ \ D\nabla^4\omega - G\nabla^2\omega + k\omega = q \tag{3.39}$$

3.3.3 Plate resting on a Kerr foundation

Proceeding in a similar manner as presented in Section 3.2.2, for a two-dimensional case, one can obtain the governing equation for a Kerr foundation as,

$$\frac{GD}{k_1}\nabla^6\omega - \left(1 + \frac{k_2}{k_1}\right) D\nabla^4\omega + G\nabla^2\omega - k_2\omega = \frac{G}{k_1}\nabla^2 q - \left(1 + \frac{k_2}{k_1}\right) q \tag{3.40}$$

One can refer to the paper by Cauwelaert et al., [38] where a detailed development of the formulation for a Kerr foundation case has been provided.

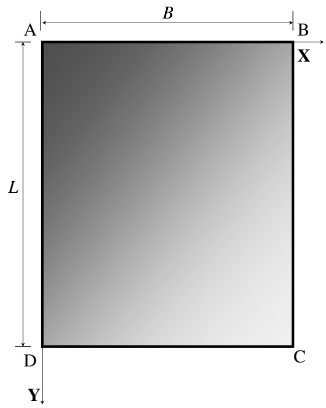

Figure 3.11: The slab boundaries may be free, fixed, or hinged.

3.3.4 Boundary conditions

Figure 3.11 shows a concrete pavement slab of dimension $L \times B$, idealized as a thin plate. For solving the plate equation (that is, Equation 3.33) suitable boundary conditions (of the individual four edges) need to be incorporated. The following boundary conditions are possible for any of the edges (say for the edge $y = L$) [134, 276]

- The edge $y = L$ may be fixed. Then, the deflection and the slope will be equal to zero. That is, $\omega \mid_{y=L}= 0$ and $\left(\frac{\delta\omega}{\delta y}\right) \mid_{y=L}= 0$
- The edge $y = L$ may be hinged. Then, the deflection and the moment along that direction will be equal to zero. That is, $\omega \mid_{y=L}= 0$ and $M_{yy} = 0$. The second condition implies, $-D\left(\frac{\delta^2\omega}{\delta y^2} + \mu\frac{\delta^2\omega}{\delta x^2}\right) \mid_{y=L}= 0$. Further, it may be noted that since there will be no deflection along $y = L$ line, $\left(\frac{\delta^2\omega}{\delta x^2}\right)_{y=L}$ will be equal to zero. This will finally result the second

condition as, $\frac{\delta^2\omega}{\delta y^2} \mid_{y=L} = 0$

- The edge $y = L$ may be free. In that case, moments will be zero. That is, $M_{yy} = 0$ and $M_{yx} = 0$.

However, for a concrete pavement the edges are not exactly free, fixed, or hinged. The presence of the dowel and tie bars (along the longitudinal and transverse direction respectively) makes the edge conditions somewhere in between. Although researchers have addressed such issues [171, 319], a simple situation with all the edges as free is taken up in the next section.

3.4 Load stress in a concrete pavement slab

If a concrete pavement slab can be idealized as a thin plate resting on a Winkler foundation, the solution of Equation 3.33 will provide an estimate of the stresses due to load. The dimension of the plate is assumed as $L \times B$ and all edges are considered as free. It is assumed that a uniform loading of magnitude q_o per unit area is acting on a rectangular area of dimension $l \times b$. The center of this area is located at $(\bar{x}, \bar{y})$. The arrangement is schematically presented in Figure 3.12.

Let a loading expressed in the form of Equation 3.41 be applied[2] to the plate [99, 134, 276]

$$q = q_o \sin\frac{m\pi x}{L} \sin\frac{n\pi y}{B} \tag{3.41}$$

where, m and n are any numbers.

Then, Equation 3.41 is a possible solution to Equation 3.33. The boundary conditions, as all edges are free (Refer to Section 3.3.4 for

[2]That is, the loading is assumed to be different than uniformly distributed loading on the rectangular area shown in Figure 3.12.

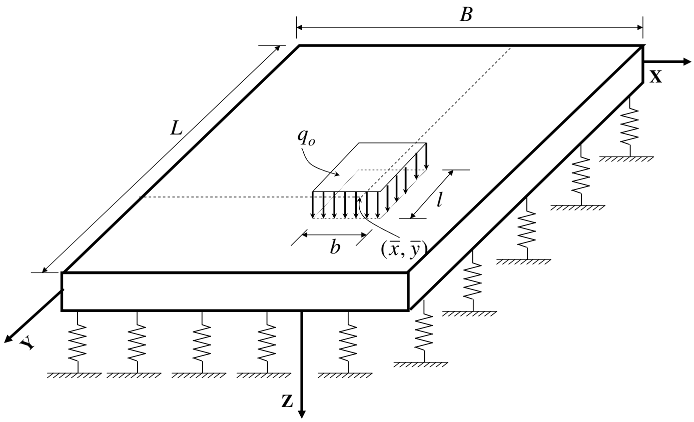

Figure 3.12: A slab resting on a Winkler spring acted upon by a rectangular patch loading.

a discussion on boundary conditions) are satisfied if ω is expressed as [99, 134, 276, 295],

$$\omega = c \sin \frac{m\pi x}{L} \sin \frac{n\pi y}{B} \tag{3.42}$$

where, c is a constant. The value of c can be obtained by putting Equations 3.41 and 3.42 in Equation 3.33, as [134, 276]

$$c = \frac{q_o}{\left(\pi^4 D \left(\frac{m^2}{L^2} + \frac{n^2}{B^2}\right)^2 + k\right)} \tag{3.43}$$

Thus, the expression for deflection ω becomes,

$$\omega = \frac{q_o}{\left(\pi^4 D \left(\frac{m^2}{L^2} + \frac{n^2}{B^2}\right)^2 + k\right)} \sin \frac{m\pi x}{L} \sin \frac{n\pi y}{B} \tag{3.44}$$

Equation 3.44 provides a solution for single sinusoidal loading (Equation 3.41). It is possible to express any loading function $q = f(x, y)$ (acting over a given area), as the sum of a series of sinusoidal loadings [99, 134, 276], as per Navier's transformation. That is,

$$\begin{aligned} q &= f(x, y) \\ &= \sum_{m=1}^{\infty} \sum_{n=1}^{\infty} c_{mn} \sin \frac{m\pi x}{L} \sin \frac{n\pi y}{B} \end{aligned} \tag{3.45}$$

where,

$$c_{mn} = \frac{4}{LB} \int_{\text{Area}} f(x, y) \sin \frac{m\pi x}{L} \sin \frac{n\pi y}{B} dxdy \tag{3.46}$$

The expression for ω in the present case, therefore, becomes [99, 134, 276],

$$\omega = \sum_{m=1}^{\infty} \sum_{n=1}^{\infty} \frac{c_{mn}}{\left(\pi^4 D \left(\frac{m^2}{L^2} + \frac{n^2}{B^2}\right)^2 + k\right)} \sin \frac{m\pi x}{L} \sin \frac{n\pi y}{B} \tag{3.47}$$

In the present case, the load is uniformly distributed over a rectangular area of $l \times b$, the center of which is located at $(\bar{x}, \bar{y})$. That is $q = f(x, y) = \frac{Q}{l\, b}$ within the region bound between $x = \bar{x} - \frac{b}{2}$ and $\bar{x} - \frac{b}{2}$ and $y = \bar{y} - \frac{l}{2}$ and $\bar{y} - \frac{l}{2}$ (refer to Figure 3.12). The value of c_{mn} is calculated as [99, 134, 276],

$$\begin{aligned} c_{mn} &= \frac{4Q}{LBlb} \int_{\bar{x}-\frac{b}{2}}^{\bar{x}+\frac{b}{2}} \int_{\bar{y}-\frac{l}{2}}^{\bar{y}+\frac{l}{2}} \sin \frac{m\pi x}{L} \sin \frac{n\pi y}{B} dxdy \\ &= \frac{16Q}{\pi^2 LBlbmn} \sin \frac{m\pi \bar{x}}{L} \sin \frac{n\pi \bar{y}}{B} \sin \frac{m\pi l}{2L} \sin \frac{n\pi b}{2B} \end{aligned} \tag{3.48}$$

The expression for ω is therefore [99, 134, 276],

$$\omega = \frac{16Q}{\pi^2 LBlb} \sum_{m=1}^{\infty} \sum_{n=1}^{\infty} \frac{1}{mn\left(\pi^4 D\left(\frac{m^2}{a^2}+\frac{n^2}{b^2}\right)^2 + k\right)} \sin\frac{m\pi\bar{x}}{L}$$
$$\sin\frac{n\pi\bar{y}}{B} \sin\frac{m\pi l}{2L} \sin\frac{n\pi b}{2B} \sin\frac{m\pi x}{L} \sin\frac{n\pi y}{B} \tag{3.49}$$

Once the expression for ω is obtained (from Equation 3.49), it can be used to find the bending moment (refer to Equations 3.24, 3.25 and 3.26) or the bending stress (refer to Equation 3.23). This is one of the possible approaches for obtaining the solution of Equation 3.33, and one may refer to, for example, [247, 276, 295] for alternative approaches and numerical methods of solution.

Figure 3.13 presents a schematic diagram showing the variation of maximum bending stress with slab thickness (h) and a modulus of subgrade reaction (k) (these terms appear in the expressions of D and q^* respectively in Equation 3.33). It may be noted that the maximum bending stress will always occur below the wheels. Figure 3.13 shows that the maximum bending stress (at the interior) decreases with (i) the increase in the slab thickness and/or (ii) the increase in the modulus of the subgrade reaction.

In the above formulation the springs can take tension as well; however, in reality underlaying layer does not pull back the concrete slab when it tries to bend upward. Thus tension, if it arises in the analysis, should be made equal to zero; yet, the portion (in which tension would arise) is not known *a priori*. Thus, the solution needs to be obtained iteratively, and achieving a closed-form solution may become difficult.

Further, it is assumed that the rectangular loaded area approximately represents the tire imprint. However, actual tire imprint may not necessarily be rectangular in shape, nor be uniform in loading (refer to Figure 5.7).

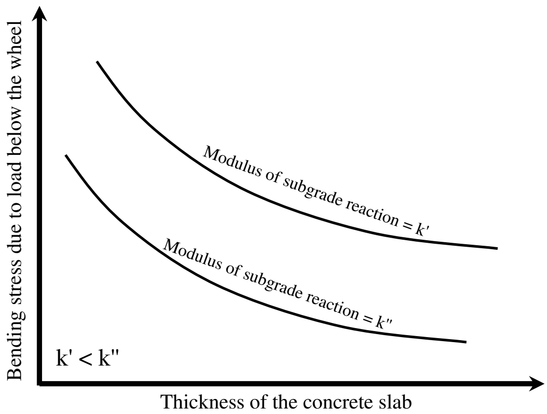

Figure 3.13: Schematic diagram showing variation of bending stress (due to load at interior) with slab thickness and modulus of subgrade reaction.

3.5 Closure

Individual solutions have been obtained for edge, interior, and corner loading, and varied boundary and loading conditions using the basic Equation 3.33. Pioneering works were done by Westergaard through his publications ranging from 1923 to 1946 [303, 304, 305, 306]. Interested readers can refer to [124, 129] for the background and historical details on the analysis of concrete pavements.

Researchers have provided solutions for thick and thin plates with various foundations; for example, a thick plate resting on a Pasternak foundation [254, 255], a thick plate resting on a Winkler foundation [92], a thin plate resting on a Kerr foundation [38], and various other boundary and foundation conditions [126, 147].

A number of softwares/algorithms have been developed which can perform analyses of concrete pavements, for example [49, 64, 120, 121, 124, 132, 211, 266]. Formulas and analysis charts/tables are also available in books/codes/guidelines for the estimation of load stress in concrete pavements for various given loading configurations, base/sub-base strength, and trial slab thickness [1, 132, 206, 211, 279, 281].

Chapter 4

Temperature stress in concrete pavement

4.1 Introduction

A pavement can be considered thermally stress-free at a given temperature (in fact, it is not a single value of a temperature, but a thermal profile, as discussed later in Section 4.3). Any temperature other than the zero-stress temperature will induce thermal strains to the pavement. If the pavement is free to move, no thermal stress will be generated. But restraint (full or partial) provided by the self-weight of the concrete slab, and/or the friction between the concrete slab and the underlying layer may prevent free movement of the slab, and hence thermal stress will be generated. These issues are covered in this chapter.

4.2 Thermal profile

The top surface of the pavement and the layers below do not have the same temperature. Thus, a thermal gradient exists across the pavement thickness. The top surface of the pavement is ex-

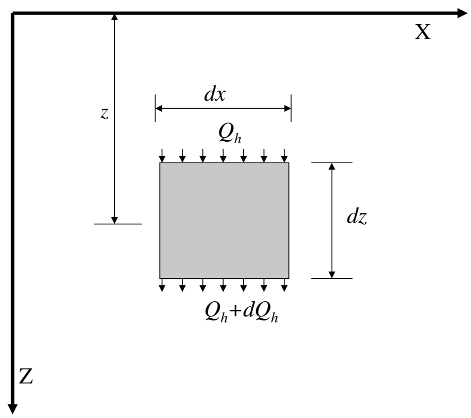

Figure 4.1: Schematic diagram showing one-dimensional steady-state heat flow across a medium.

posed to the weather conditions. Hence, the pavement surface temperature undergoes variations with the variation of the weather conditions. The angle of incidence of sun-rays, sky cover, wind speed, humidity, rain, etc. affect the pavement surface temperature [100, 108, 139, 301]. In the following, a one dimensional formulation has been presented for estimation of the thermal profile across the depth of the pavement under steady-state condition.

Consider an element[1] of unit thickness on the X−Z plane, as shown in Figure 4.1. The diagram shows that under a steady state condition, heat of Q_h per unit area is entering the element and heat of $Q_h + dQ_h$ per unit area is leaving the element due to temperature difference of dT between the thickness of the element dz. Thus, the heat balance equation can be written as,

$$Q_h dxdt - (Q_h + dQ_h)dxdt = dx\, dz\, \rho\, C^h\, dT \tag{4.1}$$

where, ρ is the density of material and C^h is the heat capacity. Thus,

$$-\frac{dQ_h}{dz} = \rho C^h \frac{dT}{dt} \tag{4.2}$$

[1] Homogenous, isotropic, and constant thermal properties.

As per Fourier's law of heat conduction, one can write,

$$Q_h = -k^{td}\rho C^h \frac{dT}{dz} \tag{4.3}$$

where, k^{td} is the coefficient of thermal diffusivity. Putting Equation 4.3 in Equation 4.2, one obtains,

$$k^{td}\frac{d^2T}{dz^2} = \frac{dT}{dt} \tag{4.4}$$

The solution of Equation 4.4 provides the thermal profile of the material, $T(z)$ across its depth. Since the present formulation is one dimensional, at a given value of z, the $T(z)$ value would remain the same for any (x, y). Given that the typical dimension of a pavement $(L \times B)$ is considerably large with respect to its height (h), this may be a reasonable assumption. Past studies (theoretical as well as experimental) suggest that the thermal profile $(T(z))$ in a concrete slab is generally nonlinear for most of the time during the day and night [16, 49, 50, 168, 180, 238, 320].

For a multi-layered structure, the Equation 4.4 can be presented as [302],

$$k_i^{td}\frac{d^2T_i}{dz^2} = \frac{dT_i}{dt} \tag{4.5}$$

where, k_i^{td} presents the thermal diffusivity of the ith layer, and T_i represents the thermal profile of the ith layer. Equation 4.5 can be solved using appropriate boundary conditions. These are discussed in the following.

4.2.1 Surface boundary conditions

The ambient air temperature adjacent to the pavement may be assumed to be varying in a sinusoidal pattern with 24 hours as the cycle length. Accordingly, the pavement surface temperature also may be assumed to vary in a sinusoidal pattern [139, 168]. Thus, the surface boundary condition can be written as,

$$T_1^{\text{top}} = T_a + T_f sin\omega_f t \tag{4.6}$$

where, T_a is the mean pavement temperature, T_f is the amplitude of the temperature variation, and ω_f is the frequency. Alternatively, the pavement surface temperature can be modeled [100] considering the exchange of heat between the pavement surface and the surrounding atmosphere through convection and radiation.

4.2.2 Interface condition

The temperatures at the interface should be the same. That is, the temperature at the bottom of the *i*th layer should be equal to the temperature at the top of the *i+1*th layer. That is, for an interface of *i*th and *i+1*th layers, it can be written as [168, 302],

$$T_i^{\text{bottom}} = T_{i+1}^{\text{top}} \tag{4.7}$$

Since at the interface, heat flow should be equal, one can write [100, 168, 302],

$$-k_i^{td}\rho_i C_i^h \frac{dT_i}{dz}\bigg|_{\text{bottom}} = -k_{i+1}^{td}\rho_{i+1}C_{i+1}^h \frac{dT_{i+1}}{dz}\bigg|_{\text{top}} \tag{4.8}$$

where, ρ_i, C_i^h and k_i^{td}, represent the density, heat capacity, and coefficient of the thermal diffusivity of the *i*th layer respectively.

4.2.3 Condition at infinite depth

The temperature at the bottom of the *n*th layer (which is a half-space) may be assumed as constant (say, T_∞) [168]. Thus,

$$T_n^{\text{bottom}} = T_\infty \tag{4.9}$$

The above boundary conditions can be used for obtaining the thermal profile in a layered pavement structure. One may, for example, refer to [168] for a closed formed solution for a three-layered structure.

4.3 Thermal stress in concrete pavement

As mentioned earlier (refer to Section 4.1) the resistance to movement (which evolves due to thermal variations) causes thermal stress. This resistance to movement may be provided by the weight of the concrete slab (when the slab is trying to bend upward), the underlying layer (when the slab is trying to bend downward) and friction between the slab and the underlying layer (when the slab is trying to move horizontally). If T_o is assumed as the temperature at which the pavement is stress-free, one can write,

$$\epsilon_{xx}^T = \epsilon_{yy}^T = -\alpha\left(T(z) - T_o\right) \tag{4.10}$$

where, α is the coefficient of thermal expansion. It is interesting to note that T_o may not necessarily be a uniform temperature, as assumed in Equation 4.10. In fact, experimental studies show that T_o rather assumes a non-uniform temperature distribution [184]. It may be noted that a negative sign has been used to indicate that this strain will generate compressive stress (with an assumption that $T(z) > T_o$ for any value of z), if restrained. The concept of the development of thermal stress has been schematically presented in Figure 4.2.

4.3.1 Thermal stress under a fully restrained condition

If the strain represented as Equation 4.10 is restrained, thermal stress will occur. The thermal stress (under a fully restrained

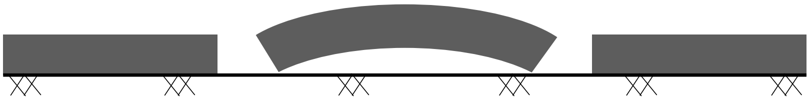

Figure 4.2: A one-dimensional schematic representation of development of thermal stress in concrete slab.

condition), therefore, can be written [232] as (refer to Equation 1.30 for the plane stress condition),

$$\sigma_{xx}^T = \tfrac{E}{1-\mu^2}\epsilon_{xx}^T + \mu\tfrac{E}{1-\mu^2}\epsilon_{yy}^T = -\frac{E\alpha\left(T(z)-T_o\right)}{1-\mu} \tag{4.11}$$

$$\sigma_{yy}^T = \tfrac{E}{1-\mu^2}\epsilon_{yy}^T + \mu\tfrac{E}{1-\mu^2}\epsilon_{xx}^T = -\frac{E\alpha\left(T(z)-T_o\right)}{1-\mu} \tag{4.12}$$

Thus, it can be seen that (with the current assumption that the thermal profile only varies along Z direction) the thermal stress $\sigma_{xx}^T = \sigma_{yy}^T = \sigma^T$ (say). The moment due to temperature stress can be calculated[2] as follows:

$$\begin{aligned} M_{xx}^T = M_{yy}^T &= -\int_{-h/2}^{h/2} \frac{E\alpha\left(T(z)-T_o\right)}{1-\mu} z dz \\ &= -\frac{E\alpha}{1-\mu}\int_{-h/2}^{h/2} T(z) z dz = M^T \quad \text{(say)} \end{aligned} \tag{4.13}$$

The thermal stress (Equation 4.11) can be broken up into three components as axial, bending, and nonlinear [49]. This analysis becomes useful because, due to the provisions of joints (where

[2]Assuming E and α are not affected by temperature, and hence can be taken outside the integration sign.

horizontal movement is allowed) the axial stress may get dissipated, and the design is governed by the bending and the remaining nonlinear components of stresses. For a given total thermal stress (σ^T_{xx} =σ^T_{yy} = σ^T) in a concrete pavement slab (under a fully restrained condition) due to the thermal profile ($T(z)$) (refer Equation 4.11), the following sections discuss the approach to obtain the axial (σ^{TA}), bending (σ^{TB}), and nonlinear component (σ^{TN}) of the stress [49, 127].

Axial stress component

One can assume an equivalent axial stress component (σ^{TA}), due to equivalent axial (uniform) temperature profile, as T^A. Equating the total thermal force (for the unit width of the slab) due to thermal profile $T(z)$ with that of T^A one obtains [49, 127, 320],

$$\int_{-h/2}^{h/2} \sigma^{TA} dz = \int_{-h/2}^{h/2} \sigma^{T} dz \tag{4.14}$$

Considering, $\sigma^{TA} = \frac{E\alpha}{(1-\mu)}(T^A - T_o)$ and $\sigma^T = \frac{E\alpha}{(1-\mu)}(T(z) - T_o)$ (refer to Equation 4.11), one obtains,

$$T^A = \frac{1}{h}\int_{-h/2}^{h/2} T(z)dz \tag{4.15}$$

Thus, the axial component of the thermal stress (σ^{TA}) is,

$$\begin{aligned}\sigma^{TA} &= -\frac{E\alpha}{1-\mu}(T^A - T_o)\\ &= -\frac{E\alpha}{1-\mu}\left(\frac{1}{h}\int_{-h/2}^{h/2} T(z)dz - T_o\right)\end{aligned} \tag{4.16}$$

Equation 4.16 provides an estimate for the axial component of thermal stress under a full restraint condition. If it is assumed that the frictional force provides resistance to the movement, one can write,

$$\sigma^{TA} = \rho g f L \tag{4.17}$$

where, ρ = density of concrete, f = coefficient of friction, L = length of concrete slab. However, it is argued that when the slab is trying to expand/contract, full frictional force may not be realized throughout the entire slab, especially near the central portion of the slab where the force developed may be lower than the maximum frictional resistance. Hence for design purposes, the stress may be reduced by some factor [187, 279, 313, 323].

Because of the provision of the expansion joints, the axial stress may get a scope for dissipation. However, the restraint provided by the layer underneath may be partial and the slab may manage to move partially (in that case stress will be lower than in the full restraint case). A formulation for a partial axial restraint has been dealt further in Section 4.3.2.

Bending stress component

One can assume an equivalent bending stress (σ^{TB}) due to an equivalent bending (linear) temperature profile, T^B. Equating the total moment due to thermal stress (for the unit width of the slab) due to thermal profile $T(z)$, with that of T^B one obtains [49, 127],

$$\int_{-h/2}^{h/2} \sigma^{TB} z dz = \int_{-h/2}^{h/2} \sigma^{T} z dz \qquad (4.18)$$

Considering, $\sigma^{TB} = \frac{E\alpha}{(1-\mu)}(T^B - T_o)$, $\sigma^T = \frac{E\alpha}{(1-\mu)}(T(z) - T_o)$ (refer to Equation 4.11), and $\frac{T^B - T_o}{z}$ is a constant parameter (because an equivalent linear profile is being considered here), one obtains,

$$T^B = T_o + \frac{12z}{h^3} \int_{-h/2}^{h/2} T(z) z dz \qquad (4.19)$$

Thus, the bending component of the thermal stress (σ^{TB}) is:

$$\sigma^{TB} \;\; = -\tfrac{E\alpha}{1-\mu}\left(T^B - T_o\right) \;\; = -\frac{12Ez\alpha}{(1-\mu)h^3} \int_{-h/2}^{h/2} T(z) dz \qquad (4.20)$$

The bending moment can be expressed as (refer to Equations 4.11, 3.24 and 3.25)

$$M_{xx}^{TB} = M_{yy}^{TB} = -\int_{-h/2}^{h/2} \frac{E\alpha\left(T^B - T_o\right)}{1-\mu} zdz$$
$$= -\frac{E\alpha}{1-\mu}\int_{-h/2}^{h/2} T^B zdz = M^{TB} \quad \text{(say)} \qquad (4.21)$$

Equation 4.20 is the expression for bending stress under full restraint conditions, due to the bending component of the thermal profile. The self-weight of the concrete slab provides this restraint. However the restraint provided by the self-weight may be partial, and the slab may manage to move partially (in that case the stress will be lower than in the full restraint case). A formulation for partial bending restraint will be dealt further in Section 4.3.2.

Nonlinear stress component

Since the thermal profile $T(z)$ may have an arbitrary shape, the axial (σ^{TA}) and bending stress (σ^{TB}) added together may not necessarily make up to the total stress. Thus, the nonlinear component of stress, σ^{TN} can be obtained by subtracting the sum of σ^{TA} and σ^{TB} from total stress σ^T. Thus [49, 127, 232],

$$\sigma^{TN} = \sigma^T - \left(\sigma^{TA} + \sigma^{TB}\right)$$
$$\text{Or,} = -\frac{E\alpha}{1-\mu}\left(T(z) - \frac{1}{h}\int_{-h/2}^{h/2} T(z)dz \frac{12z}{h^3}\int_{-h/2}^{h/2} T(z)zdz\right) \qquad (4.22)$$

The nonlinear component temperature T^N can be calculated as [127],

$$\left(T^N - T_o\right) = \left(T(z) - T_o\right) - \left(T^A - T_o\right) - \left(T^B - T_o\right) \qquad (4.23)$$
$$T^N = T_o + T(z) - \frac{1}{h}\int_{-h/2}^{h/2} T(z)dz - \frac{12z}{h^3}\int_{-h/2}^{h/2} T(z)zdz$$

Thus simple formulation for the calculation of T^A, T^B, T^N and corresponding σ^{TA}, σ^{TB} and σ^{TN} is presented for a single concrete layer under plane stress case. For further studies on two slabs with and without bonding one can refer to [127].

Example problem

The thermal profile of a concrete pavement slab is given as,

$$T(z) = \frac{T_t + T_b}{2} - \frac{T_t - T_b}{b} z \tag{4.24}$$

where T_t and T_b are the temperatures at the top and bottom of the concrete slab respectively. Estimate the axial (σ^{TA}) and bending (σ^{TB}) component of the thermal stress. Show that the nonlinear thermal stress (σ^{TN}) is nil in this case [232].

Solution

Incorporating $T(z)\left(= \frac{T_t+T_b}{2} - \frac{T_t-T_b}{b} z\right)$ in Equation 4.16, one obtains

$$\sigma^{TA} = -\tfrac{E\alpha}{1-\mu}\left(\tfrac{T_t+T_b}{2} - T_o\right) \tag{4.25}$$

Similarly, incorporating $T(z)$ in Equation 4.20, one obtains

$$\sigma^{TB} = \frac{E\alpha z}{h(1-\mu)}(T_t - T_b) \tag{4.26}$$

From Equation 4.11, the total stress is calculated as,

$$\sigma^T = -\frac{E\alpha}{1-\mu}\left(\frac{T_t + T_b}{2} - \frac{T_t - T_b}{h} z - T_o\right) \tag{4.27}$$

It can be seen, that for the present case

$$\sigma^T = \sigma^{TA} + \sigma^{TB}$$

That is, $\sigma^{TN} = 0$

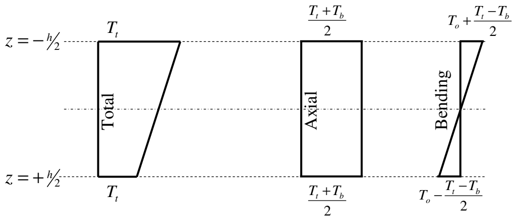

(a) Thermal profile and its components

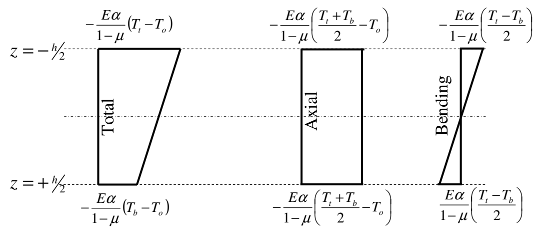

(b) Thermal stress and its components

Figure 4.3: The thermal profile and thermal stress components for the example problem (when $T_t > T_b$).

Discussions

From Equation 4.26, the bending stress at the top fiber of the slab is calculated as $\sigma^{TB}|_{z=-h/2} = -\frac{E\alpha(T_t-T_b)}{2(1-\mu)}$. This means that during daytime when $T_t > T_b$, the thermal stress (bending) is compressive (as per the sign convention adopted) at the top. This is what is expected. The thermal profile and the stress profile (for $T_t > T_b$) are shown in Figure 4.3. During the daytime, the top portion of the slab tries to expand more than the bottom portion. However, the self-weight of the slab restrains it from bending, causing compressive stress to develop at the top. Using the same logic it can be said that the stress will be tensile at the bottom portion (during daytime, when $T_t > T_b$). The formulation for bending stress for the linear thermal profile under fully restrained conditions (infinite slab) was originally derived by Westergaard [124, 168, 304].

If a finite slab is fully restrained, σ^{TB} will keep on increasing with the increase of $T_t - T_b$ (refer to Figure 4.4). If it is assumed that the

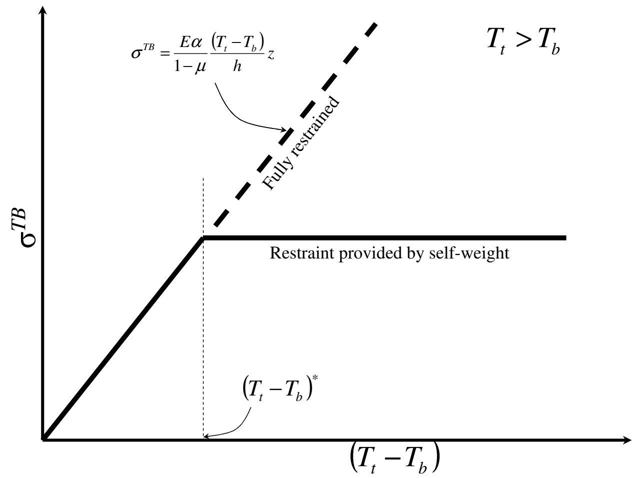

Figure 4.4: Schematic diagram showing variation σ^{TB} for $T_t > T_b$ when (i) fully restrained and (ii) finite restraint is provided by self-weight.

self-weight of the finite slab is acting as a restraint against bending, it can be argued that such a resistance may have a finite limit even if $T_t - T_b$ increases (say) in an unlimited manner. Therefore, if the $T_t - T_b$ increases beyond a certain threshold value, say $(T_t - T_b)^*$, the σ^{TB} should assume a fixed value beyond a specific level (refer to Figure 4.4). That means, the weight in this case only provides a partial restraint. A simple formulation considering the combined effect of bending due to temperature and weight is presented in Section 4.3.2.

4.3.2 Thermal stress under a partially restrained condition

The restraints cause hindrances to the free movement of the slab due to temperature change. The resistance provided by the restraints (against thermal movements) may have finite limits, hence

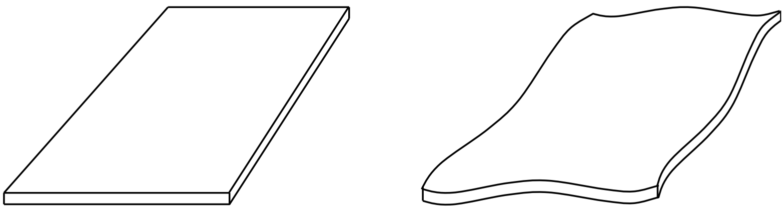

(a) Slab under fully restrained condition

(b) Slab under partially restrained condition

Figure 4.5: Shape of the slab under full and partial restraint conditions.

the slab may become partially restrained. Figure 4.5 shows a schematic diagram indicating the shapes of the concrete slab under full and partial[3] restraint conditions.

In the following, formulations for thermal stress due to partial restraint (for axial and bending) are discussed. The solutions converge to the full-restraint situation, if the movement of the slab is assumed to be zero, that is, $u = 0$ (for the axial restraint case) or $\omega = 0$ (for the bending restraint case).

Partial axial restraint

The axial restraint is provided by the layer underneath the concrete slab. A free-body diagram of an element of length dx and width B of the slab is shown in Figure 4.6, where τ_{zx} is the shear stress at the interface. From force equilibrium it can be

[3]One of the possible shapes.

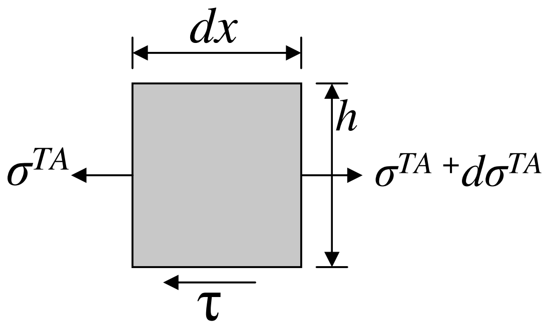

Figure 4.6: Free-body diagram of an element of length dx and width B of the slab.

written [44, 252, 273],

$$\tau_{zx} B dx = d\sigma^{TA} B h \tag{4.28}$$

where, dx is an elemental length, τ_{zx} = shear stress at the interface, B is the width of the concrete slab, and h is the height of the concrete slab. It is considered that the pavement is supported by spring sliders (of spring constant k_{ss}) as shown in Figure 4.7. Substituting,

$$\tau_{zx} = k_{ss} u \tag{4.29}$$

in Equation 4.28, it can be written as [44, 252],

$$\frac{d\sigma^{TA}}{dx} = \frac{k_{ss} u}{h} \tag{4.30}$$

It may be noted that the k_{ss} represents a condition similar to the horizontal spring constant of the underlying layer. Interested readers may refer to [270], for example, for discussions on the physical

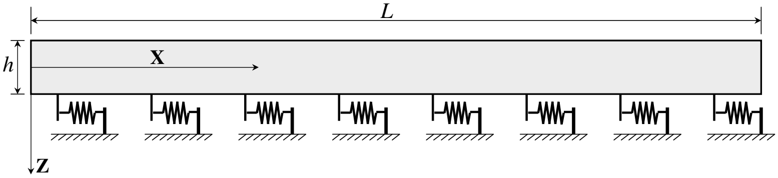

Figure 4.7: Slab resting on spring sliders.

interpretation and evaluation of this parameter. Since the thermal stress is generated from the restrained strain (partially restrained strain in the present case, because some displacement (u) is being allowed), one can write [187, 273],

$$\sigma^{TA} = E\left(\frac{du}{dx} - \alpha(T^A - T_o)\right) \tag{4.31}$$

Combining Equations 4.30 and 4.31, one obtains [44, 114],

$$\frac{d^2u}{dx^2} - \frac{k_{ss}}{hE}u = 0 \tag{4.32}$$

This equation can be solved to obtain the value of u and subsequently, the value of σ^{TA} can be obtained by using Equation 4.31.

Since the length of the slab is L, it can be assumed that $\sigma_{xx}|_{x=0} = 0$, and $u|_{x=L/2} = 0$. With these boundary conditions, the solution obtained by Timm et al. [273] can be presented as Equation 4.32,

$$u = \alpha\left(T^A - T_o\right)\frac{e^{-\xi(L-x)} - e^{-\xi x}}{\xi(1 + e^{-\xi L})} \tag{4.33}$$

$$\sigma_{xx} = E\alpha\left(T^A - T_o\right)\left[\frac{e^{-\xi(L-x)} + e^{-\xi x}}{1 + e^{-\xi L}} - 1\right] \tag{4.34}$$

for, $0 \leq x \leq L/2$ where, $\xi = \sqrt{\frac{k_{ss}}{Eh}}$

A schematic diagram showing variations of σ_{xx} and u for such a model are shown in Figure 4.8.

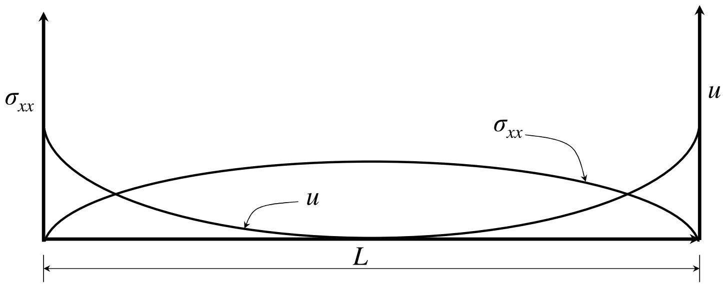

Figure 4.8: A schematic diagram representing the variation of σ_{xx} and u along the length of the slab for the partial restraint condition in the model shown in Figure 4.7.

Partial bending restraint

The self-weight of the slab (or any other external loading applied to the slab), the hypothetical springs (as a foundation) and the bending due to the temperature profile determine the final shape (hence the degree of restraint), and subsequently the overall stress in the pavement (refer to Figure 4.5(b)). The equivalent bending temperature (T^B) has been considered in the following formulation. It may be noted that one can use $T(z)$ as well (in that case, it will not represent pure bending). Considering Equations 4.10 and 3.22, one can write [168],

$$\begin{aligned}
\epsilon_{xx} &= -z\frac{\delta^2\omega}{\delta x^2} - \alpha\left(T^B - T_o\right) \\
\epsilon_{yy} &= -z\frac{\delta^2\omega}{\delta x^2} - \alpha\left(T^B - T_o\right) \qquad (4.35) \\
\epsilon_{zz} &= -z\frac{\delta^2\omega}{\delta x\delta y}
\end{aligned}$$

Referring to Equation 3.23, one obtains [127, 168, 295],

$$\begin{aligned}
\sigma_{xx} &= -\frac{Ez}{1-\mu^2}\left(\frac{\delta^2\omega}{\delta x^2}+\mu\frac{\delta^2\omega}{\delta y^2}\right)-\frac{E\alpha(T^B-T_o)}{1-\mu} \\
\sigma_{yy} &= -\frac{Ez}{1-\mu^2}\left(\frac{\delta^2\omega}{\delta y^2}+\mu\frac{\delta^2\omega}{\delta x^2}\right)-\frac{E\alpha(T^B-T_o)}{1-\mu} \\
\tau_{xy} &= \frac{E\gamma_{xy}}{1+\mu}=-\frac{Ez}{1+\mu}\frac{\delta^2\omega}{\delta x\delta y}
\end{aligned} \tag{4.36}$$

Considering Equations 3.24, 3.25 and 3.26 one can write [168, 254, 304],

$$\begin{aligned}
M_{xx} &= -D\left[\frac{\delta^2\omega}{\delta x^2}+\mu\frac{\delta^2\omega}{\delta y^2}\right]-\frac{E\alpha}{1-\mu}\int_{-h/2}^{h/2}\left(T^B-T_o\right)zdz \\
M_{yy} &= -D\left[\frac{\delta^2\omega}{\delta y^2}+\mu\frac{\delta^2\omega}{\delta x^2}\right]-\frac{E\alpha}{1-\mu}\int_{-h/2}^{h/2}\left(T^B-T_o\right)zdz \\
M_{xy} &= D(1-\mu)\frac{\delta^2\omega}{\delta x\delta y}
\end{aligned} \tag{4.37}$$

Putting Equation 4.37 in Equation 3.32, recalling Equation 4.21 and further simplification yields,

$$D\nabla^4\omega+\nabla^2M^{TB}=q^\star \tag{4.38}$$

where, $M^{TB} = \frac{E\alpha}{1-\mu}\int_{-h/2}^{h/2}\left(T^B-T_o\right)zdz = \frac{E\alpha}{1-\mu}\int_{-h/2}^{h/2}\left(T^B\right)zdz$ (that is, the same as Equation 4.21). It may be recalled that it has been assumed that T^B (so also, $T(z)$) varies only along Z direction, hence M^{TB} is only a function of z, hence $\nabla^2M^{TB}=0$. Hence, the equation takes the following form,

$$D\nabla^4\omega=q^\star$$

which is same as Equation 3.33. Thus, it is interesting to note that the thermal profile does not show up in the final equation; however, it participates in the solution when appropriate boundary conditions are invoked during solving the equation. That is, the moment expressions (refer to Equation 4.37) have thermal profile terms, and depending on the boundary condition (free, hinged, or fixed) these conditions participate in the solution process of the equation. One can refer to Section 3.3.4 to see how the boundary conditions are used with reference to the calculation of load stress in a plate.

The closed form solution of the above equation (for the partial restraint case) is, however, a complex task, although there are solutions available for various slab geometries [267]. This work (that is, work done by Tang et al. [267]) also provides derivations for the situation when the slab is curled up (that is with loss of contact) and the springs become ineffective for that region.

For slabs with finite dimensions, it was suggested that the deflected shape (ω) can be represented by the superposition of deflections of the slab when it is assumed to be finite in one direction and infinite along the other direction [124, 267, 304]. And subsequently, the proposed solutions for maximum stresses at the interior (at $B/2$, $L/2$) for linear thermal profile are,

$$\sigma_{xx} = \frac{E\alpha(T_t - T_b)}{2(1-\mu^2)}(C_x + \mu C_y) \tag{4.39}$$

$$\sigma_{yy} = \frac{E\alpha(T_t - T_b)}{2(1-\mu^2)}(C_y + \mu C_x) \tag{4.40}$$

where, C_x and C_y are two coefficients related to the shape of the slab [28, 124, 267, 304].

4.4 Closure

Simple formulations for the computation of thermal stress (for both partial and full restraint) of concrete pavement have been presented in this chapter. Formulas or charts for the estimation of thermal stress are available in various documents and guidelines [1, 126, 206, 279].

Chapter 5

Load stress in asphalt pavement

5.1 Introduction

It is in general assumed that asphalt pavement does not have any bending moment carrying capacity, unlike concrete pavement. Thus, the equilibrium equations which are developed to estimate stresses in asphalt pavements should not contain any bending moment term. In this chapter, first, the approach to analyze a single layer continuum (that is, a half-space) is presented. Subsequently, the approach is extended for a multi-layered case (with a smooth or rough interface), representing an idealized asphalt pavement structure.

5.2 General formulation

To formulate a problem (so as to obtain its mechanical response), one needs to have (i) the strain displacement relationship (hence strain compatibility conditions), (ii) the stress and strain relationship (that is the constitutive relationship), (iii) the equilibrium condition and the (iv) geometry (that is the boundary conditions) of the problem (refer to Section 1.2 for the background information). In the following an expression is developed as a combined form of the first three considerations. Finally, the boundary conditions will be used to analyze (as a typical boundary value problem) a half-space, and subsequently, it will be extended to solve for a multi-layered structure.

Let a plain strain condition (X$-$Z plane) in a Cartesian coordinate be assumed. The strains (ϵ_{xx}, ϵ_{zz} and γ_{xz}) can be expressed as Equation 1.31. Putting the above in a relevant strain compatibility equation (refer to the 3rd equation of the set of Equations 1.19), one obtains,

$$\frac{\partial^2}{\partial x \partial z}\left(\frac{2(1+\mu)}{E}\tau_{zx}\right) = \frac{\partial^2}{\partial x^2}\left(\frac{1-\mu^2}{E}\sigma_{zz} - \frac{\mu(1+\mu)}{E}\sigma_{xx}\right) + \frac{\partial^2}{\partial z^2}\left(\frac{1-\mu^2}{E}\sigma_{xx} - \frac{\mu(1+\mu)}{E}\sigma_{zz}\right) \tag{5.1}$$

Or,

$$2(1+\mu)\frac{\partial^2\tau_{zx}}{\partial x\partial z} = (1-\mu^2)\frac{\partial^2\sigma_{zz}}{\partial x^2} - \mu(1+\mu)\frac{\partial^2\sigma_{xx}}{\partial x^2} + (1-\mu^2)\frac{\partial^2\sigma_{xx}}{\partial z^2} - \mu(1+\mu)\frac{\partial^2\sigma_{zz}}{\partial z^2} \tag{5.2}$$

Now, the equilibrium equation (refer to Equation 1.33) for the present case (considering a plane strain along the X–Z plane) can be written as,

$$\frac{\partial\sigma_{xx}}{\partial x} + \frac{\partial\tau_{zx}}{\partial z} + BF_x = 0 \tag{5.3}$$

$$\frac{\partial\tau_{zx}}{\partial x} + \frac{\partial\sigma_{zz}}{\partial z} + BF_z = 0 \tag{5.4}$$

Differentiating Equation 5.3 with respect to x, and differentiating Equation 5.4 with respect to z, and adding, one obtains,

$$2\frac{\partial^2\tau_{zx}}{\partial z\partial x} = -\left(\frac{\partial^2\sigma_{xx}}{\partial x^2} + \frac{\partial^2\sigma_{zz}}{\partial z^2}\right) - \left(\frac{\partial BF_x}{\partial x} + \frac{\partial BF_z}{\partial z}\right) \tag{5.5}$$

Substituting $2\frac{\partial^2 \tau_{zx}}{\partial z \partial x}$ from Equation 5.5 to Equation 5.2 and simplifying further, one obtains,

$$\nabla^2 \left(\sigma_{xx} + \sigma_{zz}\right) = -\frac{1}{1-\mu}\left(\frac{\partial BF_x}{\partial x} + \frac{\partial BF_z}{\partial z}\right) \tag{5.6}$$

where, $\nabla^2 = \left(\frac{\partial^2}{\partial x^2} + \frac{\partial^2}{\partial z^2}\right)$

Proceeding in a similar manner for the plain stress condition (that is, using Equation 1.30 instead of Equation 1.31 and considering the X−Z coordinate system), one obtains,

$$\nabla^2 \left(\sigma_{xx} + \sigma_{zz}\right) = -(1+\mu)\left(\frac{\partial BF_x}{\partial x} + \frac{\partial BF_z}{\partial z}\right) \tag{5.7}$$

Equation 5.7 is also known as the stress compatibility equation. Now, if the body forces are assumed to be zero (if weight is the only body force considered then $BF_x = 0$, further, if the medium is also considered as weightless then $B_z = 0$), then the equation reduces to the form

$$\nabla^2 \left(\sigma_{xx} + \sigma_{zz}\right) = 0 \tag{5.8}$$

Assuming, ϕ is a function of x and z which can be expressed in the following form (so that it follows the equilibrium equation in two dimensions, without body-forces),

$$\begin{aligned} \sigma_{xx} &= \frac{\partial^2 \phi}{\partial z^2} \\ \sigma_{zz} &= \frac{\partial^2 \phi}{\partial x^2} \\ \tau_{xz} &= -\frac{\partial^2 \phi}{\partial x \partial z} \end{aligned} \tag{5.9}$$

Then by putting Equation 5.9, in Equation 5.8

$$\nabla^4 \phi = 0 \tag{5.10}$$

The function ϕ is known as Airy's stress function. For a cylindrical coordinate system and an axi-symmetrical case (that is, $\frac{\partial}{\partial \theta} = 0$ in the present case, refer to Section 1.2.3 for further discussions), the stresses in terms of differentiation of the ϕ function can be expressed as [174, 222, 277]

$$\sigma_{zz} = \frac{\partial}{\partial z}\left((2-\mu)\nabla^2\phi - \frac{\partial^2\phi}{\partial z^2}\right) \tag{5.11}$$

$$\sigma_{rr} = \frac{\partial}{\partial z}\left(\mu\nabla^2\phi - \frac{\partial^2\phi}{\partial r^2}\right) \tag{5.12}$$

$$\sigma_{\theta\theta} = \frac{\partial}{\partial z}\left(\mu\nabla^2\phi - \frac{1}{r}\frac{\partial\phi}{\partial r}\right) \tag{5.13}$$

$$\tau_{rz} = \frac{\partial}{\partial r}\left((1-\mu)\nabla^2\phi - \frac{\partial^2\phi}{\partial z^2}\right) \tag{5.14}$$

Further from Equations 1.20 and 1.26, and considering an axi-symmetric case,

$$\begin{aligned} \omega &= \frac{1+\mu}{E}\left[(1-2\mu)\nabla^2\phi + \frac{\partial^2\phi}{\partial r^2} + \frac{1}{r}\frac{\partial\phi}{\partial r}\right] \\ u &= -\frac{1+\mu}{E}\frac{\partial^2\phi}{\partial r\partial z} \end{aligned} \tag{5.15}$$

Proceeding in the similar manner, one obtains,

$$\nabla^4\phi = 0 \tag{5.16}$$

where, $\nabla^2 = \frac{\partial^2}{\partial r^2} + \frac{1}{r}\frac{\partial}{\partial r} + \frac{\partial^2}{\partial z^2}$.

The equation (Equation 5.10 or Equation 5.16) represents a combined form of strain compatibility, constitutive relationship (for plane strain or plane stress or axi-symmetric case), and the equilibrium condition. Interested readers can refer to, for example, Poulos and Davis [222] for the equations that arise for a 3-D linear elastic case.

The following steps are involved to obtain the stresses (and subsequently the strains and displacements) of such a continuum media.

- Obtain a suitable ϕ function which satisfies Equation 5.10 or Equation 5.16 depending on the choice of coordinate system.

- Obtain the constants of the ϕ function from the boundary conditions of a given problem.
- Obtain the stresses from Equation 5.9 or from Equation 5.11–5.14 depending on the choice of coordinate system.

The above approach can be used to solve for stresses in the continuum for various loading and geometries. This has been discussed further in the following.

5.3 Solution for elastic half-space

Figure 5.1 shows a point load of magnitude of Q that is acting vertically on an elastic half-space; the objective is to find out the stress-strain-displacement of any point (r, z) within the half-space. This problem is commonly known as Boussinesq's problem, and its solution is well known and widely used in the literature. One may refer to [142] for a discussion of the history and background of the Boussinesq's problem. The boundary conditions for this problem can be identified as follows:

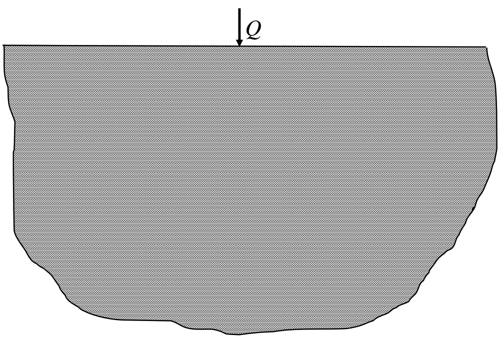

Figure 5.1: A point load acting vertically on a half-space.

1. At infinity all stresses should vanish. That is, as $z \to \infty$, $\sigma_{zz} = \sigma_{rr} = \sigma_{\theta\theta} = \tau_{rz} = 0$

2. Shear stress at the surface should be zero. That is, $\tau_{rz}|_{z=0} = 0$.

3. The σ_{zz} at the surface should be zero except at the point of the application of load. That is, $\sigma_{zz}|_{z=0} = 0$, except at the point of load application.

4. The sum of total force at any given horizontal plane within the half-space should be equal to Q. That is, $\int_A \sigma_{zz} dA = Q$, where A indicates area of the infinite horizontal plane.

To solve such a problem, first a suitable (biharmonic) ϕ function needs to be selected. The discussions in the following is the based on the solution presented in [140]. The following ϕ function is proposed [140] for the present case. It may be verified that the condition given by Equation 5.16 holds for this ϕ function.

$$\phi \quad = \quad C_1 z ln_e r + C_2(r^2 + z^2)^{1/2} + C_3 z ln_e \frac{(r^2 + z^2)^{1/2} - z}{(r^2 + z^2)^{1/2} + z} \tag{5.17}$$

From the above mentioned conditions, the constants are obtained as [140],

$$C_3 = -\frac{1 - 2\mu}{4\mu} C_2 \qquad C_2 = -\frac{\mu}{\pi} Q \qquad C_1 = -\frac{1 - 2\mu}{2\pi} Q$$

After evaluating the constants of the ϕ function, it can be used in Equation 5.11 to obtain the stresses. The widely used expressions for stresses (due to the vertical point load at the surface of an elastic half-space) can be presented as [63, 104, 140, 162],

$$\sigma_{zz} = \frac{3Q}{2\pi} \frac{z^3}{R^5} \tag{5.18}$$

$$\tau_{rz} = \frac{3Q}{2\pi} \frac{z^2 r}{R^5} \tag{5.19}$$

$$\sigma_{rr} = \frac{Q}{2\pi}\left(\frac{3zr^2}{R^5} - \frac{1-2\mu}{R(R+z)}\right) \tag{5.20}$$

$$\sigma_{\theta\theta} = \frac{Q}{2\pi}(1-2\mu)\left(\frac{1}{R(R+z)} - \frac{z}{R^3}\right) \tag{5.21}$$

where $R = (r^2 + z^2)^{1/2}$.

A brief solution to the Boussinesq's problem has been presented in the above. One can reach the same solution with any other ϕ function, provided it satisfies Equation 5.10 or Equation 5.16 (depending on the choice of coordinates) and the boundary conditions yield meaningful solutions to the unknown constants. One can, for example, refer to [247, 248, 310] for more information on alternative approaches.

Further, the vertical displacement can be derived in the following manner. The vertical strain (ϵ_z) in a cylindrical coordinate system is given as (refer to Equations 1.20 and 1.26)

$$\epsilon_{zz} = \frac{1}{E}\left(\sigma_z - \mu(\sigma_r + \sigma_\theta)\right) = \frac{\partial \omega}{\partial z} \tag{5.22}$$

Thus, displacement at any depth z (ω) is given as,

$$\omega = \frac{1}{E}\int_z^\infty \left(\sigma_{zz} - \mu(\sigma_{rr} + \sigma_{\theta\theta})\right) dz \tag{5.23}$$

Putting the expressions of σ_{zz}, σ_{rr} and $\sigma_{\theta\theta}$ from Equations 5.18, 5.20, and 5.21 (respectively), in Equation 5.23 and performing integration, one obtains the displacement due to point load Q,

$$\omega = \frac{Q(1+\mu)}{2\pi E}\left[\frac{z^2}{(r^2+z^2)^{3/2}} + \frac{2(1-\mu)}{(r^2+z^2)^{1/2}}\right] \tag{5.24}$$

In line with the problem of the point load on a half-space, there were similar such developments proposed by various researchers, for example, a line load acting vertically on the surface (by Flamant) of the half-space, the point load acting inside an infinite space (by Kelvin) or inside a half-space (by Mindlin), the point load acting horizontally on the surface of a half-space (by Cerrutti) etc. [65, 104, 138, 140]. One can refer to, for example, [142] for an exhaustive review (and the historical context) of the contributions made by various researchers in this field, and can refer to, for example, [97] for the issues related to heterogeneous, anisotropic, and incompressible media.

Boussinesq's approach can be extended further to find the response due to, for example, line loading, uniform strip loading, uniform circular loading, uniform elliptical loading, triangular strip loading, Hertz loading, eccentric loading, anisotropy, and a heterogeneous condition, etc. Some relevant but simple example problems are discussed in the following. For further study, interested readers can refer to, for example, [37, 63, 65, 104, 138, 140, 222, 247, 277] etc.

Example problem

Circular uniform loading on an elastic half-space is shown in Figure 5.2. It may be assumed that a total load of Q is distributed uniformly over a circular area of radius a. Obtain an expression for σ_{zz} at a point inside the half-space (that is, at a point (r'',z) shown as A in Figure 5.2).

Solution

The stresses can be obtained, assuming that linear superposition is valid. That is, contributions by all infinitesimally small point loads located at (r',θ) can be summed (by integration) to obtain the overall effect. The magnitude of a point load over an elemental area $r'\,d\theta\,dr'$ is given as $q\,r'\,d\theta\,dr'$ where, $q = q_{av} = \frac{Q}{\pi a^2}$. Thus, using Equation 5.18, the vertical stress (σ_{zz}), in this case, can be

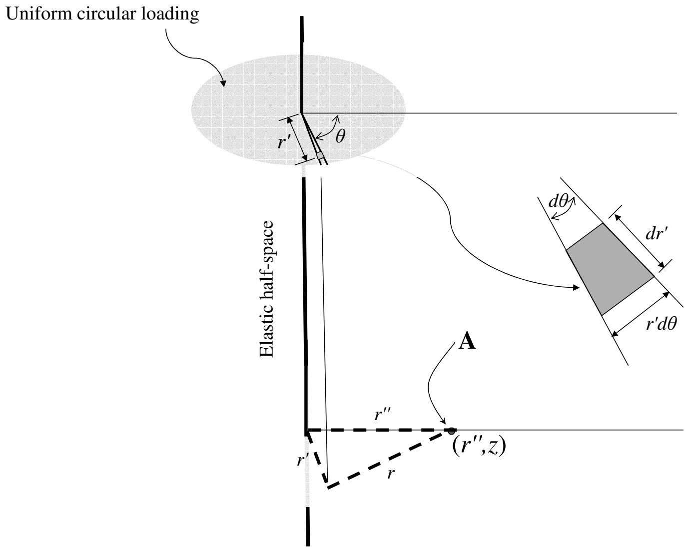

Figure 5.2: Circular loading on an elastic half-space.

written as,

$$\sigma_{zz} = \int_0^a \int_0^{2\pi} \frac{3(qr'd\theta dr')}{2\pi} z^3(r^2+z^2)^{-\frac{5}{2}} \tag{5.25}$$

where, r is the distance between the elemental area and point A. The r in the above equation can be substituted with $(r'^2 + r''^2 - r'r''2\cos\theta)^{1/2}$ and integration can be performed numerically to obtain the value of σ_{zz}.

Example problem

Figure 5.3 shows a flexible uniformly loaded circular plate. Estimate the maximum surface deflection.

Solution

By "flexible plate" it is understood that the plate does not have any flexural rigidity of its own, therefore, it takes the same shape as that of the elastic medium after deformation.

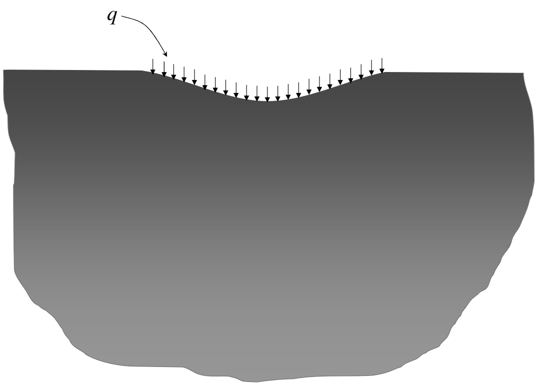

Figure 5.3: Displacement of an elastic half-space due to a flexible uniformly loaded circular plate.

The deflection due to point load Q at the surface can be obtained from Equation 5.24 (by putting $z = 0$)

$$\omega|_{z=0} = \frac{(1-\mu^2)Q}{\pi E r} \tag{5.26}$$

Taking an elemental area of $r'\,d\theta\,dr'$ on the loaded region, and assuming superposition is valid, one can calculate the central deflection ($\omega|_{z=0,r=0}$) as,

$$\omega|_{z=0,r=0} = \int_0^a \int_0^{2\pi} \frac{(1-\mu^2)(qr'd\theta\,dr')}{\pi E r} \tag{5.27}$$

where, $q = q_{av} = \frac{Q}{\pi a^2}$. Since the central deflection is being calculated, one can write $r = r'$ in this case[1]. Thus,

$$\omega|_{z=0,r=0} = \frac{2(1-\mu^2)qa}{E} \tag{5.28}$$

[1] For any point other than the center point, $r \neq r'$, an appropriate relationship needs to be developed from geometrical considerations (refer to [65], for example).

Assuming $\mu = 0.5$ as a special case, one can obtain,

$$\omega_{z=0,r=0} = \frac{1.5 q_{av} a}{E} \tag{5.29}$$

Equation 5.29 is popularly used for the estimation of an elastic modulus of soil (a subgrade or embankment structure made up of homogeneous material with sufficiently thickness or height so that it can be assumed as an elastic half-space) by plate load test, while a flexible plate is used.

Example problem

Figure 5.4 shows a rigid circular frictionless plate. Estimate the maximum surface deflection.

Solution

By "rigid plate" it is understood that the plate has high flexural rigidity, and therefore, it does not deform itself when load is applied. The pressure distribution may no longer be uniform, in this case. Two conditions need to be satisfied, as follows:

- The total force at the bottom of the plate (due to the non-uniform pressure distribution) should be equal to force Q externally applied. That is,

  $$\int_A q dA = Q \tag{5.30}$$

  where, A is the area of the plate, and dA is the elemental area.

- The deflection at each point of the circular plate should be the same (since it is a rigid plate).

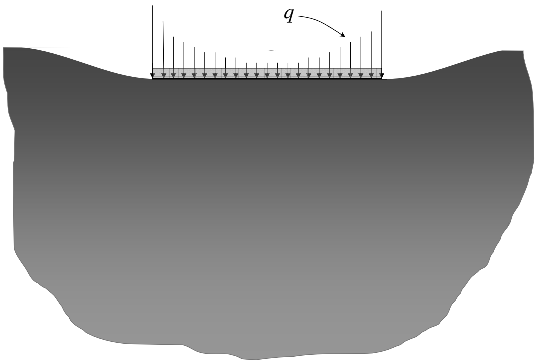

Figure 5.4: Displacement of an elastic half-space due to a rigid circular plate

For the flexible plate case (that is, the last example) it is found that the deflection at the center of the plate is maximum and at its edge it is minimum. For the present case of a rigid plate, the deflection within the plate region should be the same everywhere. This may possibly be achieved if the pressure is higher along the edges than at the center [65]. Thus, the pressure distribution can be assumed to take a shape as shown in Figure 5.4. It appears that the following pressure distribution satisfies the above two conditions [65, 140].

$$q \quad = \sigma_{zz}|_{z=0} \quad = \frac{Q}{2\pi a(a^2 - r^2)^{1/2}} \quad \text{for } 0 \le r \le a \tag{5.31}$$

It is interesting to note that the proposed pressure distribution shows that the pressure theoretically will be infinite along the edge. One can refer to [65] for further discussions on this.

Thus, the deflection at the center of the plate can be obtained as (derived from Equation 5.24 by putting $z = 0$, taking an elemental area of $r' d\theta\, dr'$, substituting the value of q from Equation 5.31, and considering $r = r'$, for the present case),

$$\begin{aligned} \omega\big|_{z=0,r=0} &= \int_0^a \int_0^{2\pi} \frac{(1-\mu^2)(\frac{Q}{2\pi a (a^2-r^2)^{1/2}} r' d\theta\, dr')}{\pi E r} \\ &= \frac{(1-\mu^2) q_{av} a \pi}{2E} \end{aligned} \tag{5.32}$$

Assuming, $\mu = 0.5$, as a special case, one can obtain,

$$\omega_{z=0,r=0} = \frac{1.18 q_{av} a}{E} \tag{5.33}$$

Equation 5.33 is popularly used for estimation of an elastic modulus of soil by a plate load test, while a rigid plate is used. Further calculations can show that for the assumed pressure distribution (that is, Equation 5.31), the deflection at every other point within the rigid circular disk is the same and can be given by Equation 5.33 for $\mu = 0.5$.

5.4 Multi-layered structure

An idealized multi-layered asphalt pavement structure is shown in Figure 5.5. A total load of Q is assumed to act uniformly on a circular area of radius a (that is, $q = \frac{Q}{\pi a^2}$, and this is equal to the tire contact pressure). The layers are identified as 1st layer, 2nd layer, ith layer and so on, starting from top to bottom. The last layer (typically a subgrade) is the nth layer. The assumptions of a multi-layer asphalt pavement structure can be mentioned as following,

- The structure is constituted with n number of layers.
- Each layer is assumed to be made up of homogeneous, isotropic, and linearly elastic material. Thus, elastic modulus (E_i) and Poisson's ratio (μ_i) characterize each layer.

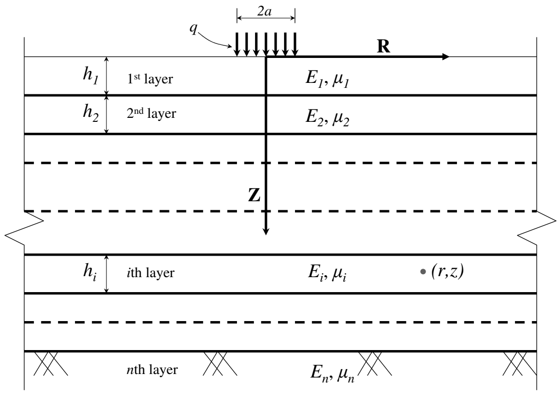

Figure 5.5: A multi-layered asphalt pavement structure.

- Each layer (except the subgrade) has finite uniform thickness (h_i) and the subgrade is assumed as semi-infinite (that is, half-space).
- The pavement structure is assumed to be weightless (that is, $BF_z = 0$). That is, compared to the contact pressure (q) applied, the pressure created due to the self-weight of the pavement itself is negligible.
- The structure is also assumed to be free from any other kind of existing stresses.

5.4.1 Formulation

The formulation presented in Section 5.2 can be utilized to analyze a multi-layered structure. The solution approach is the same as summarized toward the end of Section 5.2; however, a transformation needs to be applied so as to match the loading geometry.

The approach for the elastic analysis of a multi-layered structure was originally developed by Burmister [33, 34, 35]. Various researchers have further extended the formulation (general enough to handle n layers), developed algorithms, performed numerical studies [6, 135, 218, 246, 289, 296, 297], and have been widely used in various analysis [46, 121, 128, 148, 165, 310]. The analysis approach is presented in the following.

The following ϕ function is used for this analysis (and it satisfies Equation 5.16),

$$\begin{aligned}\phi^i(m) &= \left[A^i(m)e^{mz} - B^i(m)e^{-mz}\right.\\ &\quad \left.+C^i(m)ze^{mz} - D^i(m)ze^{-mz}\right] J_o(mr) \end{aligned} \tag{5.34}$$

where J_o is the Bessel function of 0th order, $A^i(m)$, $B^i(m)$, $C^i(m)$ and $D^i(m)$ are coefficients for the ith layer, r is the radial distance and z is the depth, and m is any number.

Using the ϕ function (that is, putting Equation 5.34 into Equation 5.11) the stresses (in the ith layer) and subsequently the displacement values (refer to Equation 5.15), for an axi-symmetric case, are calculated as follows [128, 148, 165, 296, 297],

$$\begin{aligned}
\hat{\sigma}^i_{zz} &= -mJ_o(mr)\left[A^i(m)m^2e^{mz} + B^i(m)m^2e^{-mz}\right.\\
&\quad \left.-C^i(m)m(1-2\mu_i - mz)e^{mz} + D^i(m)m(1-2\mu_i - mz)e^{-mz}\right]\\
\hat{\sigma}^i_{rr} &= mJ_o(mr)\left[A^i(m)m^2e^{mz} + B^i(m)m^2e^{-mz} + C^i(m)m(1+2\mu_i+mz)e^{mz}\right.\\
&\quad \left.-D^i(m)m(1+2\mu_i - mz)e^{-mz}\right] - m\frac{J_1(mr)}{mr}\left[A^i(m)m^2e^{mz}\right.\\
&\quad \left.+B^i(m)m^2e^{-mz} + C^i(m)m(1+mz)e^{mz} - D^i(m)m(1-mz)e^{-mz}\right]\\
\hat{\sigma}^i_{\theta\theta} &= \frac{J_1(mr)}{r}\left[A^i(m)m^2e^{mz} + B^i(m)m^2e^{-mz}\right.\\
&\quad \left.+C^i(m)m(1+mz)e^{mz} - D^i(m)m(1-mz)e^{-mz}\right]\\
&\quad +2\mu_i mJ_o(mr)\left[C^i(m)me^{mz} - D^i(m)me^{-mz}\right]\\
\hat{\tau}^i_{rz} &= mJ_o(mr)\left[A^i(m)m^2e^{mz} - B^i(m)m^2e^{-mz}\right.\\
&\quad \left.+C^i(m)m(2\mu_i+mz)e^{mz} + D^i(m)m(2\mu_i - mz)e^{-mz}\right]\\
\hat{\omega}^i &= -\frac{1+\mu_i}{E_i}mJ_o(mr)\left[A^i(m)m^2e^{mz} - B^i(m)m^2e^{-mz}\right.\\
&\quad \left.-C^i(m)m(2-4\mu_i - mz)e^{mz} + D^i(m)m(2-4\mu_i+mz)e^{-mz}\right]\\
\hat{u}^i &= \frac{1+\mu_i}{E_i}J_1(mr)\left[A^i(m)me^{mz} + B^i(m)me^{-mz}\right.\\
&\quad \left.+C^i(m)(1+mz)e^{mz} - D^i(m)(1-mz)e^{-mz}\right]
\end{aligned} \tag{5.35}$$

From Equation 5.35, it can be seen that, $\hat{\sigma}_{zz}^{1,t} = -mJ_o(mr)$, where $\hat{\sigma}_{zz}^{1,t}$ represents σ_{zz} at the top of the first layer[2]. That means, the $\hat{\sigma}_{zz}^{i}$, $\hat{\sigma}_{rr}^{i}$, $\hat{\sigma}_{\theta\theta}^{i}$, $\hat{\tau}_{rz}^{i}$, $\hat{\omega}^{i}$ and $\hat{u}^{i}$ values calculated from Equations 5.35 are the solutions due to $mJ_o(mr)$ loading at the surface. However, one is rather interested in a solution for the case represented in Figure 5.5, that is,

$$\begin{aligned} \sigma_{zz}^{1,t} &= q \quad \text{for } \; 0 \le r \le a \\ &= 0 \quad \text{otherwise} \\ \tau_{rz}^{1,t} &= 0 \end{aligned} \tag{5.36}$$

Therefore, further conversion is needed to derive the stress and the displacement values due to loading as per Equation 5.36 (and not as per $mJ_o(mr)$). This is accomplished by invoking the Henkel transform. The Henkel transform for a pair of function ($f(r)$ and $f(m)$) can be given follows,

$$f(m) = \int_0^\infty rJ_o(mr)f(r)dr \tag{5.37}$$

$$f(r) = \int_0^\infty mJ_o(mr)f(m)dm \tag{5.38}$$

For the present case, $f(r)$ can be assumed to be the same as $\sigma_{zz}^{1,t}$ mentioned in Equation 5.36. Thus, using Equation 5.37

$$\begin{aligned} f(m) &= -\int_0^a qrJ_o(mr)dr + \int_a^\infty 0dr \\ &= -\frac{qa}{m}J_1(ma) \end{aligned} \tag{5.39}$$

This expression of $f(m)$ can be put back into Equation 5.38 to re-derive an expression for $f(r)$. That is,

$$\begin{aligned} f(r) &= \int_0^\infty mJ_o(mr)\left(-\frac{qa}{m}J_1(ma)\right)dm \\ &= qa\int_0^\infty (-mJ_o(mr))\frac{J_1(ma)}{m}dm \end{aligned} \tag{5.40}$$

[2]Superscript t indicates top and b indicates bottom.

It may be recalled that the loading $mJ_o(mr)$ is the expression obtained for $\hat{\sigma}_{zz}$ at the surface, whereas $f(r)$ presents the actual stress due to the loading shown in Figure 5.5. Thus, Equation 5.40 can be used as a transformation for obtaining the stresses or displacements due to loading as per Figure 5.5. Thus [128, 148, 165, 296, 297],

$$
\begin{aligned}
\sigma^i_{zz} &= qa\int_0^\infty J_o(mr)J_1(ma)\left[A^i(m)m^2e^{mz} + B^i(m)m^2e^{-mz}\right.\\
&\quad \left.-C^i(m)m(1-2\mu_i - mz)e^{mz} + D^i(m)m(1-2\mu_i - mz)e^{-mz}\right]dm\\
\sigma^i_{rr} &= -qa\int_0^\infty J_o(mr)J_1(ma)\left[A^i(m)m^2e^{mz}\right.\\
&\quad +B^i(m)m^2e^{-mz} + C^i(m)m(1+2\mu_i+mz)e^{mz}\\
&\quad \left.-D^i(m)m(1+2\mu_i - mz)e^{-mz}\right]dm + qa\int_0^\infty \frac{J_1(mr)}{mr}J_1(ma)\left[A^i(m)m^2e^{mz}\right.\\
&\quad \left.+B^i(m)m^2e^{-mz} + C^i(m)m(1+mz)e^{mz} - D^i(m)m(1-mz)e^{-mz}\right]dm\\
\sigma^i_{\theta\theta} &= -qa\int_0^\infty \frac{J_1(mr)}{mr}J_1(ma)\left[A^i(m)m^2e^{mz} + B^i(m)m^2e^{-mz}\right.\\
&\quad \left.+C^i(m)m(1+mz)e^{mz} - D^i(m)m(1-mz)e^{-mz}\right]dm\\
&\quad -2\mu_i qa\int_0^\infty J_o(mr)J_1(ma)\left[C^i(m)me^{mz} - D^i(m)me^{-mz}\right]dm\\
\tau^i_{rz} &= -qa\int_0^\infty J_o(mr)J_1(ma)\left[A^i(m)m^2e^{mz} - B^i(m)m^2e^{-mz}\right.\\
&\quad \left.+C^i(m)m(2\mu_i+mz)e^{mz} + D^i(m)m(2\mu_i - mz)e^{-mz}\right]dm\\
\omega^i &= -\frac{1+\mu_i}{E_i}qa\int_0^\infty J_o(mr)J_1(ma)\left[A^i(m)m^2e^{mz} - B^i(m)m^2e^{-mz}\right.\\
&\quad \left.-C^i(m)m(2-4\mu_i - mz)e^{mz} + D^i(m)m(2-4\mu_i+mz)e^{-mz}\right]dm\\
u^i &= \frac{1+\mu_i}{E_i}qa\int_0^\infty J_1(mr)J_1(ma)\left[A^i(m)me^{mz} + B^i(m)me^{-mz}\right.\\
&\quad \left.+C^i(m)(1+mz)e^{mz} - D^i(m)(1-mz)e^{-mz}\right]dm
\end{aligned}
\tag{5.41}
$$

However, one needs to know the values of the coefficients $A^i(m)i$, $B^i(m)$, $C^i(m)$, and $D^i(m)$. These are obtained from the boundary conditions. The boundary conditions for the present problem (at the surface, at the interface, and at infinite depth) are discussed in the following,

5.4.2 Boundary conditions

At the surface, as discussed earlier, the vertical stress at the circular region will be equal to the tire contact pressure (q), and shear stress will be equal to zero (that is Equation 5.36).

For a perfectly bonded interface (also called a rough interface, when the layers cannot slide over each other) between the ith and $(i+1)$th layer the σ_{zz} at the bottom of the ith layer should be equal to that at the top of the $(i+1)$th layer. So also will be ω, u and τ_{rz}. Thus, the boundary conditions will be,

$$\begin{aligned} \hat{\sigma}_{zz}^{i,b} &= \hat{\sigma}_{zz}^{i+1,t} \\ \hat{\omega}^{i,b} &= \hat{\omega}^{i+1,t} \\ \hat{\tau}_{rz}^{i,b} &= \hat{\tau}_{rz}^{i+1,t} \\ \hat{u}^{i,b} &= \hat{u}^{i+1,t} \end{aligned} \tag{5.42}$$

For a perfectly smooth interface (that is, when the layers can slide over each other) the σ_{zz} and ω at the bottom of the ith layer should be equal to that of at the top of the $(i+1)$th layer. However, the shear stresses for both the ith and $(i+1)$th should individually be equal to zero, since sliding is allowed. Hence the boundary condition becomes,

$$\begin{aligned} \hat{\sigma}_{z}^{i,b} &= \hat{\sigma}_{z}^{i+1,t} \\ \hat{\omega}^{i,b} &= \hat{\omega}^{i+1,t} \\ \hat{\tau}_{rz}^{i,b} &= 0 \\ \hat{\tau}_{rz}^{i+1,t} &= 0 \end{aligned} \tag{5.43}$$

It may be mentioned that a perfectly smooth or perfectly bonded interface condition is a theoretical idealization. In reality, a situation somewhere in between may be realized. Bonding may be improved by texturing or by applying adhesive agent at the interface level, bonding may be reduced by constructing a smooth surface or by providing a separation layer.

At infinite depth one can assume that the stresses and displacements are zero, that is,

$$\begin{aligned} \hat{\sigma}_{zz} = \hat{\sigma}_{rr} = \hat{\sigma}_{\theta\theta} = \hat{\tau}_{rz} &= 0 \\ \hat{u} = \omega &= 0 \end{aligned} \tag{5.44}$$

This condition leads to, $A^n(m) = 0$ and $B^n(m) = 0$. If, however, there is a rigid base at the bottom of nth layer, for a rough interface, one can write [128]

$$\begin{aligned} \hat{\omega}^{n,b} &= 0 \\ \hat{u}^{n,b} &= 0 \end{aligned} \tag{5.45}$$

For a smooth interface between the nth layer and a rigid base, one can write [128],

$$\begin{aligned} \hat{\omega}^{n,b} &= 0 \\ \hat{\tau}_{rz}^{n,b} &= 0 \end{aligned} \tag{5.46}$$

Since this is an n-layered structure, there will be $4 \times n$ number of unknowns for each value of m. An n-layered pavement has $(n-1)$ interfaces. Thus, from Equation 5.42 or 5.43 (as the case may be) one obtains $4 \times (n-1)$ number of equations. The Equations 5.36, and 5.44 (or Equation 5.45 or Equation 5.46 as the case may be) provide an additional 4 equations. Thus, a total of $4 \times n$ equations are obtained which can be used to solve $4 \times n$ of unknowns, for each value of m. Figure 5.6 shows a typical output from an analysis of a multi-layered elastic structure.

It may be noted that in Equations 5.42 to 5.46 the expressions without a Henkel transform has been used. These expressions do not involve integrations and can be handled algebraically. It is assumed that if the boundary conditions are satisfied without the Henkel transform (that is, Equations 5.35), the boundary conditions will be satisfied with the Henkel transform (that is, Equations 5.41) as well [128].

5.4.3 Discussions

The present ϕ function (refer to Equation 5.34) can as well be used for solving the half-space problem (as discussed in Section 5.3), and one may refer to [37] for a worked out solution.

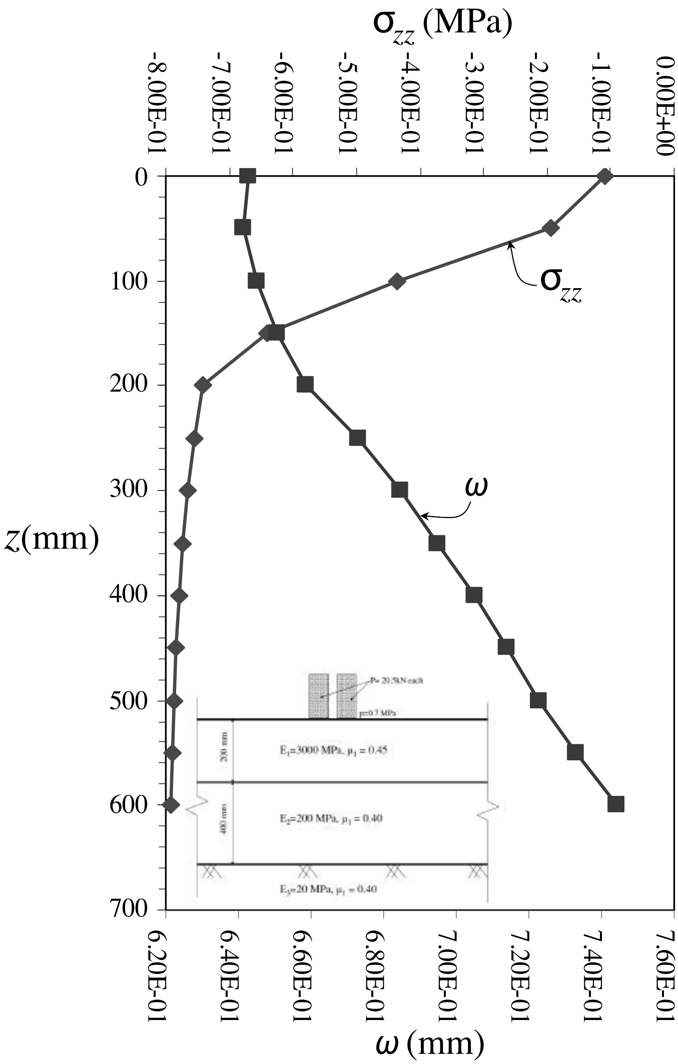

Figure 5.6: Typical output from an analysis of a multi-layered elastic structure.

It may be noted that circular uniform loading is generally assumed for analysis of asphalt pavement idealized as a multi-layered structure. It also synchronizes well with the axi-symmetric cylindrical coordinate system assumed for the analysis. However, a typical tire imprint neither may look circular nor the loading be uniform

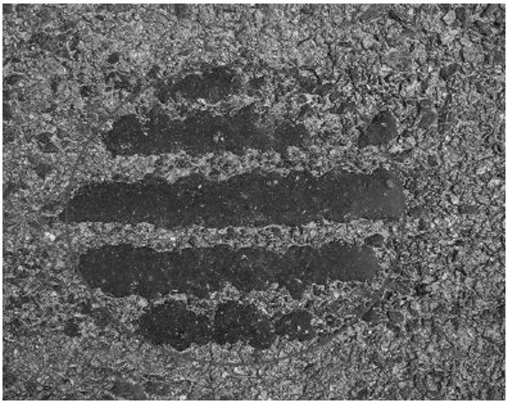

Figure 5.7: A typical tire imprint.

(refer to Figure 5.7). If the weight of the wheel is Q and the tire contact pressure is q, then the equivalent radius (a) of the tire imprint can be calculated as,

$$a = \sqrt{\frac{Q}{q\pi}} \tag{5.47}$$

Instead of vertical pressure, one can also assume that a horizontal shear stress (q_s) is applied by the wheels (refer to Figure 5.8). In that case, the surface boundary condition becomes the following,

$$\begin{aligned} \tau_{rz}^{1,t} &= q_s \quad \text{for} \;\; 0 \leq r \leq a \\ &= 0 \quad \text{otherwise} \\ \sigma_{zz}^{1,t} &= 0 \end{aligned} \tag{5.48}$$

In fact, a wheel applies both vertical pressure (q) and horizontal shear stress (q_s), and one can solve the multi-layer problem separately using Equation 5.36 and Equation 5.48, and superimpose them to predict the overall effect.

It is possible to extend the n layer analysis further for a situation where some of the layers are assumed to show viscoelastic behavior.

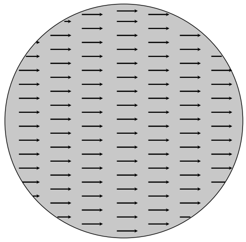

Figure 5.8: Shear stress acting within a circular area of radius a.

Use of the elastic-viscoelastic correspondence principle [84] (refer to Equations 2.41 and 2.42) can be one of the ways of handling such a problem. In this approach (i) the expressions of stress-strain-displacements are taken to the Laplacian domain (s), (ii) the expression of E_i can be replaced by $sE_i(s)$ (so also for μ_i, if it is assumed to be a function of time), and (iii) an inversion can be performed to bring it back to the time domain. A number of researchers have worked on this problem [213]. Interested readers can refer to, for example [46, 148, 213] as some of the relatively recent works.

As is apparent from the above discussions, a closed-form analytical solution of an n-layered elastic structure may be difficult. However, the results can be easily obtained using numerical schemes. Further, some alternative approximate approaches have been suggested where the multi-layered problem is solved using a single layer formulation (that is, a half-space), with certain additional simplifications. One can refer to [65, 256, 290] for discussions on such methods.

5.5 Closure

A number of softwares/algorithms are available which perform such analyses of multi-layered structures, for example, [56, 61, 66, 103, 121, 143, 154, 215, 217, 227, 283] and one can refer

Figure 5.9: Superposition may be assumed for computing response due to multi-axle loading.

to [46, 121, 131, 279] for more discussions on such available tools. Some of the softwares/algorithms have provisions for incorporating advanced material models. Since it is possible to analyze multi-layered structures with various material behavior and geometry [165] using efficient computational systems, there may not be any need to estimate an equivalency factor between two layers made up of different materials, or the equivalent single layer strength (elastic modulus) of two or multiple layers, etc. Such computational power also enables one to analyze a complex arrangement of axle and wheel configurations (refer Figure 5.9). With this, assumption of load dispersion angle or equivalent single wheel load (ESWL) etc., may no longer be required.

This page intentionally left blank

Chapter 6

Temperature stress in asphalt pavement

6.1 Introduction

Change in temperature other than the temperature profile at which the pavement is stress-free (refer to the discussions in Section 4.3 in the beginning) is expected to cause thermal stress to a pavement structure. However, the asphalt mix being a rheologic material also dissipates the stress thus developed. That is, continuous variation of the thermal profile induces thermal stress to the asphalt pavement which also continuously gets dissipated. Thus, thermal stress in asphalt pavement may be negligible in moderately cold to warm places. However, in the regions with an extremely cold climate, there can be a significant accumulation of thermal stress within a short time-period (shorter than the time needed for its dissipation). This chapter presents a formulation to estimate the thermal stress in an asphalt layer (for known rheological properties) due to any given variation of temperature.

6.2 Thermal profile

A simple formulation for the estimation of a thermal profile across pavement layers has already been presented in Section 4.2. Various researchers have studied the thermal profile of asphalt pavement theoretically and experimentally [108, 301, 311]. Past studies suggest that the thermal profile ($T(z)$) in the asphalt layer of an asphalt pavement is generally nonlinear [72].

6.3 Thermal stress in asphalt pavement

For a viscoelastic material, the thermal stress dissipates over time. If temperature T did not vary with time (t), the thermal stress (for fully a restrained condition) in the asphalt layer could be calculated (refer to Equation 4.11) as follows,

$$\begin{aligned} \sigma_{xx}^T(t) &= \sigma_{yy}^T(t) \\ \sigma^T(t) &= -\frac{E_{rel}^T \alpha (T - T_o)}{1 - \mu} \end{aligned} \tag{6.1}$$

where, $E_{rel}(t)$ is the relaxation modulus of the asphlatic material. The $\sigma^T(t)$ will gradually decrease even if the temperature remains constant over time. Further, $\sigma^T(t)$ will be higher if the temperature is low. This has been schematically presented in Figure 6.1.

However, the temperature in a pavement structure does not remain constant; the temperature ($T(z, t)$) varies both with depth (z) and time (t) (refer to Section 4.2). Such a variation will affect the restrained strain (refer to Equation 4.10), which in turn will influence $\sigma^T(z, t)$. Asphalt mix being rheologic material, $\sigma^T(z, t)$ will be affected by the history of the temperature variation as well. Thus, the considerations involved in deriving an expression for $\sigma^T(z, t)$ are presented in the following,

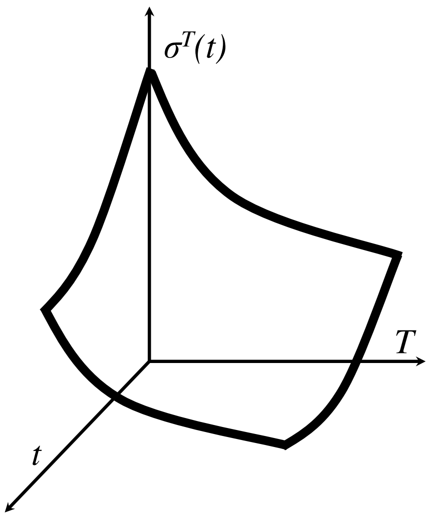

Figure 6.1: A conceptual diagram of the variation of thermal stress ($\sigma^T(t)$) with temperature (T) and time (t).

- Assuming that asphalt mix is a linear viscoelastic material, the thermal stress can be determined by using the Boltzman's superposition principle (refer to Equation 2.39), as follows [43, 111, 187, 188, 213, 229, 253].

$$\sigma^T(t) = \frac{1}{(1-\mu)} \int_{-\infty}^{t} E_{rel}^{T(t)}(t-\zeta) \frac{\partial \epsilon(\zeta)}{\partial \zeta} d\zeta \tag{6.2}$$

  where, ζ = dummy variable for time.

- Using Equation 4.10 one can write [187, 229],

$$\frac{\partial \epsilon(\zeta)}{\partial \zeta} = -\alpha \frac{\partial T}{\partial \zeta} \tag{6.3}$$

  where, α = coefficient of thermal expansion (of the asphalt in this case). It is assumed that α does not vary with temperature.

- It may be noted that since temperature is constantly changing, the $E_{rel}^{T(t)}$ needs to be converted to a equivalent value $E_{rel}^{T_r}$ at some standard temperature [188, 213, 229, 253], where T_r is a reference temperature. This can be done by invoking the time-temperature superposition principle, and assuming that asphalt is a thermorheologically simple material [253].

  Using Equation 2.51 and considering that the reduced time at a given time $(t-\zeta)$ is the sum of all the reduced times up to this time [84, 188, 213, 253], one can derive the function for calculation of the reduced time as follows [213, 229],

$$f(t-\zeta) = \int_{-\infty}^{(t-\zeta)} \frac{dt''}{\alpha_T} \tag{6.4}$$

  where, t'' = a dummy variable representing time. A suitable expression for α_T can be chosen in the form of Equation 2.53 or Equation 2.54. It is assumed that the reduced time is calculated with reference to some standard temperature, T_r. It may be noted that α_T is a function of T_r and $T(t'')$, where $T(t'')$ represents the temperature of the asphalt layer (at a given z) which is constantly varying with time, t''.

- The above considerations are assumed to hold independently for each value of z.

Considering the above, the thermal stress into asphalt layer at any t and z can be expressed as [188, 206, 213, 229, 253],

$$\sigma^T(z,t) = \frac{-\alpha}{(1-\mu)} \int_{-\infty}^{t} E_{rel}^{T_r}(z, f(t-\zeta)) \frac{\partial T(z,\zeta)}{\partial \zeta} d\zeta \tag{6.5}$$

Equation 6.5 can be used for the calculation of thermal stress within the asphalt layer at any time and depth. One can choose a suitable rheologic model for asphalt material (refer to the discussions in Section 2.3.1) and numerically obtain the estimated value of $\sigma^T(z,t)$. One can refer to, for example, [229, 253] for such a study on a single layer, [213] for a study on multiple layers, and [225] for more complex geometry. A typical expected variation of temperature, restrained strain, and viscoelastic stress is schematically shown in Figure 6.2.

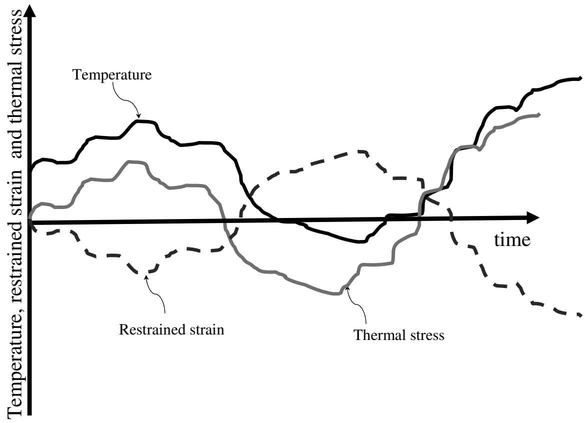

Figure 6.2: Schematic representation of variation of temperature, restrained strain, and viscoelastic stress in an asphalt layer.

6.4 Closure

$\sigma^T(z,t)$ is a function of both the temperature and the rate of drop of temperature (refer to Equation 6.5). For low temperature and a high rate of cooling, the stress developed will be high. If the drop of temperature is slow, the asphalt layer may get time to dissipate the thermal stress. If the thermal stress developed is more than the tensile strength of the material (at that z and t), a thermal crack may originate [78, 112]. The issues related to the estimation of thermal crack spacing will be taken up in the next chapter (Chapter 7).

This page intentionally left blank

Chapter 7

Pavement design

7.1 Introduction

A pavement design may involve structural, functional, and drainage design. This chapter deals with the basic principles of structural design of a pavement. The goal of this chapter is to establish a link between the analysis schemes developed in the previous chapters and the current approaches to pavement design. A large pool of documents is available on the design of pavement structure, in the form of textbooks [94, 121, 186, 212, 313], codes/guidelines [1, 86, 131, 132, 198, 206, 211, 216, 217, 260, 281, 284] and various background papers [53, 256, 257, 280], and interested readers can refer to these for further study. The discussions in this chapter, therefore, have been kept brief.

The structural design of pavement primarily involves the estimation of thickness. The thicknesses are so provided so that the pavement is able to survive the structural distresses. It may be reminded that there can be various other distresses which are non-structural in nature. Some of the primary modes of structural distresses are, load fatigue, thermal fatigue, rutting, low temperature shrinkage cracking, top-down cracking, punchouts (generally relevant for continuously reinforced cement concrete pavements), crushing, etc. One can refer to, for example [199, 260], for an overview of various types of distresses that may occur to a pavement structure.

For asphalt pavement, the structural design generally involves estimation of the thicknesses of the base, sub-base, and surfacing. For concrete pavement, structural design generally involves estimation of the thicknesses of the base and the concrete slab; for concrete pavements it also includes an estimation of the joint spacing and detailing (spacing, diameter, and length) of the dowel and tie bars. In principle, there is not much of a difference between the pavement design approaches for a highway pavement and a runway/taxiway pavement [83, 116, 211] or a dockyard pavement—the input parameters may be different (for example, load application time in a dockyard [259] may be longer than on a taxiway, the lateral wander of wheels on a runway may be distributed over a larger length than on highways and so on), but the design philosophy (in terms of the mechanistic-empirical design approach), in general, remains the same.

7.2 Design philosophy

Historically, a number of approaches have been suggested to design the pavement structure, ranging from empirical, to semi-empirical to mechanistic-empirical methods. Some of the earlier approaches were based on (i) experience (ii) bearing capacity (iii) shear strength (iv) deflection and so on. In some of these methods the layer thickness values are so designed that the maximum value (of bearing stress or shear stress or deflection) does not exceed the strength (say, bearing strength or shear strength of the material) or the limiting criterion (say, deflection). Certain initial design approaches did not originally include traffic repetition as a parameter [313]. However, it was realized that a pavement structure does not necessarily fail due to single application of load due to ultimate load bearing conditions (although there are some exceptions, as discussed toward the end of Section 7.4.1), rather it is the repetitions of load (or environmental variations) that cause failure. Repetition gradually emerged as one of the important considerations in the pavement design process.

One can refer to various other books/papers, for example, [121, 202, 290, 310] etc., for a brief review of the historical perspective of pavement design[1].

In the mechanistic-empirical pavement design approach, mechanistically estimated initial stress-strain values at critical locations are empirically related to the cumulative repetitions for individual distresses. Such relations are also known as transfer functions. For example, horizontal tensile stress/strain at the bottom of any bound layer can be related to fatigue life [216, 217, 260, 284], vertical compressive strain(s) on individual layers [216, 217, 260, 284] or the shear stress or principal stress can be related to permanent deformation (rutting) [260], vertical compressive stress can be related to the crushing of a cemented layer [260] and so on. Some of the initial works which formed the basis of the mechanistic-empirical method are due to [74, 204, 240]. Now, this approach is quite widely being used in various countries, and a number of guidelines/codes follow the mechanistic-empirical method of pavement design [1, 86, 198, 206, 216, 217, 260, 281, 284]. Some of the structural distresses considered in mechanistic-empirical pavement design are discussed further in the following:

- **Load fatigue**: Repetitive application of load causes load fatigue failure to the bound layer of the pavement [204, 251]. In the laboratory this is simulated by applying repetitive flexural loading on beams of various geometry (refer to Section 2.3.2 for a brief discussion). Since the maximum tensile

[1] It must, however, be pointed out that some of the earlier design approaches may still be quite relevant, for example deflection is used as a criteria for overlay design [13, 133, 217], bearing capacity can be used to evaluate stress and bearing capacity of individual layers [280], shear strength can be used as a criteria in an integrated approach for a mix-design-pavement-design [93] and so on.

stress strain occurs at the bottom of the bound layer, cracks initiate there and propagate upward as repetitions progress, hence are known as bottom-up cracking. The laboratory conditions of fatigue testing being different than in the field (for example, differences in loading pattern, rest period, temperature, boundary conditions of the sample etc.), calibration/adjustment is needed on the laboratory equation to make it usable as a design equation [8, 286]. Further, the definitions of fatigue failure in laboratory (which may be based on reduction of stiffness modulus by a pre-specified fraction [2, 176], or by the amount of energy absorbed [96, 269]) may be different than those in the field (which may be based on the percentage of appearance of a characteristic surface crack). One can refer to, for example [15, 258, 263] for a brief overview of the various load fatigue transfer functions used for pavement design purposes.

- **Rutting**: Permanent deformation in pavement is called rutting. Rutting generally occurs along the most traversed wheel path and is measured at the surface of the pavement. Rutting can happen due to (ii) compaction (reduction) of air-voids and/or (i) shear flow of the material. Since rutting is measured at the surface, the contribution may come from one or more layers due to either of these mechanisms. Figure 7.1 schematically shows the rutting contributed by the ith layer due to compaction (Figure 7.1(a)) and shear flow (Figure 7.1(b)).

  Various empirical, semi-empirical, or mechanistic (viscoelastic/viscoplastic) models have been suggested where elastic strain(s) of pavement layer(s), pavement thickness(es), temperature, asphalt content, airvoids, dynamic modulus, resilient modulus, aggregate gradation, traffic repetition, moisture content, state of stress, rheological parameters, etc., have been used to predict the rut depth of asphalt layer or granular layer or overall rutting [47, 54, 119, 122, 175, 206, 226, 234, 261, 322]. One can, for example, refer to [226] for a review on rutting in an asphalt layer, and

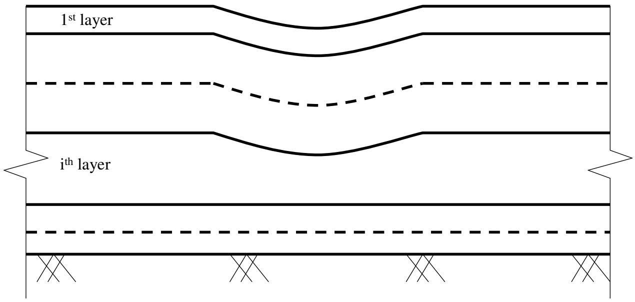

(a) Rutting of ith layer due to compaction

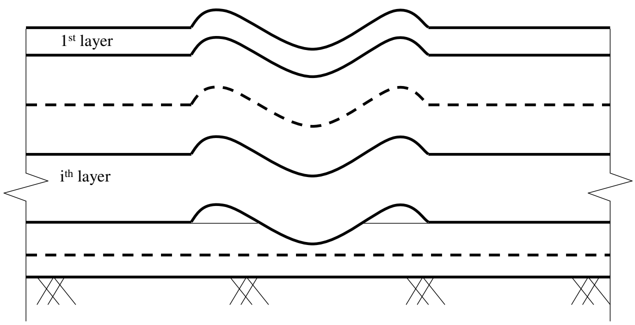

(b) Rutting of ith layer due to shear movement

Figure 7.1: Schematic diagram representing two possible mechanisms of rutting.

to [164, 288] for a review of rutting in a granular layer, and to [307] for a study on the relative contribution of different pavement layers to rutting.

- **Low temperature shrinkage cracking**: Low temperature shrinkage cracks run along the transverse direction of the road. Such cracks are prevalent in the roads of the colder regions [187]. It originates when the tensile stress generated within the bound layer exceeds the tensile strength of the material [78, 112]. Basic formulations for estimation of thermal stress have been developed in Sections 4.3.2 and 6.3 for cement concrete and asphalt pavement, respectively. For similar environmental conditions and mix composition, the transverse shrinkage cracks are expected to be spaced equally [229, 252, 253]. The design considerations for estimating the crack spacing has been presented in a later section in this chapter.

- **Thermal fatigue**: Temperature variations cause alternative expansion and contraction to the pavement materials. This causes damage (to the bound layers) due to thermal fatigue, which keeps on accumulating due to repetition of the thermal cycles [7, 21, 78, 298]. Past research suggests that variation of temperature, thickness of the bound layer, and the maximum thermal shrinkage stress level affect the damage due to thermal fatigue [7, 21, 228].

- **Top-down cracking**: Unlike load fatigue cracking, these cracks are seen to start from top and propagate downward, in asphalt [123, 194, 239] or concrete [25] pavements. Conventional load fatigue theory cannot explain it, which assumes that tensile strain causes fatigue cracks to initiate, whereas the top portion generally belongs to the compression zone [39]. It is postulated that the initiation of cracks at the top may be attributed to shear stress applied by the tires, non-uniform tire contact pressure, tensile stress at the surface generated due to wheels or axle placement, hardening of asphalt material, mix segregation, low temperature shrinkage cracks, and so on [39, 265]. Once initiated, it is assumed that the cracks propagate with the traffic repetitions.

7.3 Design parameters

The following paragraphs briefly discuss the various parameters associated with the pavement design.

7.3.1 Material parameters

The road materials are characterized through various tests, and the material parameters are subsequently used in pavement analysis as input. Road material characterization was covered in Chapter 2.

7.3.2 Traffic parameters and design period

Traffic parameters are used to predict the cumulative traffic count during the design period. For new road construction, traffic needs to be predicted where there is no traffic as yet. The traffic parameters include the traffic volume and its variation, axle load distribution, axle and the wheel configuration, tire contact pressure, the lateral wander of wheels, the traffic growth rate, the lane distribution and so on. This cumulative traffic is generally expressed in terms of million of standard axle load repetitions, using various empirical or theoretical equivalency factors [1, 101, 121, 206, 217, 260, 281, 284].

7.3.3 Environmental parameters

The variation of moisture and temperature may affect the layer modulus values, which in turn affect the critical stress/strain values for a multi-layered structure. The incremental damage for the same traffic repetition may differ due the effect of environmental variations. Advanced environmental models simulate the cumulative damage by considering the effects of the variation of environmental parameters [68].

7.4 Design process

The basic formulation for estimating stresses due to load has been presented in Chapters 3 and 5. The basic formulation for the estimation of stresses due to temperature has been presented in Chapters 4 and 6. The codal provisions may vary from one guideline to the other on whether the load and thermal stresses should be combined and considered in the design process.

The thermal stress in asphalt pavement at higher temperatures is generally neglected because of its quick dissipation. The thermal stress at low temperature in asphalt pavement is used for prediction of thermal shrinkage crack spacing (refer to Section 7.4.3).

The thermal stress in concrete pavement is highest at the interior portion (maximum restraint) and least at the corner (least restraint). Further, the thermal stress is tensile at the bottom of the slab during daytime (when, $T_t > T_b$) and is compressive at the bottom during the nighttime (when, $T_t < T_b$) (refer to Section 4.3.1). Thus, the load stress and the thermal stress may be additive or subtractive depending on the location and the thermal profile. A schematic diagram indicating relative magnitudes (not to scale) and the nature (tension/compression) of load and thermal stresses (typically bending) in concrete pavement has been presented in Figure 7.2. In the diagram, edge stress due to load, means the maximum stress is at the edge due to wheels positioned near the edge and so on (also refer to Section 3.4). Further, the existence of a moisture gradient (typically opposite to temperature gradient) may also affect the overall stress value [12]. Hence, considering only the bending stress due to the load and temperature (and ignoring the stress due to the moisture gradient) makes the design conservative.

7.4.1 Thickness design

Figure 7.3 shows a generic pavement thickness design scheme. The predicted cumulative traffic is used in the transfer functions to

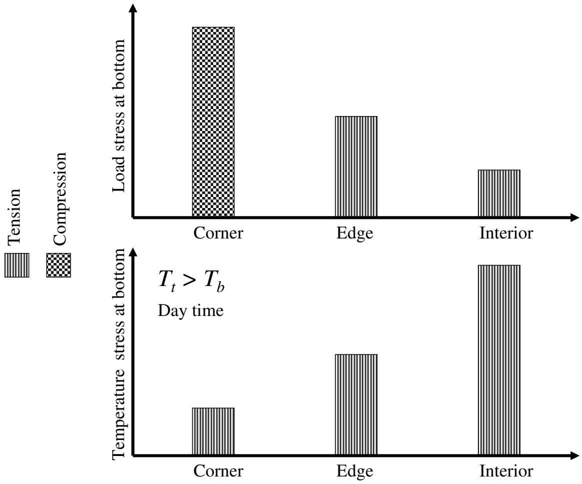

Figure 7.2: A schematic diagram indicating the possible relative magnitudes (not to scale) and nature (tension/compression) of load and thermal bending stresses in concrete pavement at the corner, edge, and interior.

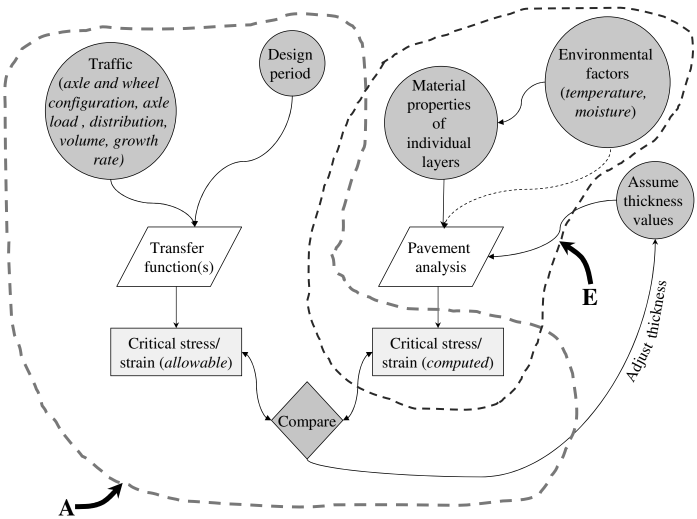

Figure 7.3: A generic pavement design scheme, where thicknesses are decided based on critical stresses/strains.

obtain the allowable values of critical stress/strain for a given type of structural distress. Further, from the assumed values of the thicknesses and the material properties, environmental parameters, and for a standard loading configuration, the stress/strain at the critical locations are computed using pavement analysis. These computed stress/strain values are compared with the corresponding allowable values. The thicknesses are adjusted iteratively until the values become approximately equal, and subsequently the design is finalized.

As per Figure 7.3, the iteration for design thicknesses is based on the comparison between the allowable and computed critical stress/ strain values. Alternatively, comparison can be also performed in terms of the traffic repetitions, that is, comparison between the number of expected traffic repetitions ($\boldsymbol{T}$) and number of traffic repetitions the pavement can sustain ($\boldsymbol{N}$). Thus, the portion marked "A" of Figure 7.3 can be changed to develop Figure 7.4, as an alternative design scheme. The value of $\boldsymbol{N}$ for a given distress can be obtained by putting the critical stress/ strain values to the corresponding transfer function.

For a deterministic design, a designer tries to adjust the thicknesses so that $\boldsymbol{N} \approxeq \boldsymbol{T}$. That means,

$$\frac{\boldsymbol{T}}{\boldsymbol{N}} \approxeq 1 \tag{7.1}$$

Given that there are seasonal variations (for example, variation of temperature affects the modulus of the asphalt layer, the variation of moisture affects the modulus of the subgrade etc.), variations in axle load (different axle loads result in different strain levels), during the design period, one may like to divide the design period into smaller time periods and calculate the fractional damage (due to different phases of environmental variations [284], different axle load groups [243], etc.) for each of these time periods. The smaller time periods may be constituted with groups of seasons, months, days or even hours. For example, stresses may be different in summer and winter months due to differences in the strength, interface,

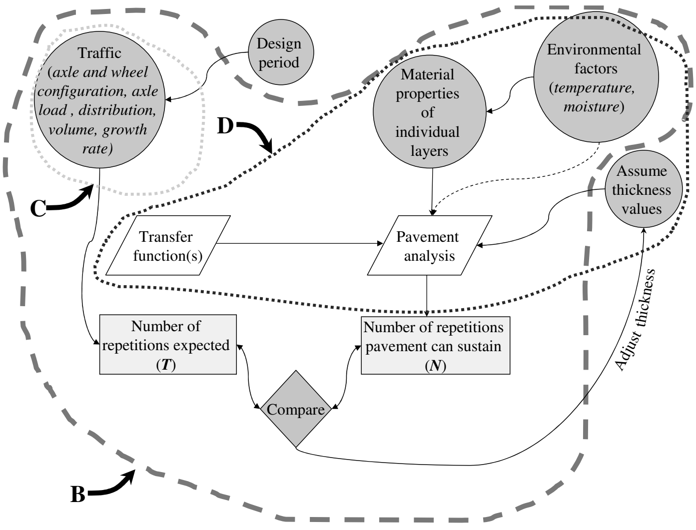

Figure 7.4: A generic pavement design scheme where thicknesses are decided based on the number of repetitions.

and restraint conditions; further, on a given month the daytime and nighttime stresses in a pavement might differ, and one might like to consider these separately. Assuming fractional damages are linearly additive (refer to Equation 2.55 and discussions thereof), one can write,

$$\sum_{\mathrm{EC}} \sum_{\mathrm{AL}} \frac{\boldsymbol{T}}{\boldsymbol{N}} \approxeq 1 \qquad (7.2)$$

where EC = different groups of environmental conditions, and AL = different groups of axle loads. Thus, the portion marked as "B" in Figure 7.4 goes through a loop (for calculation of fractional damages for different axle load, seasons, months, days etc., and one can have many such summations), before the design thicknesses are finalized.

In the above example, the damage (as per Equations 7.1 or 7.2) is made equal to one for design purposes. That is, expected traffic repetitions ($\boldsymbol{T}$) is made equal to the traffic repetitions the pavement can sustain ($\boldsymbol{N}$). One may, however, decide to take into account the uncertainties and inherent variabilities in various associated parameters [58, 121, 183, 262, 263, 313], which affects the performance of the pavement. This can be done by increasing the design traffic by a factor. Reliability analysis provides a basis for deciding this factor for a given reliability level of the pavement design. The reliability analysis for pavement design will be briefly dealt in Section 8.5.

Discussions

The same principle of pavement design (discussed above) holds for the design of the overlay, which involves the provision of an additional layer over the existing pavement. In this case, the pavement structure, including the proposed overlay, needs to be analyzed to obtain the stress/ strain parameters at the critical locations. For this analysis, one needs to consider the present strength (say, modulus) of the existing pavement, which might have deteriorated over the passage of time (due to traffic repetitions and temperature variations). The present strength of the pavement layers (at any given time during the service life) can be experimentally evaluated through a structural evaluation. Depending on the type of equipment used in the evaluation process, it may involve a solution to handling inverse problems (refer to Section 8.6 for discussion on inverse problems). Besides the mechanistic-empirical approach for overlay design, other approaches also have been suggested. For example:

- In the deflection based approach, the overlay is recommended (based on the experience gained from past studies) if the surface deflection (caused by some static or impact loading) is observed to be beyond some specified permissible limit and subsequently the overlay thickness is estimated from the observed deflection [133, 217].
- In the effective thickness approach (or, equivalent thickness

approach) [1, 13, 206], the overlay thickness is stipulated as follows,

$$h_o^B = h_1^{(A+B)} - kh_1^A \tag{7.3}$$

where, h_o^B = overlay thickness required to extend the longevity of pavement by an additional amount of B traffic repetition, after the pavement has undergone traffic repetition of A. $h_1^{(A+B)}$ = thickness of the surfacing to be provided if it had been designed for a total traffic of $A + B$, h_1^A = initial thickness of surfacing provided for design traffic A, k = a factor less than one, which takes care of the fact that the initial thickness of the surfacing provided for the design traffic A is no longer h_1^A, because, the layer must have undergone deterioration while serving the traffic A. If an asphalt overlay is to be provided on concrete pavement, or a concrete overlay is to be provided on asphalt pavement, then Equation 7.3 can be modified as follows,

$$h_o^B = C\left((h_1^{(A+B)})^m - k(h_1^A)^m\right) \tag{7.4}$$

C = empirical thickness conversion factor from one type of material to the other (say, from asphaltic to concrete or vice versa), m = an exponent depending on the bonding between the overlay and its underlying layer.

Sometimes, the weighted sum of the thicknesses of the layers (instead of individual thickness values) is used as an indicator of overall structural strength of the pavement [1, 83]. The formulas used for estimation of overlay thickness in different guidelines may be different from Equations 7.3 and 7.4, but all of them are generally based on the above conceptualization [1, 206, 211].

It can be shown that the above alternative approaches of overlay design can also be derived using the mechanistic-empirical design principle.

Some distresses may not be related to the critical stress strain parameters, rather they may be related to some other parameter (for example, erosion damage has been related to the energy needed to deform the slab), which in turn is dependent on traffic repetitions [206, 281]. One can still calculate cumulative damage due to traffic repetitions. Therefore, the schematic diagram presented as Figure 7.4 still holds.

Some distresses, for example, crushing, may be independent of the traffic repetitions in this case. Further, one might like to check whether the sum of maximum thermal and load stress for concrete pavement should always be less than the modulus of the rupture of the concrete. Such a check is independent of traffic repetitions. Thermal shrinkage cracking occurs at the instant when the generated tensile stress exceeds the tensile strength of the material. Thus, it also can be considered independent of traffic or the thermal loading cycle. If the pavement material is rheologic (like asphalt mix), there will be historical effect of thermal variations in terms of accumulation and dissipation of stress as discussed in Chapter 6; however, in principle one may consider thermal shrinkage cracking as a one-time failure phenomenon and that there is no accumulation of damage.

7.4.2 Design of joints

Design of joints involves considerations of joint spacing, and the design of the dowel and tie bars. These are discussed in the following.

7.4.3 Estimation of joint spacing

In concrete pavement, expansion joints are provided to allow expansion due to temperature variations.

Joint spacing for expansion joints

If the concrete pavement is freely allowed to expand or contract horizontally (refer to Figure 7.5(a)), from Equation 4.10 one can

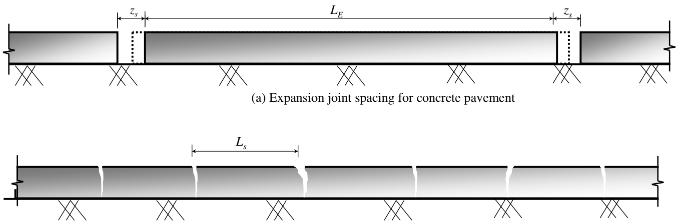

Figure 7.5: Schematic diagram explaining the thermal expansion joint spacing.

write,

$$L_E \alpha \left(T^A - T_o\right) = z_s \tag{7.5}$$

where, L_E is the spacing between the two successive expansion joints (which eventually is the length of the concrete slab). If the concrete pavement is partially restrained from moving, then from Equation 4.33 one can write,

$$\alpha \left(T^A - T_o\right) \frac{e^{-\xi L_E}}{\xi(1 + e^{-\xi L_E})} = z_s \tag{7.6}$$

The above equation provides a relationship between z_s and L_E. Thus, the spacing of expansion joints, L_E are obtained by setting limits to its displacement in terms of joint gap, z_s. If z_s provided is too small, concrete slabs may buckle at the joints (known as blow up); if it is too large it may cause hindrance to the smooth movement of wheels moving from one slab to the other (refer to Figure 3.4).

Joint spacing for thermal shrinkage crack

As discussed earlier, the thermal shrinkage crack (refer to Figure 7.5(b)) happens at that instant of time when the tensile thermal stress generated exceeds the tensile strength of the material [78]. Thus, the spacing of the contraction joint, L_C can be obtained by setting limits to the tensile stress developed as the tensile strength. That is,

$$\sigma^T(z,t) = \sigma^S \tag{7.7}$$

where, σ^S is the tensile strength of the asphalt mix. Thus, assuming a full-depth thermal shrinkage crack (refer to Figure 7.5(b)), Equation 4.17 can be used to obtain the value of L_C, if a friction model is used [188, 229, 252, 323].

Researchers have found that the σ^S of asphalt mix is sensitive to temperature [112, 298]. Approaching from low temperature (-40°C) to higher temperature, the tensile strength of asphalt material is first observed to increase then decrease [298].

The above principle also holds for the estimation of crack spacing due to the natural shrinkage of concrete (known as a contraction joint). However, stress needs to be calculated differently than the way done in Equations 4.11 and 4.33, due to thermal variations.

Contraction joints can be provided in variety of ways [313]. Primarily, a contraction joint is built as transversely placed pre-cracks (at regular intervals as estimated above), so that if the shrinkage crack grows further, it will occur along the same transverse lines. This will prevent irregular growth of cracks on the pavement surface.

7.4.4 Design of dowel bar

The dowel bars (refer to Figure 1.2) participate in the load transfer. For the design of the dowel bar the portion of the load transmitted by a single dowel bar is to be estimated first. This can be done by assuming that the dowel bar which is placed below the wheel takes the maximum share of the wheel load, and it is assumed that the subsequent dowel bars (up to some assumed length) share the load following a similar triangular rule [121, 313]. It may be noted that the total load shared by all the participating

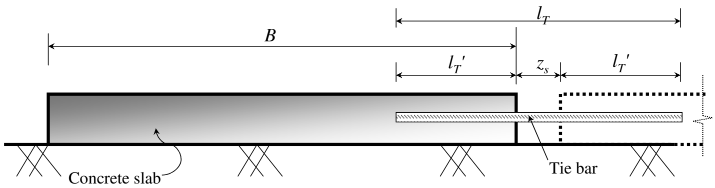

Figure 7.6: Schematic diagram of a single tie bar.

dowel bars is a fraction of the wheel load acting on the slab—the remaining load gets transmitted through the slab to the underlying layer [313].

Having obtained the maximum possible load on a single dowel bar (that is, load Q in Figure 3.4), the dowel bar can be analyzed (refer to Section 3.2 for the principles) for bending, bearing and shear, and accordingly its cross section (for a given type of steel) can be decided. The design can be finalized by varying the diameter or the spacing or both.

7.4.5 Design of tie bar

The tie bars (refer to Figure 1.2) are used for keeping two adjacent slabs tied to each other. Figure 7.6 schematically shows a single tie bar.

The strength of the tie bar should be just adequate so that it does not snap when the slab is pulled (a situation may arise due to any lateral displacement of a slab). Considering the unit length of the slab, one can write,

$$f\rho g(B \times h \times 1) = \sigma_{st}.A_{st} \tag{7.8}$$

where f= coefficient of friction between the concrete slab and the underlying layer, ρ = density of concrete material, g = gravitational acceleration, h = thickness of the concrete slab, σ_{st} = tensile strength of steel, A_{st} = area of the steel per unit length. Equation 7.8 provides the total area of steel required per unit length of the concrete slab. Further, considering the pull-out strength of a single tie bar one can write,

$$a_{st}\sigma_{st} = l'_T.2\pi a.\tau^b \tag{7.9}$$

where, a_{st} = cross sectional area of a single tie bar, l'_T is the length embedded inside one of the slabs (refer to Figure 7.6)), a = radius of the tie bar, τ^b = bond strength between the tie bar and concrete. Thus, the total length of the tie bar can be calculated as,

$$l_T = 2l'_T + z_s \tag{7.10}$$

where, z_s = gap between the two adjacent slabs.

7.5 Maintenance strategy

A pavement which is designed for a specified design period will undergo deterioration. There is a need to maintain the pavement from time to time. The maintenance strategy may involve minor maintenance, repair, or rehabilitation. It may involve recycling or may even require reconstruction. The choice of the type of maintenance and its timing is an interesting problem [287]. This is briefly introduced in the following,

Figure 7.7 shows schematic diagram of the variation of the structural health of pavement over the maintenance cycles. The beginning of each cycle may be considered to start with a maintenance activity.

Referring to a typical ith cycle (between time t^i and t^{i+1}) shown in Figure 7.7, the structural health is improved by ΔS^i (that is, the structural health is improved from S^i_S to S^i_E) due to maintenance. The cost of the maintenance (that is, Agency cost) may be

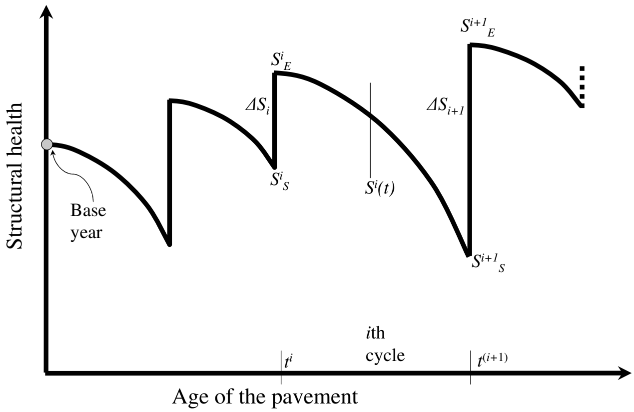

Figure 7.7: Schematic diagram showing variation of structural health of pavement over maintenance cycles.

considered as,

$$\text{Agency cost} = \Delta S^i M_c \quad \text{for } t^i < t \leq t^{i+1} \tag{7.11}$$

where M_c is the cost of maintenance for a unit of improvement of the structural health of the pavement. After each act of maintenance, the structural health will drop gradually (to S_S^{i+1}, in this case) until the next maintenance is initiated, and so on. This trend may be given by a function as [159],

$$S^i(t) = S_E^i f(t) \quad \text{for } t^i < t \leq t^{i+1} \tag{7.12}$$

One may further assume that the deterioration of the road condition causes an increase in the road users' cost (in terms of an increase in the wear and tear of tires, an increase in the consumption of fuel due to road roughness, the increase in the travel time and so on). Thus, the road users' cost can be calculated as [166, 210, 287],

$$\int_{t^i}^{t^{i+1}} S_E^i f(t') M_u dt' \quad \text{for } t^i < t \leq t^{i+1} \tag{7.13}$$

where, M_u is road users' cost. Now, one may add the agency cost and user cost to obtain the total cost, and further add these costs for all the cycles. Since these costs will be incurred at different times, one needs to consider the discounted cost for a specific base year. If the year in which the pavement is opened to the traffic is considered to be the base year (refer to Figure 7.7), then one can write the total cost as [159, 166, 287],

$$\text{TDC} = \sum_{\forall i} \left(\Delta S^i M_c e^{-rt^i} + \int_{t^i}^{t^{i+1}} S_E^i f(t') M_u e^{-rt'} dt' \right) \quad (7.14)$$

where, TDC is the total discounted cost, and r is the discount rate.

For a given road project, one may like to minimize the total discounted cost, and obtain the optimal maintenance strategy and timing for a steady-state situation [166, 197]. However, there are complexities associated with the real-life problems, for example,

- There are multiple pavement stretches in a road network and one might like to develop an optimal maintenance scheme for the entire network [159, 210], given that for each of the pavement stretches,
  - the health status may be different.
  - the deterioration trends may be different, and may not be deterministically known [48, 115]. There is an uncertainty of the predicted longevity of the pavement due to the inherent variability associated with the pavement design parameters [69, 196, 244, 272].
  - the maintenance needs of individual stretches may be different, and each stretch may have multiple maintenance alternatives [42].
  - the maintenance priorities may be different [81].
  - and so on.

- There may be constraints in terms of resources. These resource constraints may include budget, manpower, and equipment constraints [42].
- The pavement health parameters for making a decision about maintenance options [130] among preventative maintenance [220], repair, rehabilitation, recycling, or reconstruction need to be identified.
- One may like to take the energy and greenhouse gas emissions into consideration [14] while deciding from among the maintenance alternatives [170].
- and so on.

7.6 Closure

In this chapter, an overview is presented on the principles used in the structural design of pavement. Like any other design process, pavement design is also an iterative process in which the best thickness combinations are estimated from several possible design alternatives. Design alternatives arise because of choices available in the selection of layer compositions, their relative costs, and the reliability level to be achieved [231]. However, the readily available design charts and softwares provide support to a pavement designer to finalize the pavement design [1, 206, 211, 216, 217, 281, 284].

Pavement design uses the analysis (generally for static load conditions) results to obtain the predicted critical stress-strain values. For most of the distresses, failure of a pavement is a function of traffic repetition (or environmental cycles). And these are generally linked through empirical relationships and the calibration essentially depends on the local conditions [202, 282].

Given that pavement design is primarily governed by the number of traffic repetition (and not by the ultimate load bearing conditions, except for a few types of distresses) it becomes critical to understand how damage propagates due to repetition of traffic and environmental cycles for these distresses [40, 224]. Implementation of such understanding in the analysis process would eventually minimize the uncertainties in the pavement performance.

Chapter 8

Miscellaneous topics

8.1 Introduction

Some miscellaneous analyses will be discussed in this chapter. This includes the beam resting on a half-space, plates/beams resting on elastic foundations and subjected to dynamic loading, the analysis of composite pavements, reliability issues in pavement design, and the inverse problem in pavement engineering.

8.2 Plate/beam resting on a half-space

Biot [23] provided a solution on an infinite beam resting on a half-space—this is discussed here. Figure 8.1 shows an infinite beam (of a unit width) resting on a half-space, acted upon a sinusoidal loading as,

$$q = q_o \cos \kappa x \tag{8.1}$$

It can be assumed [23, 107] that this loading also produces a sinusoidal pressure distribution on the half-space, given as,

$$p = p_o \cos \kappa x \tag{8.2}$$

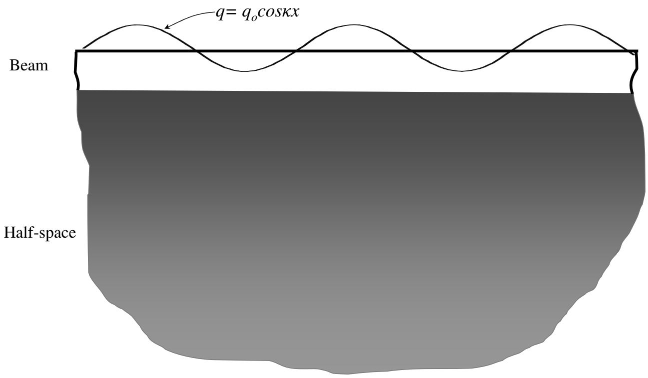

Figure 8.1: An infinite beam resting on an elastic half-space.

For the elastic half-space, the ϕ function (refer to Equation 5.10) is assumed as [23],

$$\phi = \frac{p_o}{\kappa^2} \cos \kappa x e^{-\kappa z} (1 + \kappa z) \tag{8.3}$$

The stresses can be calculated using Equation 5.9. The boundary conditions are $\sigma_{xx} = \sigma_{zz} = \tau_{xz} = 0$ for $z \to \infty$ and $\sigma_{zz} = -p_o \cos \kappa x$. Thus [23],

$$\begin{aligned} \omega = \int_0^\infty \epsilon_z dz &= \frac{1}{E} (\sigma_{zz} - \mu\sigma_{xx}) \\ &= \frac{2p_o}{E\kappa} \cos \kappa x \end{aligned} \tag{8.4}$$

where, E is the elastic modulus of the half-space. Putting the value of p_o from Equation 8.4, one obtains

$$p = \frac{1}{2} E\kappa\omega \tag{8.5}$$

The equation of the beam will be the same as in Equation 3.10. Putting Equation 8.1 and Equation 8.5 into Equation 3.10, one obtains

$$E_b I \frac{d^4\omega}{dx^4} = q_o \cos \kappa x - \frac{1}{2} E \kappa \omega \tag{8.6}$$

where E_b is the elastic modulus of the beam. The solution of the above equation is obtained as [23],

$$\omega = \frac{q_o \cos \kappa x}{E_b \kappa \left(1 + \frac{2E_b I}{E}\kappa^3\right)} \tag{8.7}$$

Thus, the deflection of an infinite beam resting on an elastic half-space due to sinusoidal loading is obtained. One can employ a suitable transformation to obtain the response due to other loading, and can refer to the Biot's paper [23] for further reading.

A number of studies are available on the analysis of plates resting on half-space. The deflection of a plate resting on a half-space acted upon by load Q uniformly distributed over a circular area of radius a is given as [113, 221, 276, 310],

$$\omega = \frac{2(1-\mu^2)}{E\pi a} \int_0^\infty \frac{Q}{m(1+m^3 l_o^3)} J_1(ma) J_0(mr) dm \tag{8.8}$$

where, $l_o^3 = \frac{2D(1-\mu^2)}{E}$, and $D =$ the flexural rigidity of the plate. Interested readers can refer to, for example, [107] for a treatise on this topic.

Dense liquid (that is, springs) and continuum (that is, half-space) are two alternative models (characterized by k and E respectively) used to represent soil subgrade. Conventionally, k is used for analysis of the concrete pavements (refer to Chapters 3 and 4) and E is used for analysis of the asphalt pavements (refer to Chapters 5 and 6), because of the mathematical compatibility with the respective equations. Researchers have opined that the actual field behavior possibly lies somewhere in between the responses predicted by these two models [91, 124]. It is argued that the k value at a point is dependent only on the vertical displacement at this point, whereas the continuum model is dependent on the wavelength (refer to Equation 8.5), therefore it involves interaction from the other parts of the medium too [23, 153]. It is interesting to examine an equivalency between E and k that may exist.

For a perfectly rigid plate of radius a acted upon by a uniform pressure q, one can write,

$$\omega = \frac{q}{k} \tag{8.9}$$

If the rigid plate rests on an elastic half-space (of elastic modulus E), where a force Q causes an average pressure[1] as q_{av} (that is $q_{av} = \frac{Q}{\pi a^2}$), the deflection can be calculated using Equation 5.32

Equating Equations 8.9 and 5.32, one obtains [249]

$$k = \frac{2E}{\pi(1-\mu^2)a} \tag{8.10}$$

One may refer to [249] for further discussions on this topic.

8.3 Plates/beams resting on an elastic foundation subjected to dynamic loading

On a pavement structure, load is applied as a pulse [9, 18]. The governing equation of a horizontal beam (Euler−Bernoulli beam) resting on an elastic foundation (represented by a lumped parameter model) subjected to a concentrated oscillating force of $Q \cos w_f$ acting at an angle of β with the horizontal line, and moving with a speed V_o (refer to Figure 8.2) can be written as,

$$\begin{aligned} EI\frac{\partial^4\omega}{\partial x^4} + \rho A\frac{\partial^2\omega}{\partial t^2} + C_d\frac{\partial^4\omega}{\partial x^4} + Q\cos(w_f t).\cos\beta\frac{d^2\omega}{dx^2} \\ = Q\cos(w_f t).\sin\beta.\partial(x - V_o t) + q* \end{aligned} \tag{8.11}$$

[1]It may be noted that the pressure distribution is expected to be non-uniform, as discussed in Section 5.3.

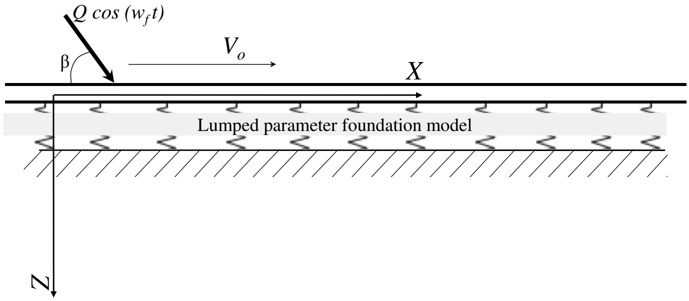

Figure 8.2: An infinite beam subjected to a moving dynamic load.

where, EI = flexural rigidity of the beam, ρ = density of the beam, A = cross-sectional area, C_d = coefficient of damping ∂ = Dirac delta function. One can see that when the load is constant (that is, $Q\cos(w_f t) = q$), vertical (that is, $\beta = 0$), and stationary (that is, $V_o = 0$), Equation 8.11 reduces to Equation 3.10. A large number of research publications are available where researchers have derived a steady-state closed-form solution of such equation; for example, solutions for

- a vertical concentrated oscillating load moving with constant speed on an infinite Euler−Bernoulli beam resting on Winkler's foundation [193].
- a vertical concentrated load of constant magnitude moving with constant speed and a constant horizontal axial load on an infinite Euler−Bernoulli beam resting on Winkler's foundation [146].
- a vertical concentrated load of constant magnitude moving with constant speed on an infinite Euler−Bernoulli beam resting on a Vlasov foundation [185] or a viscoelastic foundation [20, 264].
- a vertical concentrated load of constant magnitude moving with constant speed on an infinite Timoshenko beam resting on a viscoelastic foundation [45].

- a tandem-axle with varying amplitude moving on a plate resting on a viscous Winkler's foundation [152].

One may refer to, for example, [22] for a review, or [39, 89, 189] for a detailed discussion on this topic.

For a static concentrated vertical oscillating load of $Q\cos(w_f t)$ acting on an infinite beam resting on a Winkler's foundation, the solution is obtained as [193],

$$\omega = \frac{Q\lambda'}{2(k - A\rho\omega_f^2)} e^{-\lambda' x} \left(\cos\lambda' x + \sin\lambda' x\right) \cos(w_f t) \tag{8.12}$$

where, $\lambda' = \left(\frac{k - A\rho w_f^2}{4EI}\right)^{\frac{1}{4}}$. It is interesting to compare Equation 8.12 to Equation 3.5. From Equation 8.12 it can be shown that the amplitude becomes very large (that is, resonance occurs) when,

$$\omega_f^2 = \frac{k}{A\rho} \tag{8.13}$$

One of the ways to obtain a solution for a viscoelastic foundation is by using the elastic–viscoelastic correspondence principle briefly discussed in Section 5.4. One can refer to [84], for example, for an illustrative example of the response of an infinite Euler−Bernoulli beam resting on a viscoelastic foundation subjected to a load $F(x,t)$ along its length.

For a constant load Q moving with constant speed V_o, the deflection is obtained as [193],

$$\omega = \frac{Q}{2EI} \frac{e^{-c_2(x - V_o t)}}{2c_1 c_2 (c_1^2 + c_2^2)} \left(c_1 \cos c_1(x - V_o t) + c_2 \sin c_1(x - V_o t)\right) \tag{8.14}$$

where, c_1 and c_2 are constants expressed as functions of k, ρ, A, V_o, E and I [193]. The deflection under the load Q can be calculated by putting $x = 0$ into Equation 8.14, and it can be shown that the deflection due to load Q moving with constant speed V_o is larger than the deflection under the static load Q (refer to Equation 3.7) [193].

8.4 Analysis of composite pavements

Composite pavements are those where, in principle, any combination of asphaltic cement concrete or cemented layer can be provided anywhere within the pavement structure. Thus, the formulation will involve consideration of spring, plate, or continuum layers anywhere in the pavement structure. One may refer to [128, 153, 155] for an approach to solving such problems.

For analysis of such a pavement, the individual governing equations remain the same. That is, for a plate Equation 3.33 and for a continuum layer or half-space Equation 5.10 (or Equation 5.16 depending on the choice of coordinate) need to be used. If an ith layer is a spring, then it will be governed by (similar to Equation 2.6),

$$\sigma_{zz}^{i} = k\left(\omega^{(i-1),b} - \omega^{(i+1),t}\right) \tag{8.15}$$

Equation 5.34 can also be assumed as the ϕ function for the solution [128, 155]. In line with the deflection profile of the multi-layered structure (refer to Equation 5.41), the deflection of the plate can be expressed [128] as Equation 8.8.

The solution can be performed in the same manner as discussed in Section 5.4, and the boundary conditions can be imposed after the Henkel transformation.

For the top surface, the same boundary conditions as mentioned in Equation 5.36 hold. If the top surface is a plate, it may be noted that $\sigma_{zz}^{1,t}$ is the same parameter used as q in the expression of $q^* = q - p$ in the plate equation (that is, Equation 3.33).

The interface conditions mentioned in Section 5.4 can be used when additional boundary conditions arise; for example, for an interface between a continuum layer (the ith layer) and a plate (the

$(i+1)$th layer), the conditions can be written as [128, 153, 155],

$$
\begin{aligned}
\tau_{rz}^{i,b} &= 0 \\
\tau_{rz}^{(i+1),t} &= 0 \\
\omega^{i,b} &= \omega^{(i+1),t} = \omega^{(i+1),b}
\end{aligned}
\tag{8.16}
$$

This is because it can be assumed that shear stresses are dissipated at the boundary between the plate and the continuum layer, and the vertical deformation at the interface is equal (it also remains the same throughout the plate). If the $(i+1)$th layer is a spring instead of a plate, then the first two conditions above may be assumed to hold, and, instead of the third condition, one can write [128],

$$
\sigma_{zz}^{i} = \sigma_{zz}^{(i+1)} \tag{8.17}
$$

If two consecutive layers are plates, then these can be replaced by one equivalent plate, depending on whether the interface is smooth or rough [37, 121, 153].

8.5 Reliability issues in pavement design

The reliability of a pavement is the probability that it survives within the design period. In Section 7.4.1 estimation of $\boldsymbol{N}$ and $\boldsymbol{T}$ and their participation in pavement design has been explained. Deterministically, these parameters assume fixed values. However, variabilities in the parameters marked in the portion "C" in Figure 7.4 causes variation in the $\boldsymbol{T}$ and variabilities in the parameters marked in the portion "D" in Figure 7.4 causes variation in the $\boldsymbol{N}$. Therefore, $\boldsymbol{T}$ and $\boldsymbol{N}$ can then be represented in the form of a distribution, as shown in Figure 8.3. The distributions of $\boldsymbol{T}$ and $\boldsymbol{N}$ can be obtained analytically or numerically by simulation. One can

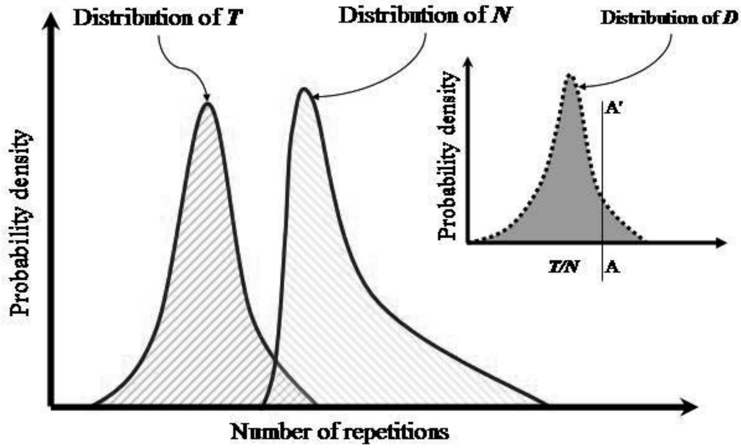

Figure 8.3: Estimation of reliability from distributions of $\boldsymbol{N}$ and $\boldsymbol{T}$.

refer to, for example [105, 183, 274], for background information on this.

It can be said that if $\boldsymbol{N}$ always assumes higher value than $\boldsymbol{T}$, then the pavement will be safe during the design period, hence reliability will be 100%. If however, there is some overlap, (as is shown in Figure 8.3), the reliability value will be lower than 100%. Recalling Equation 7.1 a term for damage ratio, $\boldsymbol{D}$ can be defined as,

$$\boldsymbol{D} = \frac{\boldsymbol{T}}{\boldsymbol{N}} \tag{8.18}$$

The reliability (R) can be defined as,

$$\begin{aligned} R &= \text{Probability}(T < N) \\ &= \text{Probability}(D < 1) \end{aligned} \tag{8.19}$$

The reliability value can be estimated from the distribution of $\boldsymbol{D}$ (refer to Figure 8.3). The distribution of $\boldsymbol{D}$ can be derived from

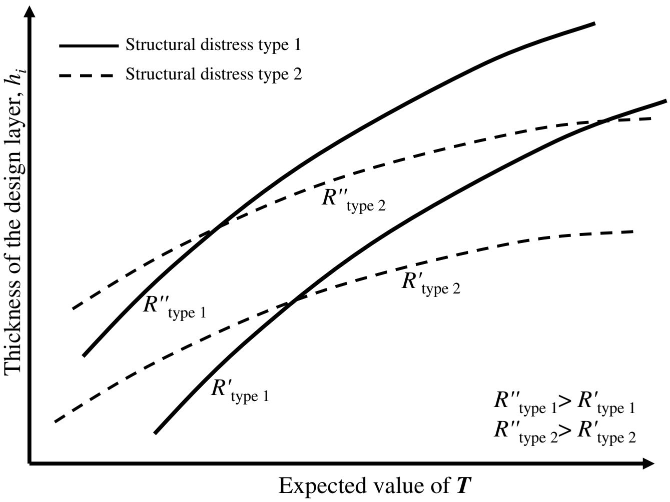

Figure 8.4: Schematic diagram of pavement design chart.

the known distributions of $\boldsymbol{T}$ and $\boldsymbol{N}$ analytically [52, 158, 230] or by simulation [59, 183, 275].

For a pavement design problem, the position of $\boldsymbol{T}$ is rather fixed, a designer can move the position of $\boldsymbol{N}$ (that is by iteratively varying the thickness) so that the reliability attains the designed reliability level. One can refer to [231] for a suggested procedure for designing a pavement for a given reliability level. It can be said that if the design reliability is increased, more thickness will be required for any given pavement layer (h_i) for a given structural distress type. This is schematically shown in Figure 8.4.

8.6 Inverse problem in pavement engineering

An analysis provides information on the expected response of the pavement. For example, for a given geometry of the pavement structure, material characteristics and the wheel loading configuration, it is possible to obtain the response of the pavement in terms of stress/strain/displacement etc. (refer to the portion marked "E" in Figure 7.3). During the structural evaluation of pavements, the reverse situation arises. For example, the pavement may be subjected to an impact load and the information about its response (in terms of the instantaneous surface deflection) may be collected, and the objective is to predict the parameters of the pavement structure. These parameters may include the layer thicknesses, the physical (for example, density, thermal conductivity etc.) and mechanical (for example, material constants needed to describe the constitutive behavior) properties of the individual layers. This is an example of an inverse problem in pavements. The response typically contains mixed-up information of all the layers: so the task is to decipher the individual properties of the each layer.

Typically, an inverse problem (also known as back-calculation) algorithm involves (i) assuming of initial values for the unknown parameters and performing analysis (that is, forward calculation), (ii) comparing the analysis results with the field observations and (iii) revising the trial values of the unknown parameters for the next iteration, until the observed and calculated analyses results become comparable (in terms of any suitable error function), and subsequently convergence is said to have achieved. Figure 8.5 provides a schematic diagram explaining this approach.

For an idealized multi-layered structure, theories have been formulated to predict the response due to static (as discussed in Sections 5.4 and 3.4) and dynamic load (refer Section 8.3), due to propagation of elastic [80] or eletromagnetic waves [36] and so on.

Various optimization (classical and evolutionary) schemes are suggested in order to perform iteration and subsequent finalization of unknown parameters. The complexity (in terms of problem formulation, convergence, computational time, etc.) increases as the number of unknowns increases. For example, it is more difficult to back-calculate the parameters for the non-linear constitutive models of the individual pavement layers of a n layered structure, than to obtain, (say) the elastic moduli of a pavement structure

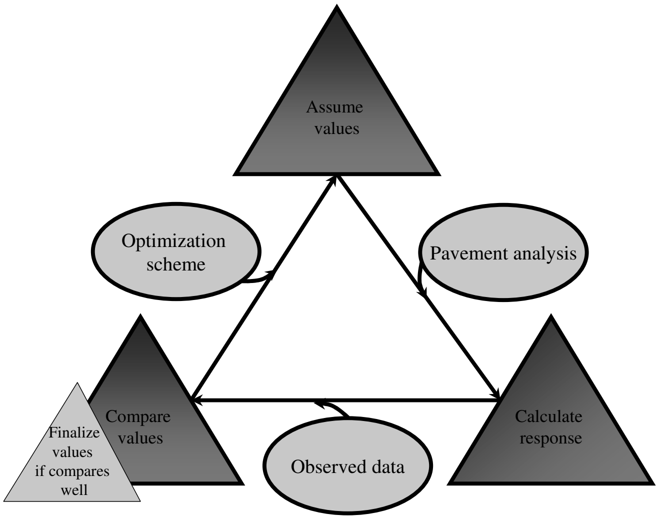

Figure 8.5: Schematic diagram explaining an approach to solve the inverse problem in the structural evaluation of pavements.

made with two homogeneous isotropic continuum layers. Clearly, inverse solutions are quite straightforward when closed form analysis results are available (for example, refer to Equations 3.5, 5.29 etc.), and may not involve any iteration.

With an assumed pavement structure with known material properties and an associated theory, it is generally possible to uniquely obtain the predicted response within the framework of idealizations involved; however, the reverse is not true. The solution to an inverse problem may give rise to non-uniqueness [90], that is, multiple answers are possible within the permissible error-band.

8.7 Closure

Basic formulations for the estimation of load and thermal stress in concrete and asphalt pavements are dealt with in this book. The analyses involved a number of idealizations. Most of the time it has been assumed that the pavement materials behave like a linear, homogeneous elastic structure, that interface conditions are either perfectly smooth or rough (fully bonded), that load is static, that the life of the pavement can be predicted from initial stress-strain conditions, that relative damage is linearly accumulative, and so on. However, pavement materials behave in a more complex way than what are generally considered in idealized analysis schemes, and the propagation of pavement distresses are more complex a phenomena than what are generally considered in routine design processes [60].

Obtaining a closed-form solution for analysis of a pavement structure is not always easy because of the involvement of multiple layers in the formulation. The difficulty level increases further, when simplified assumptions on geometry, loading and material properties are replaced with more realistic ones. This can be handled by invoking advanced numerical methods. A number of 3-D finite element formulations have been developed for analyses [49, 64, 103, 121, 125, 271, 317] of pavement structures. Efforts are being made to develop a comprehensive model of pavement which can simulate deformation, damage, healing, and so on [79, 190]. Further, it is important to validate the analysis' results from field studies through appropriate instrumentation. Significant initiatives have also been undertaken in this direction [21, 77, 121, 122, 173, 312].

The gap between the theoretical and experimental results is gradually reducing through advanced modeling and instrumentation. This will eventually bring down the level of uncertainty. Researchers are trying to understand the pavements better.

This page intentionally left blank

References

[1] AASHTO Guide for design of pavement structures, American Association of State Highway and Transportation Officials, Washington, D. C., 1993.

[2] AASHTO-T321, Standard test method for determination of fatigue life of compacted hot mix asphalt (HMA) subjected to repeated flexural bending, AASHTO, Washington, D. C., 2007.

[3] AASHTO T307-99, Standard method for test for determining the resilient modulus of soils and aggregate materials, 2007, Washington, D. C.

[4] AASHTO TP 79-10, Standard method of test for determining dynamic modulus and flow number for hot mix asphalt using the asphalt mixture performance tester (AMPT), AASHTO, Washington, D.C., 2010.

[5] ACI Committee 318, Building code requirements for structural concrete and commentary, American Concrete Institute, 2008.

[6] Acum, W. E. A., and Fox, L., Computation of load stresses in a three-layered elastic system, *Geotechnique*, 2(4), 1951, pp. 293-300.

[7] Al-Qadi, I. L., Hassan, M. M., and Elseifi, M. A., Field and theoretical evaluation of thermal fatigue cracking in

flexible pavements, *Transportation Research Record*, 1919, TRB, Washington, D.C., 2005, pp.87-95.

[8] Al-Qadi, I. L., Nassar, W.N., Fatigue shift factors to predict HMA performance, *International Journal of Pavement Engineering*, 4 (2) , 2003, pp. 69-76.

[9] Al-Qadi, I. L., Xie, W., and Elseifi, M. A., Frequency determination from vehicular loading time pulse to predict appropriate complex modulus in MEPDG, *Journal of Association of Asphalt Paving Technologists*, 77, 2008, pp.739-772.

[10] Aragão, F., Kim, Y., Lee, J., and Allen, D., Micromechanical model for heterogeneous asphalt concrete mixtures subjected to fracture failure, *Journal of Materials in Civil Engineering*, 23, Special issue: Multiscale and Micromechanical Modeling of Asphalt Mixes, 2011, pp.30-38.

[11] Armedakàs, A. E., *Advanced Mechanics of Materials and Advanced Elasticity*, CRC Press, Taylor & Francis Group, 2006.

[12] Asbahan, R. E., and Vandenbossche, J. M., Effects of temperature and moisture gradients on slab deformation for jointed plain concrete pavements, *Journal of Transportation Engineering*, 137(8), 2011, pp.563-570.

[13] Asphalt overlays for highway and street rehabilitation, Manual Series No. 17, Asphalt Institute, 1983.

[14] Aurangzeb, Q., Al-Qadi, I. L., Ozer, H., and Yang, R., Hybrid life cycle assessment for asphalt mixtures with high RAP content, *Resources, Conservation and Recycling*, 83, 2014, pp.77-86.

[15] Baburamani, P., Asphalt fatigue life prediction models - a literature review, Australian Road Research Bureau, Report no. 334, Vermont South, 1999.

[16] Balbo, J. T., and Severi, A. A., Thermal gradients in concrete pavements in tropical environment:experimental appraisal, *Transportation Research Record*, 1809, TRB, Washington, D. C., 2002, pp.12-22.

[17] Bandyopadhyaya, R., Das, A. and Basu, S., Numerical simulation of mechanical behaviour of asphalt mix, *Construction & Building Materials*, 22(6), 2008, pp.1051-1058.

[18] Barksdale, R. G., Compressive stress pulse times in flexible pavements for use in dynamic testing, *Highway Research Record*, 345, HRB, 1971, pp.32-44.

[19] Bari, J., and Witczak, M. W., Development of a new revised version of the Witczak E* predictive model for hot mix asphalt mixtures, 2006, *Journal of Association of Asphalt Paving Technologists*, 75, pp.381-423.

[20] Basu, D., and Rao, N. S. V. K., Analytical solutions for Euler-Bernoulli beam on viscoelastic foundation subjected to moving load, *International Journal for Numerical and Analytical Methods in Geomechanics*, 37, 2013, pp.945-960.

[21] Bayat, A., Knight, M. A., and Soleymani, H. R., Field monitoring and comparison of thermal- and load-induced strains in asphalt pavement, *International Journal of Pavement Engineering*, 13(6), 2012, pp.508-514.

[22] Beskou, N. D., and Theodorakopoulos, D. D., Dynamic effects of moving loads on road pavements : a review, *Soil Dynamics and Earthquake Engineering*, 31(4), 2011, pp.547-567.

[23] Biot, M. A., Bending of an infinite beam on an elastic foundation, *Journal of Applied Mechanics*, 1937, pp.A-1-A-7.

[24] Boley, B. A., and Weiner, J. H., *Theory of Thermal Stresses*, John Wiley & Sons, Inc., 1960.

[25] Bordelon, A., Roesler, J., and Hiller, J., Mechanistic-empirical design concepts for joined plain concrete pavements in Illinois, Research Report ICT-09-052, Illinois Center for Transportation, 2009.

[26] Boyce, H. R., A non-linear model for the elastic behaviour of granular materials under repeated loading, *Proceedings of International Conference on Soils under Cyclic and Transient Loading*, Swensea, 1980, pp.285-194.

[27] Bradbury, R. D., Design of joints in concrete pavements, *Proceedings of Highway Research Board*, 12, 1932, pp.105-141.

[28] Bradbury, R. D., Reinforced concrete pavement, Wire Reinforcement Institute, Washington, D. C., 1938, pp.34-41.

[29] Brown, S. F., and Pappin, J. W., Analysis of pavement with granular bases, *Transportation Research Record*, 810, TRB, Washington, D.C., 1981, pp.17-22.

[30] Brown, S. F., and Pappin, J. W., Modelling of granular materials in pavements, *Transportation Research Record*, TRB, Washington, D.C., 1022, 1985, pp.45-51.

[31] Brown, S. F., and Pell, P. S., An experimental investigation of the stresses, strains and deflections in a layered pavement structure subjected to dynamic loads, *Proceedings of 2nd International Conference of Structural Design of Asphalt Pavements*, 1967, pp.487-504.

[32] Brown, S. F., and Pell, P. S., A fundamental structural design procedure for flexible pavements, *Proceedings of 3rd International Conference of Structural Design of Asphalt Pavements*, Vol. I, 1972, pp.369-381.

[33] Burmister, D. M.,The theory of stress and displacements in layered systems and applications to the design of airport runways, Highway Research Board, 23, 1943, pp.126-144.

[34] Burmister, D. M., Stresses and displacements in elastic layered Systems. *Proceedings of 2nd International Conference on Structural Design of Asphalt Pavements*, University of Michigan, Ann Arbor, 1945, pp.277-290.

[35] Burmister, D. M., The general theory of stresses and displacements in layered soil systems, I, II, and III. *Journal of Applied Physics*, 16. 1945, pp. 84-94 (I), 126-127 (II), 296-302 (III).

[36] Carcione, J. M., Ground-penetrating radar: wave theory and numerical simulation in lossy anisotropic media, *Geophysics*, 61(6), 1996, pp.1664-1677.

[37] Cauwelaert, F. V., Pavement design and evaluation: the required mathematics and its applications, Editor: Stet, M., Federation of Belgian Cement Industry, http://www.pavers.nl/pdf/The%20Required%20Mathematics.pdf, 2003, last accessed February 2014.

[38] Cauwelaert, V. F., Stet, M., Jasienski, A., The general solution for a slab subjected to centre and edge loads and resting on a Kerr foundation, *International Journal of Pavement Engineering*, 3(1), 2002, pp.1-18.

[39] Cebon, D., *Handbook of Vehicle-Road Interaction*, Swets & Zeitlinger, B. V., Lisse, the Netherlands, reprinted 2000.

[40] Cebon, D., Vehicle generated road damage - a review, *Vehicle System Dynamics*, 18(1-3), 1989, pp.107-150.

[41] Ceylan, H., Schwartz, C. W., Kim, S., and Gopalakrishnan, K., Accuracy of predictive models for dynamic modulus of hot-mix asphalt, *Journal of Materials in Civil Engineering*, 21(6), 2009, pp.286-293.

[42] Chakroborty, P., Agarwal, P. K., and Das, A., Comprehensive pavement maintenance strategies for road network through optimal allocation of resources, *Transportation Planning and Technology*, 35(3), 2012, pp.317-339.

[43] Chiasson, A., Yavuzturk, C., and Ksaibati, K., Linearized approach for predicting thermal stresses in asphalt pavements due to environmental conditions, *Journal of Materials in Civil Engineering*, 20(2), 2008, pp.118-127.

[44] Chen, G., and Baker, G., Analytical model for predication of crack spacing due to shrinkage in concrete pavements, *Journal of Structural Engineering*, 130(10), 2004, 1529-1533.

[45] Chen, Y. H., Huang, Y. H., Shih, C. T., Response of an infinite Timoshenko beam on a viscoelastic foundation to a harmonic moving load, *Journal of Sound and Vibration*, 241(5), 2001, pp.809-824.

[46] Chen, E. Y. G., Pan, E., and Green, R., Surface loading of a multilayered viscoelastic pavement: semianalytical solution, *Journal of Engineering Mechanics*, 135(6), 2009, pp.517-528.

[47] Chen, J-S, Lin, C-H, Stein, E., Horthan, J., Development of a mechanistic-empirical model to characterize rutting in flexible pavements, *Journal of Transportation Engineering*, 130(4), 2004, pp.519-525.

[48] Chootinan, P., Chen, A., Horrocks, M. R. and Bolling, D., A multi-year pavement maintenance program using a stochastic simulation-based genetic algorithm approach. *Transportation Research Part A*: *Policy and Practice*, 40 (7), 2005, pp.725-743.

[49] Choubane, B., and Tia, M., Nonlinear temperature gradient effect on maximum warping stresses in rigid pavements, *Transportation Research Record* 1370, TRB, Washington, D.C., 1992, pp.11-19.

[50] Choubane, B., and Tia, M., Analysis and verification of thermal gradient effects on concrete pavement, *Journal of Transportation Engineering*, 121(1), 1995, pp.75-81.

[51] Christensen, R.M., *Theory of Viscoelasticity: An Introduction*, 2nd edition, New York, Academic Press, 1982.

[52] Chua, K. H., Kiureghian, A. D., and Monismith, C. L., Stochastic model for pavement design, *Journal of Transportation Engineering*, 118(6), 1992, pp.769-786.

[53] Claussen, A. I. M., Edwards, J. M., Sommer, P., and Uge, P., Asphalt pavement design - the Shell method, *Proceedings of 4th International Conference of Structural Design of Asphalt pavements*, Vol.1, 1977, pp.39-74.

[54] Collop, A. C., Cebon, D., and Hardy, M. S. A., Viscoelastic approach to rutting in flexible pavements, *Journal of Transportation Engineering*, 121(1), 1995, pp.39-74.

[55] Costanzi, M., and Cebon, D., Generalized phenomenological model for the viscoelasticity of idealized asphalts, *Journal of Materials in Civil Engineering*, 26(3), 2014, pp.399-410.

[56] DAMA Computer Program, Pavement structural analysis using multi-layered elastic theory, User's manual, Asphalt Institute, 1983.

[57] Daniel, J. S., and Kim, Y. R., Development of simplified fatigue test and analysis procedure using a viscoelastic continumm damage model, *Journal of the Association of Asphalt Paving Technologists*, 71, 2002, pp.619-650.

[58] Darter, M. I., Hudson, W. R., and Brown, J. L., Statistical variation of flexible pavement properties and their consideration in design, *Proceedings of Association of Asphalt Paving Technologists*, 42, 1973, pp.589-615.

[59] Darter, M., Khazanovich, L., Yu, T. and Mallela, J., Reliability analysis of cracking and faulting prediction in the new mechanistic-empirical pavement design procedure, *Transportation Research Record*, No. 1936, TRB, Washington, D.C., 2005, pp.150-160.

[60] Das, A., A reliable design of asphalt pavement from structural considerations, Editor's Corner, *International Journal of Pavement Research and Technology*, 2(1), 2009, p.IV.

[61] Das, A. and Pandey, B. B., Mechanistic-empirical design of bituminous roads: an Indian perspective, *Journal of Transportation Engineering*, 1999, 125(5), pp.463-471.

[62] Daloglu, A. T., and Girijia, C. V., Values of k for slab on Winkler foundation, *Journal of Geotechnical and Geoenvironmental Engineering*, 126(5), 2000, pp.463-471.

[63] Das, B. M., *Advanced Soil Mechanics*, Taylor & Francis, 3rd edition, 2008.

[64] Davids, W. G., Turkiyyah, G. M., and Mohoney, J., EverFE - rigid pavement finite analysis tool, *Transportation Research Record*, 1629, TRB, Washington, D. C., 1998, pp.41-49.

[65] Davis, R. O., and Selvadurai, A. P. S., *Elasticity and Geomechanics*, Cambridge University Press, 1996.

[66] De Jong, D. L., Peatz, M. G., Korswagen, A. R., Computer program BISER, layered systems under normal and tangential loads, External Report AMSR.0006.73, Koninklijke/ Shell-Laboratorium, Amsterdam, Netherlands.

[67] Deacon, J. A., Fatigue of asphalt concrete, Ph.D. thesis, University of California, Berkeley, 1963.

[68] Dempsey, B. J., Herlache, W. A., and Patel, A. J., Climatic-materials-structural pavement analysis program, *Transportation Research Record*, 1095, TRB, Washington, D. C., 1986, Washington, D. C., pp.111-123.

[69] Despande, V. P., Damnjanvic, I. D., Gardoni, P., Reliability-based optimization models for scheduling pavement rehabilitation, *Computer-Aided Civil and Infrastructure Engineering*, 25, 2010, pp.227-237.

[70] Di Benedetto, H., Roche, de la C, State of the art of stiffness modulus and fatigue of bituminous mixtures, RILEM Report 17, Bituminous binders and mixes, edited by Francken, L., pp.137-180.

[71] Di Benedetto, H., Neifer, C., Suzeat, C., and Olard, F., Three dimensional thermo viscoplastic behaviour of bituminous materials: the DBN model, *International Journal of Road Materials and Pavement Design*, 8(2), 2007, pp.285-316.

[72] Diefenderfer, B. K., Al-Qadi, I. L., and Diefenderfer, S. D., Model to predict pavement temperature profile: development and validation, *Journal of Transportation Engineering*, 132(2), 2006, pp.162-167.

[73] Dinev, D., Analytical solution of beam on elastic foundation by singularity functions, *Engineering Mechanics*, 19(6), 2012, pp.381-392.

[74] Dorman, G. M., The extension to practice fundamental procedure for design of flexible pavements, *Proceedings of 1st International Conference of Structural Design of Asphalt Pavements*, Ann Arbor, Michigan, 1962, pp.785-793.

[75] Dunlap, W. S., A report on a mathematical model describing the deformation characteristics of granular materials. Technical Report 1, Project No. 2-8-62-27, Texas Transportation Institute, Texas A & M University, 1963.

[76] Dunhill, S. T., Airey, G. D., Collop, A. C. and Scarpas, A., Advanced constitutive modelling of bituminous materials, *International Journal of Pavement Engineering*, 7(3), 2006, pp.153-165.

[77] Elseifi, M. A., Al-Qadi, I. L., and Yoo, P. J., Viscoelastic modeling and field validation of flexible pavement, *Journal of Engineering Mechanics*, 132(2), 2006, pp.172-178.

[78] Epps, A., Design and analysis system for thermal cracking in asphalt concrete, *Journal of Transportation Engineering*, 126(4), 2000, pp.300-307.

[79] Eslaminia, M., Thirunavukkarasu, S., Guddati, M. N., Kim, Y. R., Accelerated Pavement Performance Modeling Using Layered Viscoelastic Analysis, *7th RILEM International Conference on Cracking in Pavements*, RILEM Bookseries, 4, 2012, pp.497-506.

[80] Ewing, W. M., and Jardetzky, W. S., and Presss, F., *Elastic Waves in Layered Media*, McGraw-Hill Book Company, 1957.

[81] Farhan, J. and Fwa, T. F., Incorporating priority preferences into pavement maintenance programming, *Journal of Transportation Engineering*, 138(6), 2012, pp.714-722.

[82] Fatemi, A., and Yang, L., Cumulative fatigue damage and life prediction theories: a survey of the state of the art for homogeneous materials, *International Journal of Fatigue*, 20(1), 1998, pp.9-34.

[83] Federal Aviation Administration (FAA), Advisory Circular 150/5320-6E, Airport pavement design and evaluation, 2009, http://www.faa.gov/airports/engineering/pavement_design/, last accessed February 12, 2014.

[84] Findley, W. N, Lai, J. S., and Onaran, K. *Creep and Relaxation of Nonlinear Viscoelastic Materials with an Introduction to Linear Viscoelasticity*, Dover Publications, Inc., 1989, New York.

[85] Francken, L., and Clauwaert, C., Characterization and structural assessment of bound materials for flexible bound structures, *Proceedings of the 6th International Conference on Structural Design of Asphalt Pavements*, University of Michigan, Ann Arbor, 1987, pp.130-144.

[86] French design manual for pavement structures, Guide Technique, LCPC and SETRA, Union Des Synducates, DeLindustrie Routiere, France, 1997.

[87] Friberg, B. F., Load and Deflection Characteristics of Dowels in Transverse Joints of Concrete Pavements, *Proceedings of the Highways Research Board*, 18, National Research Council, Washington, D.C., 1938, pp. 140-154.

[88] Friberg, B. F., Design of dowels in transverse joints of concrete pavements, *Transactions of ASCE*, 105, pp.1076-1095, 1940.

[89] Fryba, L., *Vibrations of Solids and Structures under Moving Load*, Thomas Telford Ltd., London, 1999.

[90] Fwa, T. F. and Setiadji, B. H., Evaluation of backcalculation methods for nondestructive determination of concrete pavement properties, *Transportation Research Record*, 1949, TRB, Washington, D. C., 2007, pp.75-82.

[91] Fwa, T. F. and Setiadji, B. H., Backcalculation analysis of rigid pavement properties considering presence of subbase layer, TRB 87th Annual Meeting Compendium of Papers DVD, Paper No.08-0434, 2008.

[92] Fwa, T. F., Shi, X. P., and Tan, S. A., Analysis of concrete pavements by rectangular thick plate method, *Journal of Transportation Engineering*, 122(2), 1996, pp.146-154.

[93] Fwa, T. F. and Tan, S. A., $C-\phi$ characterization model for design of asphalt mixtures and asphalt pavements, *ASTM Special Technical Publication*, 1469, 2006, pp.113-126.

[94] Garber, N. J., and Hoel, L. A., *Traffic and Highway Engineering*, West Publishing Company, St. Paul, 2009.

[95] Genin, G. and Cebon, D., Failure mechanism in asphalt concrete. *International Journal of Road Materials and Pavement Design*, 1(4), 2000, pp.419-450.

[96] Ghuzlan, K. A., Carpenter, S. H., Energy-derived, damage-based failure criterion for fatigue testing. *Transportation Research Record*, 1723, TRB, Washington, D. C., 2000, pp.141-149.

[97] Gibson, R. E., The analytical method in soil mechanics, *Géotechnique*, 24(2), 1974, pp.115-140.

[98] Gillespie, T. D., Karamihas, S. M., Cebon, D., Sayers, M. W., Nasim, M. A., Hansen, W., Ehsan, N., Effects of heavy vehicle characteristics on pavement response and performance, UMTRl 92-2, The University of Michigan, 1992.

[99] Gould, P. L., *Introduction to Linear Elasticity*, Second Edition, Springer, 1994.

[100] Gui, J., Phelan, P. E., Kaloush, K. E., Golden, J. S., Impact of pavement thermophysical properties on surface temperatures, *Journal of Materials in Civil Engineering*, 19(8), 2007, pp.683-690.

[101] Haider, S. W., Harichandran, R. S., and Dwaikat, M. B., Closed-form solutions for Bimodal Axle Load Spectra and relative pavement damage estimation, *Journal of Transportation Engineering*, 135(12), 2009, pp.974-983.

[102] Hall, K. T., Darter, M. I., Kuo, C. M., Improved methods for selection of k value for concrete pavement design, *Transportation Research Record*, 1505, TRB, Washington, D. C., 1995, pp.128-136.

[103] Harichandran, R. S., Yeh, M. S. and Baladi, G. Y., MICH-PAVE: A nonlinear finite element program for analysis of pavements. *Transportation Research Record*, 345, TRB, Washington, D. C. 1971, pp.15-31.

[104] Harr, M. E., *Foundations of Theoretical Soil Mechanics*, McGraw-Hill Inc, 1966.

[105] Harr, M. E., *Reliability Based Design in Civil Engineering*, McGraw-Hill Book Company, New York, 1987.

[106] Hausman, M. R., *Engineering Principles of Ground Modification*, McGraw Hill, 1990.

[107] Hemsley, J. A, *Elastic Analysis of Raft Foundations*, Thomas Telford. 1998.

[108] Hermansson, Å., Mathematical model for calculation of pavement temperatures : comparison of calculated and measured temperatures, *Transportation Research Record*, 1764, TRB, Washington, D. C., 2001, pp.180-188.

[109] Hetényi, M., *Beams on Elastic Foundation*, Ann Arbor, The University of Michigan Press, 11th Printing, 1979.

[110] Hicks, R. G. and Monismith, C. L., Factors influencing the resilient properties of granular materials, *Highway Research Record*, 345, HRB, National Research Council, Washington, D. C., 1971, pp.15-31.

[111] Hiltunen, D. R., and Roque, R., A mechanistic-based prediction model for thermal cracking of asphalt concrete pavements. *Proceedings of Association of Asphalt Paving Technologists*, 63, 1994, pp.81-108.

[112] Hoare, T. R. and Hesp, S. A. M., Low temperature fracture testing of asphalt binders, *Transportation Research Record*, 1728, TRB, Washington D.C., 2000, pp.36-42.

[113] Hogg, A. H. A., Equilibrium of a thin plate, symmetrically loaded, resting on an elastic foundation of infinite depth, *Philosophical Magazine*, Series 7, 25, 1938, pp.576-582.

[114] Hong, A. P., Li, Y. N., and Bažant, Z. P., Theory of crack spacing in concrete pavements, *Journal of Engineering Mechanics*, 123(3), 1997, pp.267-275.

[115] Hong, H. P., and Wang, S. S., Stochastic modeling of pavement performance, *International Journal of Pavement Engineering*, 4(4), 2003, pp.235-243.

[116] Horonjeff, R., and Mckelvey, F. X., Sproule, W. J., and Young, S. B., *Planning and Design of Airports*, McGraw-Hill Book Company, 5th edition, 2010.

[117] Horvath, J. S., Modulus of subgrade reaction: new perspective, *Journal of Geotechnical Engineering*, 109(12), 1983, pp.1591-1596.

[118] Hou, Y., Wang, L., Pauli, T., and Sun, W., An Investigation of asphalt self-healing mechanism using phase-field model, *Journal of Materials in Civil Engineering*, doi:10.1061/(ASCE)MT.1943-5533.0001047.

[119] Hu, S., Zhou, F., and Scullion, T., Development, calibration, and validation of a new M-E rutting model for HMA overlay design and analysis, *Journal of Materials in Civil Engineering*, 23(2), 2011, pp.89-99.

[120] Huang, Y. H., Finite element analysis of slabs on elastic solids, *Journal of Transportation Engineering*, 100(2), 1974, pp.403-416.

[121] Huang, Y. H., *Pavement Analysis and Design*, Pearson Prentice Hall, 2nd Edition, 2004 Englewood Cliffs, New Jersey.

[122] Hugo, F., and Martin, A. L. E., Significant findings from full-scale accelerated pavement testing, NCHRP Synthesis 325, Transportation Research Board, Washington, D. C., 2004.

[123] Hugo, F., Strauss, P. J., Marais, G. P., and Kennedy, T. W., Four asphalt pavement case studies using a mechanistic approach, *Proceedings of 5th International Conference on the Structural Design of Asphalt Pavements*, Delft, 1982, pp.275-284.

[124] Ioannides, A. M., Concrete pavement analysis: the first eighty years, *International Journal of Pavement Engineering*, 7(4), 2006, pp.233-249.

[125] Ioannides, A. M., and Donnelly, J. P., Three-dimensional analysis of slab on stress dependent foundation, *Transportation Research Record*, 1196, TRB, Washington D. C., 1988, pp.72-84.

[126] Ioannides, A. M., and Hammons, M. I., Westergaard-type solution for edge load transfer problem, *Transportation Research Record*, 1525, TRB, Washington D. C., 1996, pp.28-34.

[127] Ioannides, A. M., and Khazanovich, L. Nonlinear temperature effects on multilayered concrete pavements. *Journal of Transportation Engineering*, 124(2), 1998, pp.128-136.

[128] Ioannides, A. M., and Khazanovich, L., General formulation for multilayered pavement systems, *Journal of Transportation Engineering*, 124(1), 1998, pp.82-90.

[129] Ioannides, A. M., Stress prediction for cracking of jointed plain concrete pavements, 1925-2000 - an overview, *Transportation Research Record*, 1919, TRB, Washington D. C., 2005, pp.47-53.

[130] Irfan, M., Khurshid, M. B., Bai, Q., Labi, S., and Morin, T. L., Establishing optimal project-level strategies for pavement maintenance and rehabilitation - a framework and case study, *Engineering Optimization*, 44(5), 2012, pp.565-589.

[131] IRC:37-2012, *Guidelines for the Design of Flexible Pavements*, 3rd Revision, Indian Roads Congress, New Delhi, 2012.

[132] IRC:58-2011, *Guidelines for the Design of Plain Jointed Rigid Pavements for Highways*, 3rd Revision, Indian Roads Congress, New Delhi, 2011.

[133] IRC:81-1997, *Guidelines for Strengthening of Flexible Pavements Using Benkelman Beam Deflection Technique*, Indian Roads Congress, New Delhi, 1997.

[134] Jaeger, L. G., *Elementary Theory of Elastic Plates*, Pergamon Press, 1964.

[135] Jones, A., Tables of stresses in three-layer elastic systems, HRB Bulletin, 342, 1962.

[136] Jones, G. P., *Analysis of Beams on Elastic Foundation: Using Finite Difference Theory*, ICE Publishing, UK, 1997.

[137] Jones, R., and Xenophontos, J., The Vlasov foundation model, *International Journal of Mechanical Sciences*, 19, 1977, pp.317-323.

[138] Johnson, K. L., *Contact Mechanics*, Cambridge University Press, Cambridge, 1985.

[139] Jumikis, A. R., *The Frost Penetration Problem in Highway Engineering*, Rutgers University Press, New Brunswick, New Jersey, 1955.

[140] Jumikis, A. R., *Theoretical Soil Mechanics*, Van Nostrand Reinhold, New York, 1969.

[141] Kassem, E., Grasley, Z. C.,Masad, E., Viscoelastic Poissons ratio of asphalt mixtures, *International Journal of Geomechanics*, 13(2), 2013, pp.162-169.

[142] Kausel, E., Early history of soil-structure interaction, *Soil Dynamics and Earthquake Engineering*, doi:10.1016/j.soildyn.2009.11.001.

[143] Kenis, W. J., Predictive design procedure. VESYS users manual. An interim design for flexible pavements using VESYS structural subsystem, FHWA-RD-77-154, Federal Highway Administration, U.S. Department of Transportation, 1978.

[144] Kerr, A. D., Elastic and viscoelastic foundation models, *Journal of Applied Mechanics*, 1964, 31, pp.491-498.

[145] Kerr, A. D., A study of a new foundation model, *Acta Mech*, 1965, 2, pp.135-147.

[146] Kerr, A. D., The continuously supported rail subjected to an axial force and a moving load, *International Journal of Mechanical Science*, 1972. 14, pp. 71-78.

[147] Kerr, A. D., and Kwak, S. S., The semi-infinite plate on a Winkler base, free along the edge, and subjected to a vertical force, *Archive of Applied Mechanics*, 63, 1993, pp.210-218.

[148] Kim, J., General viscoelastic solutions fo multilayered systems subjected to static and moving loads, *Journal of Materials in Civil Engineering*, 2011, 23(7), pp.1007-1016.

[149] Kim, Y. R., *Modeling of Asphalt Concrete*, McGraw-Hill Construction, ASCE Press, 2009.

[150] Kim, Y. R., Allen, D. H., and Little, D. N., Damage-induced modelling of asphalt mixtures through computational micromechanics and cohesive zone fracture, *Journal of Materials in Civil Engineering*, 17(5), 2005, pp.477-484.

[151] Kim, Y. R., Little, D. N., and Lytton, R. L., Fatigue and healing characterization of asphalt mixtures, *Journal of Materials in Civil Engineering*, 15(1), 2003, pp.75-83.

[152] Kim, S-M., and McCullough, B. F. Dynamic response of plate on viscous Winkler foundation to moving loads of varying amplitude, *Engineering Structures*, 25, 2003, pp.1179-1188.

[153] Khazanovich, L., Structural analysis of multi-layered concrete pavement systems, PhD thesis, University of Illinois at Urbana-Champaign, 1994.

[154] Khazanovich, L., and Wang, Q., MnLayer high-performance layered elastic analysis program, *Transportation Research Record*, 2037, TRB, Washington, D. C., 2007, pp.63-75.

[155] Khazanovich, L., and Ioannides. A. M., DIPLOMAT: an analysis program for both bituminous and concrete pavements, *Transportation Research Record* 1482, TRB, Washington, D.C., 1994, pp.52-60.

[156] Krishnan, J. M., and Rajagopal, K. R., Review of the uses and modeling of bitumen from ancient to modern times, *Applied Mechanics Review*, 56(2), 2003, pp.149-214.

[157] Krishnan, J. M., Rajagopal, K. R., Masad, E., and Little, D. N., Thermomechanical framework for the constitutive modeling of asphalt concrete, *International Journal of Geomechanics*, 6(1), 2006, pp.36-45.

[158] Kulkarni, R. B., Rational approach in applying reliability theory to pavement structural design, *Transportation Research Record*, 1449, TRB, Washington, D. C., 1994, pp.13-17.

[159] Labi, S., and Sinha, K. C., Life-cycle evaluation of flexible pavement preventive maintenance, *Journal of Transportation Engineering*, 131(10), 2005, pp.744-751.

[160] Lade, P. V. and Nelson, R. B., Modelling the elastic behahiour of granular materials, *International Journal for Numerical and Analytical Methods in Geomechanics*, 11, 1987, pp.521-542.

[161] Lakes, R. S., *Viscoelastic Solids*, CRC Press, 1999.

[162] Lancellotta, R., *Geotechnical Engineering*, 2nd English Edition, Taylor & Francis, 2009.

[163] Lekarp, F., Isacsson, U., and Dawson, A., State of the art. I : resilient response of unbound granular aggregates, *Journal of Transportation Engineering*, 126(1), 2000, pp.66-75.

[164] Lekarp, F., Isacsson, U., and Dawson, A., State of the art - II: permanent strain response of unbound aggregates, *Journal of Transportation Engineering*, 126(1), 2000, pp.76-83.

[165] Levenberg, E., Analysis of pavement response to subsurface deformations, *Computers and Geotechnics*, 50, 2013, pp.79-88.

[166] Li, Y., and Madanat, S., A steady-state solution for the optimal pavement resurfacing problem, *Transportation Research Part A: Policy and Practice*, 2002, 36(2), 525-535.

[167] Li, D., and Selig, E. T., Resilient modulus for fine-grained subgrade soils, *Journal of Geotechnical Engineering*, 120 (6), 1994, pp.939-957.

[168] Liang, R. Y., and Niu, Y-Z, Temperature and curling stress in concrete pavements: analytical solutions, *Journal of Transportation Engineering*, 1998, 124(1), pp.91-100.

[169] Little, D. N., and Nair, S., Recommended practice for stabilization of subgrade soils and base materials, Web-only document 144, NCHRP, Transportation Research Board, 2009.

[170] Liu, X., Cui, Q., Schwartz, C., Greenhouse gas emissions of alternative pavement designs: framework development and illustrative application, *Journal of Environmental Management*, 132 2014, pp.313-322.

[171] Liu, W., and Fwa, T. F., Nine-slab model for jointed concrete pavements, *International Journal of Pavement Engineering*, 8(4), 2006, pp.277-306.

[172] Loulizi, A., Flintsch, G.W., Al-Qadi, I.L., Mokarem, D., Comparing resilient modulus and dynamic modulus of hot-mix asphalt as material properties for flexible pavement design, *Transportation Research Record*, 1970, Washington, D. C., 2006, pp.161-170.

[173] Loulizi, A., Al-Qadi, I.L., Elseifi, M., Difference between in situ flexible pavement measured and calculated stresses and strains, *Journal of Transportation Engineering*, 132(7), 2006, 574-579.

[174] Love, A. E. H., *Mathematical Theory of Elasticity*, 1927, Oxford University Press, Cambridge, U. K., 2nd edition, 1906.

[175] Lu, Z., Yao, H., Liu, J., and Hu, Z., Experimental evaluation and theoretical analysis of multi-layered road cumulative deformation under dynamic loads, *Road Materials and Pavement Design*, 15(1), 2014, pp.35-54

[176] Lundstrom, R., Benedetto, H. D. and Isacsson, U., Influence of asphalt mixture stiffness on fatigue failure, *Journal of Materials in Civil Engineering*, 16(6), 2004, pp.516-525.

[177] Lundstrom, R., Ekblad, J., Isacsson, U., Karlsson, R., Fatigue modeling as related to flexible pavement design, *Road Materials and Pavement Design*, 8(2), 2007, pp.165-205.

[178] Lytton, R. L., Characterizing asphalt pavements for performance, *Transportation Research Record*, No. 1723, TRB, Washington, D.C., pp.5-16.

[179] Madhav, M. R., and Poorooshasb, H. B., A new model for geosynthetic reinforced soil, *Computers and Geotechnics*, 6, 1988, pp.277-290.

[180] Mahboub, K. C., Liu, Y., Allen, D. L., Evaluation of temperature responses in concrete pavement, *Journal of Transportation Engineering*, 2004, 130(3), pp.395-401.

[181] Maheshwari, P., Chandra, S., Basudhar, P. K., Modelling of beams on a geosynthetic-reinforced granular fill-soft soil system subjected to moving loads, *Geosynthetics International*, 11(5), 2004, pp.369-376.

[182] Mahrenholtz, O. H., Beam on viscoelastic foundation: an extension of Winkler's model, *Archive of Applied Mechanics*, 2010, 80, pp.93-102.

[183] Maji, A., and Das, A., Reliability considerations of bituminous pavement design by Mechanistic-Empirical approach, *International Journal of Pavement Engineering*, 9(1), 2008, pp.19-31.

[184] Malárics, V., and Müller, H. S., Numerical investigations on the deformation of concrete pavements, *7th RILEM International Conference on Cracking in Pavements*, 2012, pp.507-516.

[185] Mallick, A. K., Chandra, S., and Singh, A. B., Steady-state response of an elastically supported beam to a moving load, *Journal of Sound and Vibration*, 291, 2006, pp.1148-1169.

[186] Mallick, R. B., and El-Korchi, T., *Pavement Engineering - Principles and Practice*, CRC Press, Taylor & Francis Group, 2nd Edition, 2013.

[187] Marasteanu, M. O., Li, X., Clyne, T. R., Voller, V. R., Timm, D. H., Newcomb, D. E., Low temperature cracking of asphalt concrete pavements, report no MN/RC - 2004-23, submitted by University of Minnesota to Minnesota Department of Transportation, 2004.

[188] Marasteanu, M., Zofka, A., Turos, M., Li, X., Velasquez, R., Li, X., Buttlar, W., Paulino, G., Braham, A., Dave, E., Ojo, J., Bahia, H., Williams, C., Bausano, J., Gallistel, A., and McGraw, J., Investigation of low temperature cracking in asphalt pavements national pooled fund study, 776, Rep. No. MN/RC 2007-43, Dept. of Civil Engineering, 2007, University of Minnesota, Minneapolis.

[189] Martinček, G., *Dynamics of Pavement Structures*, E & FN Spon, 1994.

[190] Masad, E., Al-Rub, R. A., and Little, D. N., Recent developments and applications of pavement analysis using nonlinear damage (PANDA) model, *7th RILEM International Conference on Cracking in Pavements*, RILEM Bookseries, 4, 2012, pp.399-408.

[191] Masad, E., Branco, V. T. F. C., Little, D. N., Lytton, R., A unified method for the analysis of controlled-strain and controlled-stress fatigue testing, *International Journal of Pavement Engineering*, 9(4), 2008, pp.233-246.

[192] Masad, E., Tashman, L. Little, D., Zbi, H., Viscoplastic modeling of asphalt mixes with the effects of anisotropy, damage and aggregate characteristics, *Mechanics of Materials*, 37, 2005, pp.1242-1256.

[193] Mathews, P. M., Vibrations of a beam on elastic foundation, *Journal of Applied Mathematics and Mechanics*, 38(3-4), 1958, pp.105-115.

[194] Matsuno, S. and Nishizawa, T., Mechanism of longitudinal surface cracking in asphalt pavement, *Proceedings of 7th International Conference of Structural Design of Asphalt pavements*, Vol. 2, 1992, Ann Arbor, pp.277-291.

[195] May, R. and Witczak, M. W., Effective granular modulus to model pavement responses, *Transportation Research Record*, No. 810, TRB, Washington, D. C., 1981, pp.1-9.

[196] McDonald, M., and Madanat, S., Life-cycle cost minimization and sensitivity analysis for mechanistic-Empirical pavement design, *Journal of Transportation Engineering*, 138(6), 2012, pp.706-713.

[197] Meneses, S., and Ferreira, A., Pavement maintenance programming considering two objectives: maintenance costs and user costs, *International Journal of Pavement Engineering*, 14(2), 2013, pp.206-221.

[198] Mechanistic-empirical pavement design guide, - manual of practice, AASHTO, Interim Edition, July 2008.

[199] Miller, J. S., and Bellinger, W. Y., Distress Identification Manual for Long-Term Pavement Performance Program (Fourth revised edition), FHWA-RD-03-031, Federal Highway Administration, FHWA-RD-03-031, 2003. http://www.fhwa.dot.gov/publications/research/infrastructure/pavements/ltpp/reports/03031/03031.pdf

[200] Miner, M. A., Cumulative damage in fatigue, *Proceedings of ASME*, ASME, 1945, pp.A159-A164.

[201] Mitchell, J. K., and Monismith, C. L., A thickness design procedure for pavements with cement stabilized bases

and thin asphalt surfacings, *Proceedings of 4th International Conference of Structural Design of Asphalt Pavements*, Vol. I, 1977, pp.409-416.

[202] Monismith, C. L., Analytically based asphalt pavement design and rehabilitation: theory to practice, 1992-1992, *Transportation Research Record*, 1354, TRB, Washington, D. C., 1994, pp.5-26.

[203] Mun, S., Chehab, G.R., and Kim, Y. R., Determination of time domain viscoelastic functions using optimized interconversion techniques, *Road Materials and Pavement Design*, 8, 2007, pp.351-365.

[204] Monismith, C. L., Secor, K. E. and Blackmer, W., Asphalt mixture behaviour in repeated flexure, *Proceedings of Association of Asphalt Paving Technologists*, 30, 1961, pp.188-222.

[205] Monismith, C. L., Seed, H. B., Mitry, F. G., and Chan, C. K., Prediction of pavement deflection from laboratory tests, *Proceedings of the 2nd International Conference of Structural Design of Asphalt Pavements*, University of Michigan, 1967, pp.109-140.

[206] NCHRP Design Guide, Mechanistic-empirical design of new & rehabilitated pavement structure, 1-37A, 2004, http://onlinepubs.trb.org/onlinepubs/archive/mepdg/guide.htm, last accessed January, 2014.

[207] Neville, A. M., *Properties of Concrete*, Longman, Thomson Press (India) Ltd., 1st Indian Reprint, 2000.

[208] Neville, A. M., and Brooks J. J., *Concrete Technology*, International Student Edition reprint, Longman Group, 1999.

[209] Nunn, M., Brown, A., Weston, D. and Nicholls, J. C., Design of long-life flexible pavements for heavy traffic. Report No. 250, Transportation Research Laboratory, Berkshire, United Kingdom, 1997.

[210] Ouyang, Y., and Madanat, S., Optimal scheduling of rehabilitation activities for multiple pavement facilities: exact and approximate solutions, *Transportation Research Part A: Policy and Practice*, 38(5), 2004, pp.347-365

[211] Packard, R. G., Design of Concrete Airport Pavement, Portland Cement Association, Skokie, Illinois, reprint 1995.

[212] Papagiannakis, A. T., and Masad, E. A., *Pavement Design and Materials*, John Wiley & Sons, 2007.

[213] Park, S. W., and Kim, Y. R., Analysis of layered viscoelastic system with transient temperature, *Journal of Engineering Mechanics*, Vol.124(2), 1998, pp.223-231.

[214] Park, S. W., and Kim, Y. R., Fitting prony-series viscoelastic models with power-law presmoothing, *Journal of Materials in Civil Engineering*, 13(1), 2001, pp.26-32.

[215] Pavement analysis and design software, http://asphalt.csir.co.za/samdm/, last accessed January 25, 2014.

[216] *Pavement design manual - Asphalt pavements and overlays for road traffic,* Shell International Petroleum Company Limited, London, 1978.

[217] *Pavement Design - A Guide to the Structural Design of Road Pavements*, Austroads, Sydney, 2004.

[218] Peattie, K. R., Stress and strain factors for three layered elastic systems, Highway Research Bulletin No.342, Washington D. C., 1962, pp.215-253.

[219] Pellinan, T. K., and Witczak, M. W., Stress dependent master curve construction for dynamic (complex) modulus, *Journal of Association of Asphalt Paving Technologists*, 71, 2002, pp.281-309.

[220] Peshkin, D. G., Hoerner, T. E., and Zimmerman, K. A., Optimal timing of pavement preventive maintenance treatment applications, Report 523, NCHRP, TRB, Washington, D. C., 2004.

[221] Pister, K. S., Viscoelastic plate on a viscoelastic foundation, *Journal of the Engineering Mechanics Division*, 87 (EM1), 1961, pp.43-54.

[222] Poulos, H. G., and Davis, E. H., *Elastic Solutions for Soil and Rock Mechanics*, John Wiley & Sons Inc., 1974.

[223] Porter, M. L., Dowel bar optimization: phases I and II, Final Report, Center for Portland Cement Concrete Pavement Technology, Iowa State University, 2001.

[224] Potter, T E. C., Cebon, D., Collop, A. C., Cole, D. J., Road damaging potential of measured dynamic tyre forces in mixed traffic, Proceedings of the Institution of Mechanical Engineers, Part D: *Journal of Automobile Engineering*, 210(D3), 1996, pp.215-225.

[225] Pyatigorets, A. V., Marasteanu, M. O., Khazanovich, L., and Stolarski, H. K., Application of matrix operator method to the thermoviscoelastic analysis of composite structures, *Journal of Mechanics of Materials and Structures*, 5(5), 2010, pp.837-854.

[226] Quintus, H. L. V., Mallela, J., Bonaquist, R., Schwartz, C. W., Carvalho, R. L., Calibration of rutting models for structural and mix design, Report No. 719, NCHRP, *Transportation Research Board*, Washington, D. C., 2012.

[227] Raad, L. and Figueroa, J. L., Load response of transportation support systems. *Transportation Engineering Journal*, 16 (TE1). 1980, pp.111-128.

[228] Rajbongshi, P. and Das, A., Thermal fatigue considerations in asphalt pavement design, *International Journal of Pavement Research and Technology*, 1(4), 2008, pp.129-134.

[229] Rajbongshi, P., and Das, A., Estimation of temperature stress and low-temperature crack spacing in asphalt pavements, *Journal of Transportation Engineering*, 135(10), 2009, pp.745-752.

[230] Rajbongshi, P., and Das, A., Estimation of structural reliability of asphalt pavement for mixed axle loading conditions, *Proceedings of the 6th Int. Conference of Roads and Airfield Pavement Technology* (ICPT), Sapporo, Japan, 2008, pp.35-42.

[231] Rajbongshi, P., and Das, A., Optimal asphalt pavement design considering cost and reliability, *Journal of Transportation Engineering*, 134(6), 2008, pp.255-261.

[232] Rajbongshi, P. and Das, A., Temperature stresses in concrete pavement - a review, *International Conference on Civil Engineering in the New Millennium : Opportunities and Challenges (CENeM 2007)*, Bengal Engineering and Science University, Shibpur, January 11-14, 2007, Vol. III, pp.2080-2090.

[233] Ramsamooj, D. V., Stresses in jointed rigid pavement, *Journal of Transportation Engineering*, 125(2), 1999, pp.101-107.

[234] Ramsamooj, D. V., Ramadan, J., and Lin, G. S., Model prediction of rutting in asphalt concrete, *Journal of Transportation Engineering*, 124(5), 1998, pp.448-456.

[235] Ramsamooj, D. V., Prediction of fatigue performance of asphalt concrete mixes, *Journal of Testing and Evaluation*, 27(5), 1999, pp.3343-3348.

[236] Rao, T. S. C. S., Craus, J., Deacon, J. A., Monismith, C. L., Fatigue response of asphalt mixes, Institute of Transportation Studies, SHRP-A-003-A, University of California Berkeley, California, 1990.

[237] Rhines, W. J., Elastic-plastic foundation model, *Journal of Soil Mechanics and Foundation Division*, 95, 1960, pp.819-826.

[238] Richardson, J. M., and Armaghani, J. M., Stress caused by temperature gradient in Portland cement concrete pavements, *Transportation Research Record* 1121, TRB, Washington, D.C., 1987, pp.7-13.

[239] Roque, R., Zou, J., Kim, Y. R., Baek, C., Thirunavukkarasu, S., Underwood, B. S., Guddati, M. N., Top-Down cracking of hot-mix asphalt layers: models for initiation and propagation, NCHRP web-only document 162, Washington, D. C., 2010.

[240] Saal, R. N. S. and Pell, P. S., Fatigue of bituminous road mixes, Kolloid Zeitschrift, 171(1), 1960, pp.61-71.

[241] Sadd, M. H., *Elasticity - Theory, Applications and Numerics*, Academic Press, Elsevier, 2005.

[242] Sadd, M. H., Dai, Q., Parameswaran, V., and Shukla, A., Microstructural simulation of asphalt materials: modeling and experimental studies, *Journal of Materials in Civil Engineering*, 16(2), 2004, pp.107-115.

[243] Salamaa, H. K., and Chatti, K., Evaluation of fatigue and rut damage prediction methods for asphalt concrete pavements subjected to multiple axle loads, *International Journal of Pavement Engineering* 12(1), 2011, pp.25-36.

[244] Sanchez-Silva, M., Arroyo, O., Junca, M., Caro, S. and Caicedo, B., Reliability based design optimization of asphalt pavements, *International Journal of Pavement Engineering*, 6(4), 2005, pp.281-294.

[245] Schapery, R. A., and Park, S. W., Methods of interconversion between linear viscoelastic material functions. Part IIan approximate analytical method, *International Journal of Solids and Structures*, 36(11), pp.1677-1699.

[246] Schiffman, R. L., General analysis of stresses and displacements in layered elastic systems, *Proceedings of the 1st International Conference on Structural Design of Asphalt*

Pavements, University of Michigan, Ann Arbor, 1962, pp.365-375.

[247] Selvadurai, A. P. S., *Elastic Analysis of Soil-Foundation Interaction, Development of Geotechnical Engineering*, Elsevier Scientific Publishing Company, Vol. 17, 1979.

[248] Selvadurai, A. P. S., On Boussinesq's problem, *International Journal of Engineering Science*, 39, 2001, pp.317-322.

[249] Setiadji, B. H., and Fwa, T. F., Examining $k - E$ relationship of pavement subgrade based on load-deflection consideration, *Journal of Transportation Engineering*, 135(3), 2009, pp.140-148.

[250] Seyhan U, Tutumluer E. Anisotropic modular ratios as unbound aggregate performance indicators, *Journal of Materials in Civil Engineering*, 2002, 14(5), pp.409-416.

[251] Shah, S. P., Subramaniam, K. V., and Popoovics, J. S., Fatigue fracture of concrete subjected to biaxial stresses in the tensile C-T region, *Journal of Engineering Mechanics*, 2002, 128(6), pp.668-676.

[252] Shen, W., and Kirkner, D. J., Distributed thermal cracking of AC pavement with frictional constraint, *Journal of Engineering Mechanics*, 125(5), 1999, pp.554-560.

[253] Shen, W., and Kirkner, D. J., Thermal cracking of viscoelastic asphalt-concrete pavement, *Journal of Engineering Mechanics*, 127,(7), 2001, pp.700-709.

[254] Shi, X. P., Fwa, T. F., and Tan, S. A., Warping stresses in concrete pavements on Pasternak foundation, *Journal of Transportation Engineering*, 119(6), 1993, pp.905-913.

[255] Shi, X. P., Tan, S. A., and Fwa, T. F., Rectangular thick plate with free edges on Pasternak foundation, *Journal of Transportation Engineering*, 120(5), 1994, pp.971-988.

[256] Shook, J. F., and Finn, F. N., Thickness design relations for asphalt pavements, *Proceedings of the 1st International Conference on Structural Design of Flexible Pavements*, University of Michigan, Ann Arbor, Michigan, 1962, pp.640-687.

[257] Shook, J. F., Finn, F. N., Witczak, M. W., and Monisminth, C. L., Thickness design of asphalt pavements, The Asphalt Institute Method, *Proceedings of the 5th International Conference on Structural Design of Flexible Pavement*, Delft University of Technology, Delft, 1982, pp.17-44.

[258] Shukla, P. K., and Das, A., A re-visit to the development of fatigue and rutting equations used for asphalt pavement design, *International Journal of Pavement Engineering*, 9(5), 2008, pp.355-364.

[259] Smallridge, M., and Jacob, A., The ASCE port and intermodal yard pavement design guide, Ports'01, Norfolk, 2001, p.10.

[260] South African National Road Agency, SANRAL, Chapter-10, Pavement design, http://sanral.ensight-cdn.com/content/SAPEM_Chapter_10_Jan2013.pdf, last accessed February 6, 2014

[261] Sousa, J. B., Deacon, J. A., Weissman, S., Harvey, J. T., Monismith, C. L., Leahy, R. B., Paulsen, G., and Coplantz, J. S., Permanent deformation response of asphalt-aggregate mixes, Report no. SHRP-A-415, Strategic Highway Research Program, National Research Council, Washington, D.C., 1994.

[262] Stubstad, R.N., Tayabji, S. D., and Lukanen, E. O., LTPP data analysis: variation in pavement design inputs. Final Report, NCHRP Web Document 48, TRB, National Research Council, Washington, D.C., 2002, http://gulliver.trb.org/publications/nchrp/nchrp_w48.pdf. Last accessed on February, 2014.

[263] Sun, L., Hudson, W. R., and Zhang, Z., Empirical-mechanistic method based stochastic modeling of fatigue damage to predict flexible pavement cracking for transportation infrastructure management, *Journal of Transportation Engineering*, 129(2), 2003, pp.109-117.

[264] Sun, L., A closed-form solution of beam on viscoelastic subgrade subjected to moving loads, *Computers and Structures*, 80, 2002, pp.1-8.

[265] Svasdisant, T., Schorsch, M., Baladi, G. Y., and Pinyosunun, S., Mechanistic analysis of top-down cracks in asphalt pavements, *Transportation Research Record*, 1809, TRB, Washington, D. C., 2002, pp.126-135.

[266] Tabatabaie, A. M., and Barenberg, E. J., Structural analysis of concrete pavement systems, *Transportation Engineering Journal*, 106(5), 1980, pp.493-506.

[267] Tang, T., Zollinger, G., and Senadheera, S., Analysis of concave curling in concrete slabs, *Journal of Transportation Engineering*, 119(4), 1993, pp.618-633.

[268] Tayebali, A. A., Tsai, B., Monismith, C. L., Stiffness of asphalt-aggregate mixes, SHRP-A-388, Institute of Transportation Studies, University of California, Berkeley, 1994.

[269] Tayebali, A. A., Deacon, J. A., Coplantz, J. S., Harvey, J. T., and Monismith, C. L., Fatigue Response of asphalt-aggregate mixes, SHRP-A-404, Institute of Transportation Studies, University of California, Berkeley, 1994.

[270] Terzaghi, K., Evaluation of coefficients of subgrade reaction, *Geotechnique*, 5(4), 1995, pp.41-50.

[271] Tia, M., Armaghani, J. M., Wu, C. L., Lei, S. and Toye, K. L., FEACONS III computer program for an analysis of jointed concrete pavements, *Transportation Research Record*, 1136, TRB, Washington, D.C., 1987, pp.12-22.

[272] Tighe, S., Guidelines for probabilistic pavement life cycle cost analysis, *Transportation Research Record*, 1769, TRB, Washington, D. C., 2001, pp.28-38.

[273] Timm, D. H., Guzina, B. B., and Voller, V. R. Prediction of thermal crack spacing. *International Journal of Solids and Structures*, 40, 2003, 125-142.

[274] Timm, D. H., Newcomb, D. E., Briggison, B., and Galambos, T. V., Incorporation of reliability into the Minnesota mechanistic-empirical pavement design method. Final Report, Submitted to Minnesota Department of Transportation, Department of Civil Engineering, Minnesota University, Minneapolis, 1999.

[275] Timm, D. H., Newcomb, D. E. and Galambos, T. V., Incorporation of reliability into mechanistic-empirical pavement design, *Transportation Research Record*, 1730, TRB, Washington, D. C., 2000, pp.73-80.

[276] Timoshenko, S. P. and Woinowky-Krieger, S., *Theory of Plates and Shells*, McGraw Hill, New York, 1959.

[277] Timoshenko, S., and Goodier, J. N., *Theory of Elasticity*, McGraw-Hill, 1934, New York.

[278] Titi, H. H., Elias, M. B., Helwany, S., Determination of typical resilient modulus values for selected soils in Wisconsin, University of Wisconsin - Milwaukee, Submitted to The Wisconsin Department of Transportation, 2006.

[279] *The Handbook of Highway Engineering*, Edited by: Fwa, T. F., CRC Press, Taylor & Francis Group, 2006.

[280] Theyse, H. L., de Beer, M. and Rust, F. C., Overview of the South African mechanistic pavement design method, *Transportation Research Record*, No.1539. TRB, Washington D. C. 1996, pp.6-17.

[281] *Thickness design for concrete highway and street pavements*, Portland Cement Association, 1984, Skokie.

[282] Thompson, M. R., Barenberg, E., Brown, S. F., Darter, M. M., Larson, G., Witczak, M., and El-Basyouny, M., Independent review of the Mechanistic-Empirical pavement design guide and software, NCHRP research results digest 307, NCHRP, Washington, D.C., 2006. http://onlinepubs.trb.org/onlinepubs/nchrp/nchrp_rrd_307.pdf, last accessed January 28, 2014.

[283] Thompson, M. R., and Elliott, R. P., ILLI-PAVE based response algorithms for design of conventional flexible pavements, *Transportation Research Record*, 1043, TRB, Washington D. C. 1985, pp.50-57.

[284] *Thickness Design – Asphalt Pavements for Highways and Streets*, The Asphalt Institute, Manual Series No. 1 (MS-1), 1991.

[285] *Thickness design of concrete pavements*, Portland Cement Association publication, ISO10P, 1974.

[286] Tseng, K. H., and Lytton, R. L., Fatigue damage properties of asphaltic pavements, *Transportation Research Record*, No. 1286, TRB, 1990, Washington D. C., pp.150-163.

[287] Tsunokawa, K., and Schofer, J. L., Trend curve optimal control model for highway pavement maintenance: case study and evaluation, *Transportation Research*, 28A, 1994, pp.151-166.

[288] Tutumluer, E., Practices for unbound aggregate pavement Layers - a synthesis of highway practice, NCHRP Synthesis 445, Transportation Research Board, Washington, D. C., 2013.

[289] Ueshita, K., and Meyerhof, G., G., Deflection of multilayer soil systems, *Journal of the Soil Mechanics and Foundation Division*, 93 (SM5), 1967, pp.257-282.

[290] Ullidtz, P. *Pavement Analysis*, 19, Elsevier, New York, 1986.

[291] Underwood, B. S., and Kim, Y. R., Determination of the appropriate representative elastic modulus for asphalt concrete, *International Journal of Pavement Engineering*, 10(2), 2009, pp.77-86.

[292] Underwood S., Heidari, A. H., Guddati, M., and Kim, Y. R., Experimental investigation of anisotropy in asphalt concrete, *Transportation Research Record*, 1929, TRB, Washington, D. C., 2005, pp.238-247.

[293] Uzan, J., Characterization of granular materials, *Transportation Research Record*, 1022, TRB, Washington, D. C., 1985, pp.52-59.

[294] Uzan, J., Witczak, M. W., Scullion, T., and Lytton, R. L., Development and validation of realistic pavement response models, *Proceedings of 3rd International Conference on the Structural Design of Asphalt Pavements*, Vol. I, 1972, pp.334-350.

[295] Ventsel, E., and Krauthammer, T., *Thin Plates and Shells - Theory, Analysis and Application*, Marcel Dekker, 2001.

[296] Verstraeten, J., Stresses and displacements in elastic layered systems, general theory – numerical stress calculation in four-layered systems with continuous interfaces, *Proceeding of 2nd International Conference of Structural Design of Asphalt Pavements*, 1967, pp.277-290.

[297] Verstraeten, J., Moduli and critical strains in repeated bending of bituminous mixes application to pavement design, *Proceeding of 3rd International Conference of Structural Design of Asphalt Pavements*, Vol. 1, 1972, pp.729-738.

[298] Vinson, T. S., Janoo, V. C., and Haas, R. C. G., Summary report - low temperature and thermal fatigue cracking, Report SHRP-A/ IR-90-001, Strategic Highway Research Program, National Research Council, Washington, D. C., 1990.

[299] Vlasov, V. Z., and Leont'ev, M. N., Beams, plates and shells on elastic foundations, Israel Program for Scientific Translations, translated from Russian, 1960.

[300] Von-Quintus, H. L., Hot mix asphalt layer thickness design for longer life bituminous pavements, Transportation Research Circular, Number 503, TRB, Washington, D. C., 2001, pp.66-78.

[301] Wang, D., Analytical solutions for temperature profile prediction in multi-layered pavement systems. Ph.D. Dissertation, Dept. of Civil and Environmental Engineering, Univ. of Illinois at Urbana- Champaign, IL, Open access http://hdl.handle.net/2142/18241, last accessed February 2014.

[302] Wang, D., Analytical approach to predict temperature profile in a multilayered pavement system based on measured surface temperature data, *Journal of Transportation Engineering*, 138(5), 2012, pp.674-679.

[303] Westergaard, H. M., Stresses in concrete pavements computed by theoretical analysis, *Public Roads*, 7, 1926, pp.25-35.

[304] Westergaard, H. M., Analysis of stresses in concrete pavement due to variations in temperature, Highway Research Board, National Research Council, 6, Washington, D.C., 1927, pp.201-217.

[305] Westergaard, H. M., Stresses in concrete runways of airports, *Proceedings of 19th Annual Meeting*, Highway Research Board, Washington, D.C., 1939, pp.197-203.

[306] Westergaard, H. M., New formulas for stresses in concrete pavements of airfields, *Proceedings of ASCE*, 73, 1947, pp.687-701.

[307] White, T. D., Haddock, J. E., Hand, A. J. T., and Fang, H., Contributions of pavement structural layers to rutting

of hot mix asphalt pavements, NCHRP 468, TRB, National Research Council, Washington, D. C., 2002.

[308] Williams, M. L., Landel, R. F., and Ferry, J. D., The temperature dependence of relaxation mechanisms in polymers and other glassforming liquids, *Journal of American Chemical Society*, 77, 1955, pp.3701-3707.

[309] Witczak, M., Mamlouk, M., Souliman, M., Zeiada, W., Laboratory validation of an endurance limit for asphalt pavements, NCHRP Report No. 762, Transportation Research Board, Washington, D. C., 2013.

[310] Yang, N. C., *Design of Functional Pavements*, McGraw-Hill Book Company, 1972.

[311] Yavuzturk, C., K. K. C. A., Assessment of temperature fuctuations in asphalt pavements due to thermal environmental conditions using a two-dimensional, transient finite difference approach, *Journal of Materials in Civil Engineering*, 17(4), 2005, pp.465-475.

[312] Yin, H., An analytical procedure for strain response prediction of flexible pavement, *International Journal of Pavement Engineering*, 14(5), 2013, pp.486-497.

[313] Yoder, E. J., and Witczak, M. W., *Principles of pavement design*, 2nd edition, John Wiley & Sons, Inc., 1975.

[314] You, Z., and Buttlar, W. G., Discrete element modeling to predict the modulus of asphalt concrete mixtures, *Journal of Materials in Civil Engineering*, 16(2), 2004, pp.140-146.

[315] Yusoff, M. I. Md., Chailleux, E., and Airey, G. D., A comparative study of the influence of shift factor equations on master curve construction, *International Journal of Pavement Research and Technology*, 4(6), pp.324-336.

[316] Yusoff, M. I. Md., Shaw, M. T., Airey, G. D., Modelling the linear viscoelastic rheological properties of bituminous

binders, *Construction and Building Materials*, 25, 2011, pp.2171-2189.

[317] Zaghloul, S. M, and White, T. D., Use of a three-dimensional dynamic finite element program for analysis of flexible pavement, *Transportation Research Record*, 1388, TRB, Washington, D. C., 1993, pp.60-69.

[318] Zeinkiewicz, O. C., Valliappan, S. and King, I. P., Stress analysis of rock as 'no-tension' material, *Geotechnique*, 18, 1968, pp.56-66.

[319] Zhang, J., Fwa, T. F., Tan, K. H. and Shi, X. P., Five-slab thick-plate model for concrete pavement. *Road Materials and Pavement Design*, 2000, 1, pp.10-34.

[320] Zhang, J., Fwa, T. F., Tan, K. H., and Shi, X. P., Model for nonlinear thermal effect on pavement warping stresses, *Journal of Transportation Engineering*, 129(6), 2003, pp.695-702.

[321] Zhao, Y., Ni, Y., and Zeng, W., A consistent approach for characterising asphalt concrete based on generalised Maxwell or Kelvin model, 2014, *Road Materials and Pavement Design*, DOI: 10.1080/14680629.2014.889030

[322] Zhu, H., and Sun, L., Mechanistic rutting prediction using a two-stage viscoelastic-viscoplastic damage constitutive model of asphalt mixtures, *Journal of Engineering Mechanics*, 139(11), 2013. pp.1577-1591.

[323] Zubeck, H. K., and Vinson, T. S., Prediction of low-temperature cracking of asphalt concrete mixtures with thermal stress restrained specimen test results. *Transportation Research Record*, 1545, TRB, Washington, D. C., 1996, pp.50-58.

CIVIL ENGINEERING

ANALYSIS OF PAVEMENT STRUCTURES

"A useful add-on to all those dealing with pavement structure studies, research, and consultancy."
—Dr. John N. Karadelis, Coventry University, UK

"Structured and well-organized. Thorough theoretical modelling. …The materials give a well-structured overview of the theory. Items discussed are presented in a clear way."
—C.R. Braam, Delft University of Technology, Faculty Civil Engineering and Geosciences, Netherlands

---

Predict or Explain the Pavement Response to Load: Understand the Physical Governing Principles

Analysis of Pavement Structures brings together current research and existing knowledge on the analysis and design of pavements. It provides a platform for the readers to understand the basic principles of physics and mechanics involved in pavement analyses.

From Simple to Complex Formulation: Learn to Develop Your Own Research or Field Problems

The book introduces load and thermal stress analyses of asphalt and concrete pavement structures in a simple and step-by-step manner. Uniformity of symbol and sign conventions have been maintained throughout the book. References are made to more than 300 sources for interested readers for further reading. The book helps to build confidence in the reader and allows them to formulate and solve their own research or field problems.

Analysis of Pavement Structures covers the basic approaches for pavement analysis, and highlights the fundamental principles followed in the analyses of pavement structures through numerous schematic diagrams.

CRC Press
Taylor & Francis Group
an informa business
www.crcpress.com

6000 Broken Sound Parkway, NW
Suite 300, Boca Raton, FL 33487
711 Third Avenue
New York, NY 10017
2 Park Square, Milton Park
Abingdon, Oxon OX14 4RN, UK

K15520
ISBN: 978-1-4665-5855-7
90000
9 781466 558557